



HAL
open science

Carbon Dioxide Sensing - Biomedical Applications to Human Subjects

Emmanuel Dervieux, Michael Theron, Wilfried Uhring

► **To cite this version:**

Emmanuel Dervieux, Michael Theron, Wilfried Uhring. Carbon Dioxide Sensing - Biomedical Applications to Human Subjects. *Sensors*, 2021, 22 (1), 10.3390/s22010188 . hal-03797894

HAL Id: hal-03797894

<https://hal.science/hal-03797894v1>

Submitted on 4 Oct 2022

HAL is a multi-disciplinary open access archive for the deposit and dissemination of scientific research documents, whether they are published or not. The documents may come from teaching and research institutions in France or abroad, or from public or private research centers.

L'archive ouverte pluridisciplinaire **HAL**, est destinée au dépôt et à la diffusion de documents scientifiques de niveau recherche, publiés ou non, émanant des établissements d'enseignement et de recherche français ou étrangers, des laboratoires publics ou privés.

Review

Carbon Dioxide Sensing—Biomedical Applications to Human Subjects

Emmanuel Dervieux ^{1,*} , Michaël Théron ²  and Wilfried Uhring ³ ¹ BiOSENCEY, 1137a Avenue des Champs Blancs, 35510 Cesson-Sévigné, France² ORPHY, Université de Bretagne Occidentale, 6 Avenue Victor le Gorgeu, 29238 Brest, France; michael.theron@univ-brest.fr³ ICube, University of Strasbourg and CNRS, 23 rue du Loess, CEDEX, 67037 Strasbourg, France; wilfried.uhring@unistra.fr

* Correspondence: emmanuel.dervieux@biosency.com

Abstract: Carbon dioxide (CO₂) monitoring in human subjects is of crucial importance in medical practice. Transcutaneous monitors based on the Stow-Severinghaus electrode make a good alternative to the painful and risky arterial “blood gases” sampling. Yet, such monitors are not only expensive, but also bulky and continuously drifting, requiring frequent recalibrations by trained medical staff. Aiming at finding alternatives, the full panel of CO₂ measurement techniques is thoroughly reviewed. The physicochemical working principle of each sensing technique is given, as well as some typical merit criteria, advantages, and drawbacks. An overview of the main CO₂ monitoring methods and sites routinely used in clinical practice is also provided, revealing their constraints and specificities. The reviewed CO₂ sensing techniques are then evaluated in view of the latter clinical constraints and transcutaneous sensing coupled to a dye-based fluorescence CO₂ sensing seems to offer the best potential for the development of a future non-invasive clinical CO₂ monitor.

Keywords: carbon dioxide; CO₂; transcutaneous monitoring; ptCO₂; tcpCO₂; paCO₂



Citation: Dervieux, E.; Théron, M.; Uhring, W. Carbon Dioxide Sensing—Biomedical Applications to Human Subjects. *Sensors* **2022**, *22*, 188. <https://doi.org/10.3390/s22010188>

Academic Editor: Simona M. Cristescu

Received: 8 November 2021

Accepted: 20 December 2021

Published: 28 December 2021

Publisher’s Note: MDPI stays neutral with regard to jurisdictional claims in published maps and institutional affiliations.



Copyright: © 2021 by the authors. Licensee MDPI, Basel, Switzerland. This article is an open access article distributed under the terms and conditions of the Creative Commons Attribution (CC BY) license (<https://creativecommons.org/licenses/by/4.0/>).

1. Introduction

In medical practice, the accurate monitoring of vital signs is of crucial importance to provide appropriate and effective care to the patients. In particular, the measurement of blood gases—namely di-oxygen (O₂) and CO₂—gives respiratory as well as circulatory clues on the state of a patient [1]. Yet, the continuous monitoring of the arterial partial pressure in O₂—paO₂—and CO₂—paCO₂—implies frequent arterial blood sampling, a process which is both painful and risky [2], requiring trained staff and expensive blood gas analyzers. Furthermore, the blood samples must be promptly analyzed upon collection, adding logistic constraints on the whole healthcare system [3]. Thus, the development of non-invasive paO₂ and paCO₂ monitoring techniques has been an active research field for decades [4–6], but while pulse oximetry proved to be a reliable proxy for paO₂ [7,8], no satisfactory equivalent exists for paCO₂.

On patients intubated or wearing a face mask, CO₂ may be monitored in the exhaled breath, a technique called airway capnometry, leading to the measurement of the end tidal CO₂ partial pressure, petCO₂. Despite a poor correlation between petCO₂ and paCO₂ in case of ventilation-perfusion mismatch or elevated physiologic dead space, airway capnometry makes a good surrogate for blood gases measurement in case of stable haemodynamic conditions [9,10].

The other state-of-the-art paCO₂ proxy is the transcutaneous partial CO₂ pressure—tcpCO₂: if the skin temperature is elevated enough to trigger reactive hyperaemia—and thus subcutaneous blood arterialization—tcpCO₂ correlates well with paCO₂ [11]. However, tcpCO₂ monitors are bulky, expensive (~15 k€), and—above all—need to be recalibrated at least every eight hours due to their important drift [12]. Consequently, there is a strong need

for an alternative to the existing tcpCO_2 monitors, with the aim of developing a cheap, non-invasive, stable, and accurate technique for long-term paCO_2 monitoring.

Fortunately, since CO_2 is ubiquitous in our world, its measurement has been the goal of many researchers from very different fields, each with its constraints and objectives. In particular, CO_2 sensing is used: in the food storage and agri-food industry [13], in medical science [4], in sea and environmental research [14], and of course in the laboratories themselves (e.g., analytical chemistry). Such a diversity of applications leads to different constraints in terms of operating conditions (temperature and pressure), cost, durability, maintenance, etc.

In the first part, this article reviews existing CO_2 sensing techniques available both on the market and in recent research. We aim at being exhaustive, not on the number of works gathered—we rely on external reviews on this point—but rather on the variety of techniques available. Our aim is to collect and present research works spanning the full range of CO_2 sensing.

In a second part, the main goals and constraints intrinsic to biomedical monitoring are exposed. For each sensing medium—in blood or tissues, in exhaled breath, or at the skin surface—the clinical interest of its pCO_2 is discussed. Then, the principal probing modalities routinely used in medical practice are detailed with their specificities, advantages, and drawbacks.

In a third part, a focus is made on transcutaneous sensing: past attempts to replace the ubiquitous Stow-Severinghaus electrode, specific constraints imposed by the transcutaneous sensing modality, and future direction for the development of a new kind of sensor. A brief conclusion summarising the key outcomes of this review is then drawn.

2. Review of CO_2 Sensing Techniques

2.1. Scope of the Review

As stated earlier, our aim is not to produce a complete bibliographic review of each mentioned technique. We do so for the sake of conciseness, and because comprehensive reviews focusing on one or another of the techniques presented here are available in the literature [15–23]. While the latter performs an in-depth coverage of their respective topic (e.g., nanomaterials-based sensors [18,22]), they never cover the full range of CO_2 sensing possibilities. This is partly done, however, in the book *Carbon Dioxide Sensing* [24] which covers certain aspects of the present work in much more details, although letting others aside.

The present review spans the full range of CO_2 measuring techniques with the exception of the analytical ones. That is for instance (mass) spectroscopy, magnetic resonance, chromatography, or titration. We did so because such techniques are not likely to be used for biomedical monitoring in the near future, due to the bulky and expensive apparatus they require. These methods are covered in-depth by dedicated analytical chemistry works, though [25,26].

For each technique, the underlying physical principle enabling CO_2 measurement is exposed briefly. Such explanations are often accompanied by a clear figure or schematic to allow for rapid comprehension of the presented technique. The main features, advantages, and drawbacks of the technique are also disclosed, with typical characteristics of commercial or research applications, when available or relevant. The aim of such summaries is to provide the reader with a basic understanding of each exploited phenomenon, while giving them references to research articles or reviews to dig further. At the end of this section, a table is also given to summarise all the presented techniques and to compare them on several merit criteria—e.g., lifetime, accuracy, drift, cross-sensitivities, response time, form factor, etc.—see Section 2.6.

The structure of the review is organized around the physico-chemical properties of the CO_2 molecule, namely:

1. Infrared absorption of CO_2 —Section 2.2.
2. Hydration of dissolved CO_2 into carbonic acid—Section 2.3.

3. Reduction of CO₂ into CO₂⁻ and CO₃²⁻—Section 2.4.
4. Acoustic properties of gaseous CO₂—Section 2.5.

2.2. Infrared Absorption of CO₂

2.2.1. Non Dispersive Infra-Red (NDIR) Sensors

The operating principle of NDIR CO₂ sensors is that of the Beer-Lambert law of absorption, for gaseous CO₂ exhibits an absorbance peak at 4.26 μm, as can be seen in Figure 1. Due to the absence of other commonly encountered gases absorbing at this wavelength, NDIR sensors are very specific and can reach extremely low levels of detection if the sensing cavity is long enough. They operate as follows: an infrared source is placed on one end of a cavity containing the gaseous analyte, while an infrared receptor is placed at the other end. At a given wavelength λ, the measured light flux Φ_{mes} (W) is then function of: the emitted light flux Φ₀ (W), the geometry of the sensor *k* (unit-less), the light path length *l* (m), the CO₂ volume fraction χ_{CO₂} (unit-less), and its absorbance A_{CO₂} (m⁻¹) following [27]:

$$\Phi_{mes}(\lambda) = k \cdot \Phi_0(\lambda) \cdot e^{-l \cdot \chi_{CO_2} \cdot A_{CO_2}(\lambda)} \quad (1)$$

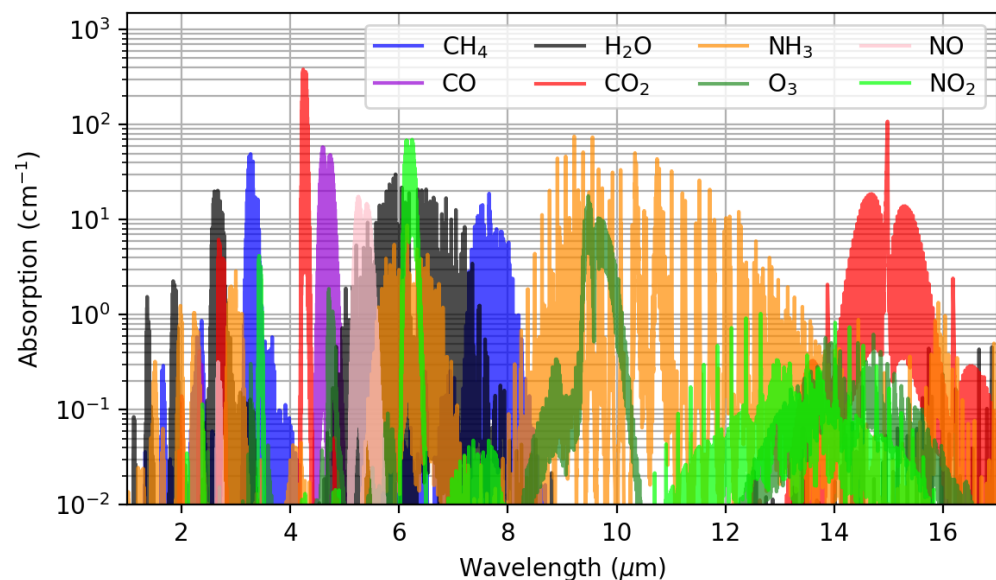


Figure 1. Mid infra-red absorption spectra of various gases, only CO₂ absorbs at 4.26 μm. Data source: HITRAN database [28]. A Lorentzian broadening profile was considered for a dilution in air at 1 atm and 296 K.

While this equation indicates a linear relationship between $\log(\Phi_{mes}/\Phi_0)$, *l*, and χ_{CO₂}, the actual linkage between the latter quantities is generally much more difficult to model accurately, due to a variety of light paths that contribute differently to the sensor response. Although this plurality of light paths can be studied beforehand by simulation—as did Hodgkinson, Liu et al. [29–31]—most sensors are calibrated empirically once manufactured.

Theoretically, only one emitter/receiver duo is needed, given one of them is narrow-band—or bandpass filtered—around 4.26 μm, so as to avoid interferences from other gases. In practice however, a *reference* channel is often placed beside the *measurement* one [32–34]. The role of this additional reference channel is to compensate for variations in the light source intensity due to temperature variations, for instance. In this case, the sensor is composed of two sensing elements, one is covered by a 4.3 μm bandpass filter, while the other one is covered by a bandpass filter in the 3.8–4.1 μm region, where no other gas absorbs. Other designs have also been proposed using a time-interleaved reference/measurement channel alternation, instead of two physically distinct light paths. In this case, a single sensing element is covered by a rotating filter wheel equipped with

multiple bandpass filters at 4.2 μm and 3.8 μm [35]. The typical design of such referenced sensors is presented in Figure 2, Left.

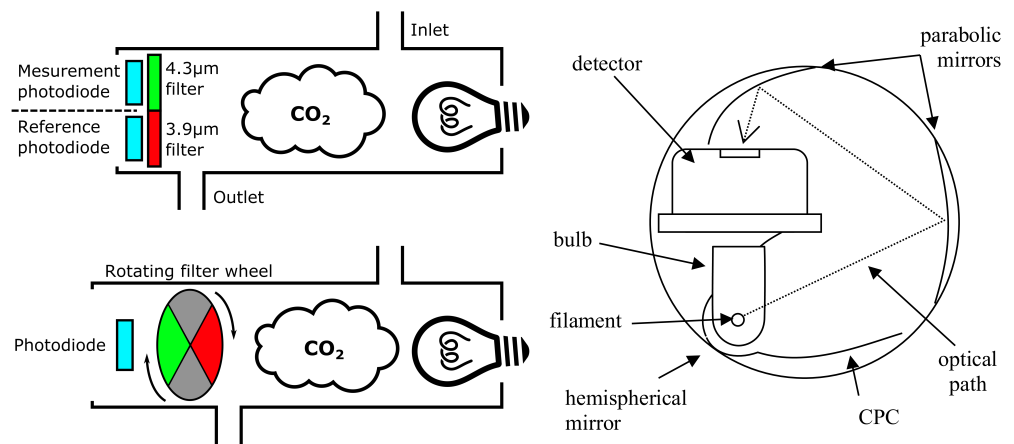


Figure 2. (Left) outline schematic of a space-interleaved (top) and time-interleaved (bottom) NDIR CO₂ sensor. In the time-interleaved sensor, a rotating filter wheel acts as a chopper, with two opaque sectors, and two sectors equipped with 4.3 μm and 3.9 μm bandpass filters, respectively. (Right) a more complex design allowing for longer light paths in a compact device. The detector has two channels, a measurement and a reference one, as in the upper left scheme. CPC stands for Compound Parabolic Collector, a type of light concentrator. Reproduced with permission from Hodgkinson et al. [30].

NDIR sensors were often criticized because of the infrared source they used—i.e., a bulb with a heating filament—which both consumed much power and generated heat [36]. However, with recent advances in the domain of infrared emission and sensing, this is no longer a source of concern. In particular, recent InAsSb semi-conductors allow for reasonably cheap, energy-efficient emitters and receiver, e.g., AK9700AE (Light Emitting Diode (LED)) and AK9710 (sensor), AKM, Japan, or Lms43 LED and photodiode, LMSNT, Russia. Alternatively, thermopiles—possibly miniaturized as Micro Electro-Mechanical Systems (MEMS)—also offer good alternatives to the aforementioned photodiodes [37]. Similarly, MEMS emitters have also been developed [31,38].

The response time of NDIR sensors is limited by the gas flow rate in the sensing chamber, while their sensing range is a function of the light path used. Thus, it is possible to create fast sensors with operating range from a few hundred ppm up to 100% CO₂ [36,39]. It should be noted, however, that since the detection of small concentrations requires a long light path—up to 80 mm for 100 ppm for instance [39]—it can lead to bulky sensors. In order to solve the latter issue, more complex sensing geometries can be envisioned to lengthen the light path while keeping a compact sensor, as can be seen in Figure 2, Right. Additionally, while NDIR CO₂ sensors are not sensitive to relative humidity levels below 100% [35,36], condensation can lead to the formation of water droplets, either in the light path as a fog, or on the surface of light emitters, receivers, or reflectors, thus disturbing the measurements [39,40]. Fortunately, this latter issue may be solved by either detecting potential dew-point situations and removing potentially polluted measurements [41], or heating the sensor itself, though at the cost of a higher power consumption [42,43].

Reviews of mid-infrared sources [44], NDIR applications for gas sensing in general [32,45], and concrete applications to CO₂ measurement [30,33,39,46] can be found in the literature. Interestingly, even if predominantly reported in the gas phase, NDIR CO₂ measurements may also be performed onto an aqueous solution containing dissolved CO₂ [47].

2.2.2. Photoacoustic Sensors

Photoacoustic sensors also use the afore-mentioned absorbance of CO₂ in the mid-infrared (4.26 μm) and periodically illuminate the CO₂ present in the sensing volume. Either a mechanical chopper with a continuous source, a low-inertia source, or even a pulsed laser is used to produce a periodic infrared illumination on the gas sample to analyze. If CO₂ is present in the gas mixture, it absorbs the infrared radiation and thus heat, dilating slightly. When the illumination is stopped, the mixture cools down and thus compresses. The alternating illumination causes a repetition of these dilatations and compressions, which is nothing more than an acoustic wave. The latter can in turn be measured with a microphone [48].

This technique requires a light source that can be modulated at high frequencies—depending on the geometry of the cell and the sensor used—which is achievable using Light Emitting Diodes (LEDs) or lasers, but precludes the use of a light bulb as an infrared light source—unless a mechanical chopper is used, of course. Depending on the targeted accuracy or measurement range, several designs may be employed. The most simple one consists of a non-resonant acoustic cell with a simple microphone and a modulated light working in the 20 Hz–20 kHz range. However, using a resonant cell design and placing the microphone at an antinode of the acoustic wave can lead to much higher output levels. Such a design is illustrated in Figure 3 with an organ-pipe-like resonant cell. With cells in the centimeter range, this translates into frequencies below 40 kHz. Further still, the microphone can consist of a quartz tuning fork—a piezoelectric transducer with a quality factor above 10,000.

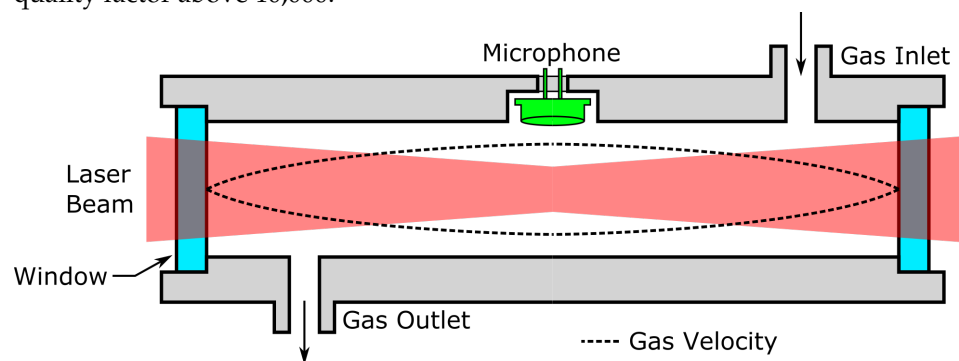
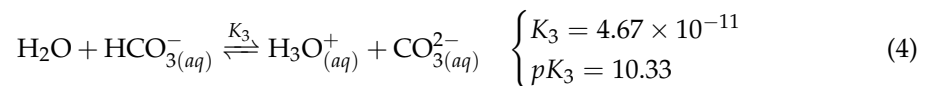
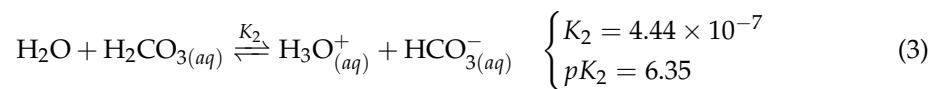
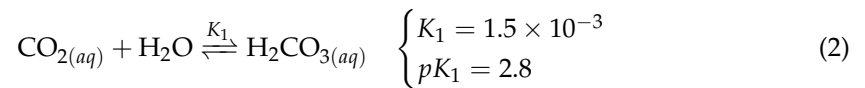


Figure 3. Outline schematic of an organ-pipe-like resonant acoustic cell. The cell consists of a pipe closed at its two ends with optical windows. A laser beam at 4.26 μm is then pulsed at the resonant frequency of the pipe, which forms a $\lambda/2$ resonator. For instance, if a 32,768 Hz quartz tuning fork is used, $\lambda \approx 10$ mm and a pipe length of ~ 5 mm would be ideal. A velocity-sensitive microphone may be placed at half the pipe as depicted. Alternatively, a pressure-sensitive microphone would rather be placed near one of its ends.

With the use of resonant photoacoustic cells or microphones—e.g., quartz tuning forks—very high sensitivities of a few ppm or even ppb can be achieved [49]. Yet, quartz tuning forks are influenced by temperature and humidity—even if this cross-sensitivity is reproducible and can thus be compensated for—and may need to be frequently recalibrated [50]. Contrariwise, MEMS microphones appear to be independent of humidity—even if being temperature-sensitive—and no frequent calibration need was reported [51]. Abundant examples of photoacoustic sensors can be found in the literature [51–53] and recent research is ongoing, targeting their miniaturization into MEMS sensors [54]. Besides, photoacoustic CO₂ sensors can be designed for the full range of CO₂ sensing—from a few ppb up to 100% CO₂—and their response time is mainly limited by the gas flow inside the sensor. It should be noted that this flow is necessarily limited since high flow value generates turbulences, which are essentially acoustic noise [48].

2.3. Hydration of CO₂ into Carbonic Acid

When presented to an aqueous medium, gaseous CO₂ dissolves into carbonic acid (H₂CO_{3(aq)}), which further dissociates into bicarbonate (HCO_{3(aq)}⁻) and carbonate (CO_{3(aq)}²⁻) ions, following [55,56]:



wherein typical values of K_i can be found in the literature [57,58] and are given here in pure water at 25 °C. The consequences of such dissociations are twofold: first, CO₂ dissolution tends to lower the pH of the aqueous medium, and second, the presence of dissolved ions induces changes in the conductance of the solution. While the former phenomenon is the basis the Stow-Severinghaus electrode, Ion-Selective Field-Effect Transistor (ISFET) sensors and dye-based sensors, the former one drives the operation of conductometric CO₂ sensors.

2.3.1. Wet Conductometric Sensors

Wet conductometric sensors take advantage of the fact that when CO₂ dissolves in an aqueous solution, it generates both HCO₃⁻ and H₃O⁺ ions, which in turn modifies the conductivity of the solution [59]. A typical static conductometric sensor is composed of a chamber filled with distilled water and containing two electrodes. The chamber is then covered with a CO₂ permeable membrane to allow outer CO₂ to diffuse inside the sensor [60–62]. Alternatively, a dynamic conductometric sensor may be built, into which distilled water is circulated between a gas diffusion area and an impedance measurement area [13,59]. A static measurement cell is depicted in Figure 4. Using such an apparatus, the sensing medium may be either liquid or gaseous, while dynamic flow-through geometries have only been reported using gaseous analytes.

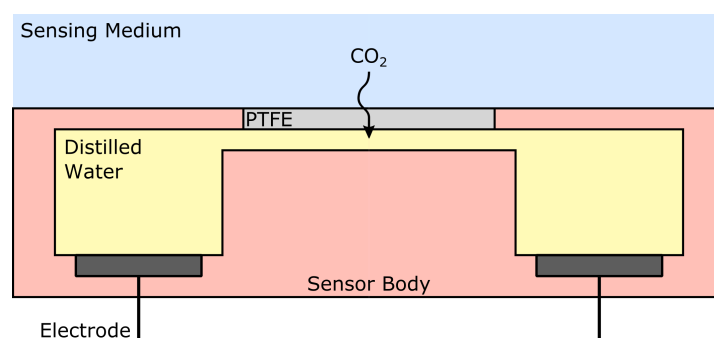


Figure 4. Outline of a static conductometric cell. CO₂ diffuses into distilled water, modifying the concentration of H₃O⁺, HO⁻ and HCO₃⁻ and thus the conductivity of the solution, which may be measured using alternative current to avoid polarisation by mean of two electrodes.

Such sensors are in theory inexpensive, easy to build, and stable. In practice however, a drift is often observed whose roots are not accurately known, even if some authors suggest contamination of the distilled water with external ions. In particular, if glues or resins are used to attach the membrane to the sensor, or to assemble the different parts of the embodiment together, they may further suffer from outgassing and release ions in the distilled water [61]. If the membrane is not tightly sealed, foreign ions may also enter the solution and thus change its conductivity. Drift correction [63] or automatic

recalibration [64] techniques have thus been developed to compensate for this phenomenon. Alternatively, other authors immersed the body of their electrode for at least two weeks in bi-distilled water to make sure that foreign ions possibly bound to the glass surface re-dissolve in the rinsing water and are thus eliminated [65]. The dynamic flow-through geometry also eludes this issue by forcing the water into a de-mineralizing resin while being recycled.

As is the case for other membrane-covered sensors—see Section 2.3.2 below, for instance—the water can still evaporate through the covering membrane depending on the ambient relative humidity, especially in the case of static sensors used on a gaseous analyte. This issue was partially addressed by Neethirajan et al. [66], who presented a polytetrafluoroethylene (PTFE) membrane-covered sensor using Nafion as a proton conductor over a layer of polyaniline boronic acid, which exhibits a conductivity change upon a change in its pH. Overall, wet conductometric CO₂ sensor can be used on the full 0–100% CO₂ range, with response times below 1 min. Still, their life has not been reported in the literature and may be seriously impacted by the afore-mentioned drift.

2.3.2. The Stow-Severinghaus Electrode

The Stow-Severinghaus electrode—named after its inventors Richard Stow [4] and John Severinghaus [67]—is the current state-of-the-art measurement method for transcutaneous pCO₂ [11]. Even if it has been miniaturized since its first introduction, its basic working principle remains unchanged. As one can see in Figure 5 it is nothing more than a pH-meter plunging in an electrolyte and covered with a thin membrane. Originally designed for ex vivo blood pCO₂ sensing, it was later modified to be used transcutaneously as well [68].

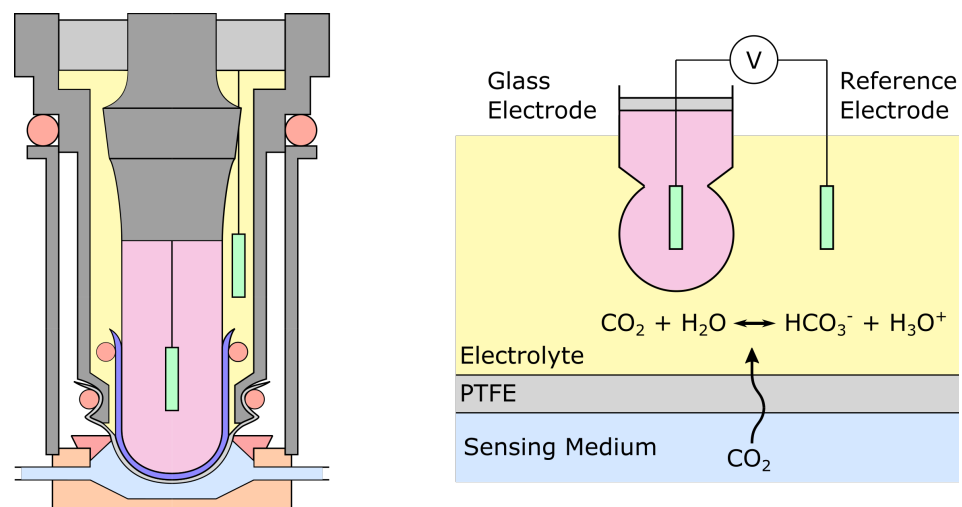


Figure 5. (Left) the Severinghaus electrode, an improvement of the Stow electrode, as first described in the 1958 publication [67]. The colour of the different elements matches that of the simplified schematic on the right. (Right) outline schematic of the Severinghaus electrode. CO₂ diffuses through a PTFE membrane into an electrolyte, causing a change in the pH of the latter. Such a change is then recorded by the mean of a pH-meter that consists of a glass electrode and a reference electrode.

Dissolved CO₂ diffuses from the outer medium into the sensor's embodiment through a membrane made of an ion-impermeable, CO₂-permeable material. A rubber membrane was originally proposed but was quickly replaced by a PTFE one [4,67], although silicone rubber is still occasionally used for its ease of application and better adhesion [69]. The electrolyte was also switched from distilled water to a solution of sodium carbonate (NaHCO₃) and sodium chloride (NaCl) in various concentrations, which influences both the sensitivity and response time of the electrode [55]. CO₂ dissociation lowers the pH of the electrolyte—as described by Equations (2)–(4)—which is then measured using a pair of electrodes: the glass electrode, and the reference electrode. The glass electrode

consists in an Ag/AgCl electrode more often than not, although a Sb/SbO_x electrode has also been occasionally reported [68], while the reference electrode can be made of Pt [67,70] or AgCl [68]. Alternatives to the glass electrode have been explored with liquid membranes instead of the traditional glass bulb [71], or a replacement of the whole electrode by an iridium oxide film grown electrochemically on an iridium wire, yielding a higher sensitivity and being easier to manufacture than the glass electrode [72,73].

Apart from miniaturization and the exploration of other membrane materials, redox electrode pairs, or pH membrane material, the electrode underwent little changes compared to its original design. The response time of the Stow-Severinghaus electrode is generally reported to lie in the 1–5 min range, although the addition of carbonic anhydrase—a catalyst to the reaction (2)—led to response times below 1 min [69,74]. Still, the long-term stability of the electrode rarely exceeds a few months and some amount of drift is always present, making it necessary to re-calibrate the electrode every few hours or days, depending on the target accuracy [71,75]. The full range of the Stow-Severinghaus electrode is usually that of physiological pCO₂ range—that is ~2.6–13.2 kPa (or ~20–100 mmHg) [11]—although applications for concentrations as low as ~0.05–0.1% have also been reported [71,76]. The temperature dependency of the electrode may be compensated for, and a mixture of water and ethylene glycol can be used as a base for the electrolyte, preventing the electrode from drying out from a loss of water vapor through the gas-permeable membrane [77].

2.3.3. ISFET Sensors

Due to the limited miniaturization potential of the Stow-Severinghaus electrode, Ion-Selective Field-Effect Transistors (ISFETs) were explored as CO₂ sensing devices. ISFETs are Metal Oxide Semiconductor Field-Effect Transistor (MOSFET) whose gate is H₃O⁺ sensitive. The addition of a reference electrode can turn them into fully functional pH meters. The use of ISFET for pH sensing has been reported as early as 1970 [78] and was later extended to CO₂ sensing with the addition of a layer of bicarbonate solution covered with a gas-permeable, ion-impermeable, silicone rubber membrane [79].

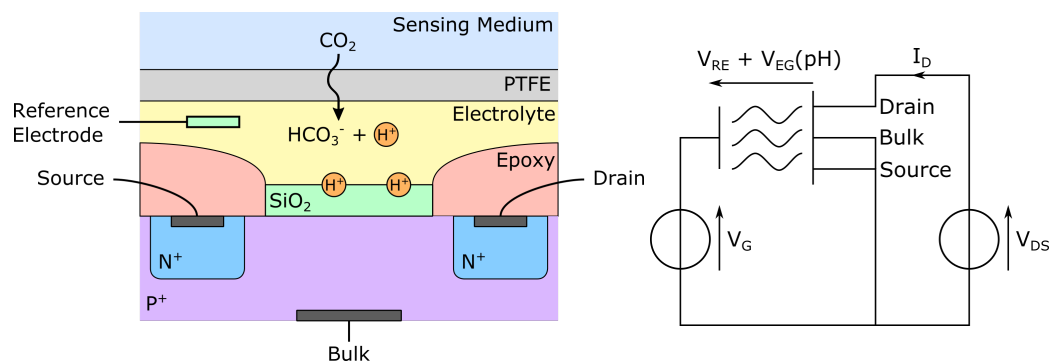


Figure 6. (Left) outline schematic of an ISFET CO₂ sensor. CO₂ diffuses from the analyte inside the inner electrolyte through a PTFE membrane, changing the pH of the electrolyte and generating hydronium ions (abbreviated H⁺). The ions will penetrate the upper layer of the porous SiO₂ gate insulator, influencing the P⁺ substrate underneath, and thus the conductance of the transistor. (Right) basic electrical implementation schematic of an ISFET sensor. The actual grid-source potential seen by the transistor is the sum of the applied grid voltage V_G , the voltage between the reference electrode and the electrolyte V_{RE} , and that between the electrolyte and the gate insulator V_{EG} , itself function of the pH of the electrolyte.

As can be seen in Figure 6, the ISFET gate insulator is not metalized but rather covered with a layer of silicon oxide (SiO₂), itself optionally covered with another layer of silicon nitride (Si₃N₄), hafnium oxide (HfO₂), aluminum oxide (Al₂O₃) or tantalum pentoxide (Ta₂O₅). Once hydrated, the upper layer of the gate insulator becomes able to exchange protons with the surrounding electrolyte, thus acting as a pH electrode. Still, another electrode—the reference electrode—is needed to apply or measure a grid-source potential

on the transistor. This latter potential— V_{GS} —itself function of the pH of the electrolyte, modulates the conductance of the transistor, hence turning it into a pH sensor [80]. CO_2 detection can then be performed by covering the electrolyte with a CO_2 -permeable membrane, impermeable to other ions. This basic approach has been successfully applied by a number of authors in the literature, either for pH measurements [79,81], or direct CO_2 sensing [14,82–84].

Among the above-mentioned gate insulators, hafnium oxide offers better performances in terms of drain current, sensitivity, and body effect than silicon nitride. Hafnium oxide may even be used alone, in place of the silicon oxide layer [85]. The inner electrolyte usually consists of a bicarbonate solution, while the reference electrode is often an AgCl/Ag electrode. ISFET CO_2 sensors are subject to the same drawbacks as the Stow-Severinghaus electrode, namely the drift of the reference electrode and temperature dependency, although the latter may be compensated for. An approach for drift correction has also been proposed with good results either on restrained [81] or wide pH ranges [86]. The dry-out and humidity sensibility problems have been addressed with a dry sensor [87], even if the drift of the latter has yet to be reported. Alternatively, a low-drift design with a deposed reference electrode has also been proposed with promising results [88].

2.3.4. Dye-Based Sensors

Dye-based CO_2 sensors also rely on the influence of CO_2 hydration and dissociation on the pH of an aqueous solution. The pH change caused by the dissociation of CO_2 translates into a change in the optical properties of a pH-sensitive dye, which can exist in either a protonated— RH —or an anionic— R^- —form. The dye is chosen so that its protonated and anionic forms differ either in their absorbance or luminescence spectra, and also for having a K_A acidity constant near that of reaction (3) ($pK_A = -\log(K_A) \approx 6.3$ in water at 25 °C [89]). It can be either dissolved in an aqueous solution—which is in turn entrapped between a substrate layer and a gas-permeable, ion-impermeable membrane—or dissolved in a thin polymer film with the aid of a phase transfer agent. These two kinds of sensors are often referred to as “wet” and “dry” sensors, respectively. A typical fluorescent sensor is depicted in Figure 7, along with the fluorescence spectrum of 1-hydroxy-pyrene-3,6,8-trisulfonate (HPTS), a commonly encountered pH-sensitive fluorophore.

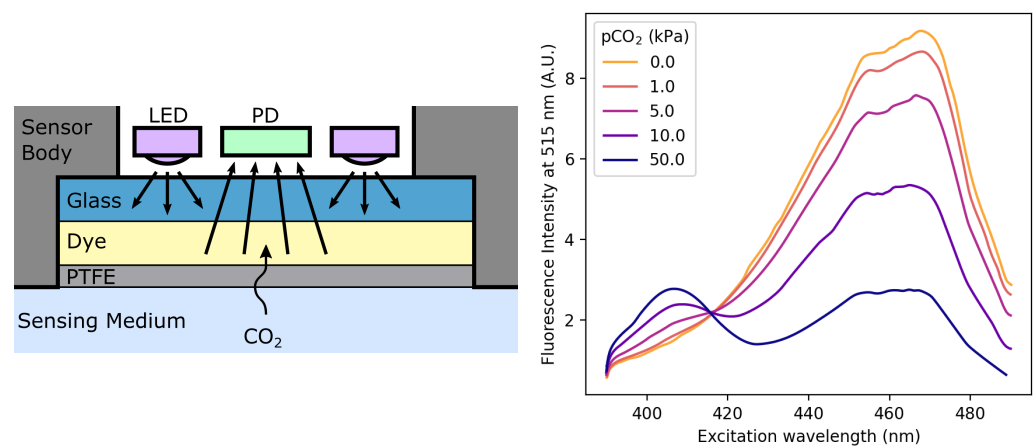


Figure 7. (Left) outline schematic of a typical dye-based CO_2 sensor. The LEDs illuminate a pH-sensitive dye, either dissolved in an aqueous solution or a polymer, through a layer of transparent substrate—here a glass slide. The dye is protected from ionic contamination by a PTFE, gas-permeable, ion-impermeable membrane. The LEDs and photodiode may additionally be covered by excitation or emission filters in case of fluorescence measurement. (Right) the fluorescence excitation spectra of 1 mM HPTS in carbonated distilled water equilibrated with different $p\text{CO}_2$ values. Data source: Uttamlal et al. [90].

The most basic sensors use a single wavelength for illumination—in case of absorbance measurements—or a pair of excitation-emission wavelengths—in case of luminescence measurement. Photobleaching may be compensated for, using more wavelengths and ratiometric methods similar to that driving pulse oximetry [90–97], while variations in the emitted light intensities or sensitivities toward received light can be addressed by using referencing—i.e., taking a measurement in pure di-nitrogen (N₂) and/or pure CO₂ prior to CO₂ measurement for sensor calibration purposes [98–114].

Three other more sophisticated sensing schemes have been developed through the years, in addition to the aforementioned techniques, using an additional pH-independent, reference fluorescent dye: namely the Inner Filter Effect (IFE), Dual Lifetime Referencing (DLR), and Fluorescent Resonance Energy Transfer (FRET). Those techniques are presented in more detail in literature reviews or research articles focusing either on dye-based sensors in general [56,115] or on specific applications such as the IFE [116–123], DLR measurements [124–130] or FRET [131–134]. Surprisingly, none of these methods appears to be notably better than another, with some state-of-the-art works using either DLR [130], IFE [122] or simple referencing [113].

In contrast, a clear distinction exists between dry and wet sensors, with dry sensors largely outperforming wet ones, would it be in terms of response time, long-term stability, or ease of manufacturing [56,135]. Dry sensors are basically made out of a substrate layer, onto which a polymer is cast. The dye(s) of interest is prior dissolved into the polymer through the mean of a phase transfer agent before casting. A plasticiser is also often added to enhance the CO₂ diffusion inside the polymer layer. Optionally, the latter may be covered by an additional protective layer, so as to prevent ionic contamination, or destruction of the sensor by acidic vapors. Apart from the optical sensing scheme, the main differences between the many dry sensors mentioned in the literature lie in the choice of the substances used for the aforementioned layers. Although no exhaustive comparison can be found, several authors compared different combinations of chemicals:

1. **Substrate:** the substrate material does not seem to have any major influence on the sensing performance and is indifferently made of polyethylene terephthalate (PET) films, glass slides, or optical fibers. Nonetheless, polyethylene naphthalate (PEN) appears to be superior to PET, because its lower diffusivity towards CO₂ yields shorter response times [128]. In addition, the adhesion of the polymer film on the glass substrate can be difficult without a cumbersome surface preparation [112,127] while PEN foils may just be roughened to enhance the sensitive layer adhesion [128].
2. **Polymer:** hydroxy propyl methylcellulose (HPMC) may be a better choice than ethyl cellulose for being more hydrophilic than the latter, allowing water molecules to be entrapped with the dye and favoring the hydration of CO₂ into bicarbonate ions [121].
3. **Plasticiser:** several plasticizers were compared in the literature, tributyl phosphate (TPB) and Tween 20 appear to be the most efficient ones in terms of sensor response time [105,121].
4. **Phase transfer agent:** cetyltrimethyl ammonium hydroxide (CTAH) tends to lead to shorter response times [125] although tetramethyl ammonium hydroxide (TMAH) may be more stable since it is less susceptible to Hofmann elimination [121].
5. **Covering membrane:** Hyflon or even Cytop if a minimal response time is not mandatory may be used to limit the sensor poisoning and humidity loss [128].

Overall, dye-based sensors cover the full 0–100% CO₂ range with response times below 1 min—a few seconds have even been seldom reported [110,113,119]—accuracies below 1%, lifetimes approaching one year [122,123] and thicknesses as low as 1 μm [112]. Still, they may be destroyed quickly by acidic vapors, and often suffer from a high cross-sensitivity towards humidity, O₂—for it is a fluorescence quencher [136,137]—and temperature. While a protective membrane may mitigate the first two drawbacks, temperature influence may be compensated for, and O₂ cross-sensitivity can be reduced, either by using polymers with a low oxygen permeability [120,122] or by fixing the O₂-sensitive luminophore on

polystyrene micro- or nano-beads [125,127,138]. Using a dual-frequency DLR scheme may also be used to compensate for O₂ luminescence quenching [124].

2.3.5. Optical Fiber Sensors

Although optical fibers have been used in some of the afore-mentioned dye-based sensors to convey light back and forth between bulky bench-top equipment and compact sensing membranes or solutions [92,94,101], they did not consist in the CO₂-sensitive part itself. On the contrary, optical fibers-based CO₂ sensors put optical fibers at the very heart of their sensing principle, using one of the four different techniques presented in Figure 8. These four sensing schemes can be grouped in two categories: either (i) the CO₂ sensitive material changes the total light path length by shrinking or dilating in response to a change in CO₂ concentration and thus turns the optical fiber into a miniaturized Fabry-Perot interferometer (case (b)), or (ii) the CO₂ sensitive material exhibits a change in its refractive index or exert a mechanical constraint on the fiber core. In these last two cases, changes are made to the evanescent modes of the fiber, introducing a shift in the transmitted or reflected wavelengths (cases (a), (c), and (d)).

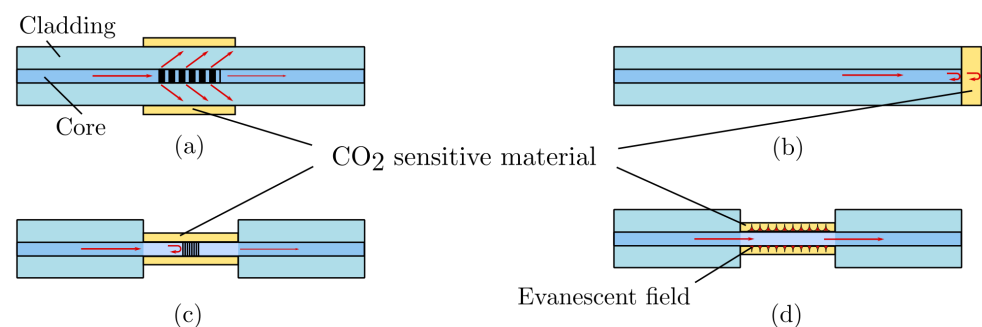


Figure 8. “Various techniques that have been employed in CO₂ sensors to cause light propagating in the core to interact with the surrounding environment: (a) [Long Period Grating]; (b) extrinsic Fabry-Perot cavity; (c) [Fiber Bragg Grating] and; (d) etched cladding. All the examples here use a material which demonstrates CO₂ sensitivity and the subsequent change in coating upon exposure to CO₂ is sensed by the interacting light”—Text and figure reproduced with permission from Barrington [20].

The principle behind end-of-fiber Fabry-Perot interferometer-based sensors is to measure the interferences between the light wave reflected by the fiber-film interface and that reflected by the film-analyte interface. Depending on the wavelength of the probing light and the thickness of the film, the interferences can be either constructive or destructive, causing notches and peaks in the observed reflected spectrum. The exact positions of those spectral features are directly linked to the thickness of the film, and the latter fluctuates with the surrounding pCO₂. Thus, accurate spectral measurements of the shift in wavelength of a given notch can yield reliable pCO₂ measurements [139,140].

As for evanescent modes-based fibers, several sensing modalities exist. Fiber Bragg gratings may be used as a strain gauge on a block of pH-sensitive hydrogel that swells or contract with pH changes, thus bending the fiber it is attached to [141]. Applying a mechanical strain on the optical fiber modifies its effective refractive index [142], inducing a wavelength shift in the evanescent modes of the grating. This technique does not require an optical fiber in itself, however, since a regular pressure sensor may be used instead, possibly much cheaper and more convenient to implement [143]. The pH-sensitive hydrogel can also directly coat the optical fiber optic, with similar consequences, as exerting strain on it [144]. Other materials, which exhibit a direct change in their refractive index upon CO₂ adsorption, have also been explored for optical fiber coatings—such as metal-organic frameworks or ionic liquids—with some success [20,145].

Alternatively, other optical fiber-based sensors have been developed relying on principles closer to NDIR absorption than CO₂ hydration. Those utilize the absorption of evanescent waves by CO₂ present in the air surrounding the fiber at $\sim 1.5 \mu\text{m}$, where CO₂

absorbs. An additional coating of the fiber was shown to greatly improve the sensitivity of such sensors towards CO₂ [146,147].

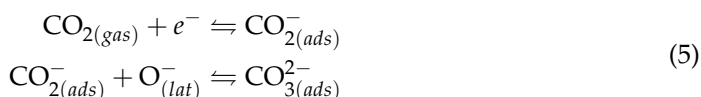
The main drawback of optical fiber-based sensors, apart from the price of the associated measurement apparatus, is their cross-sensitivity towards external strain, temperature, relative humidity, and possibly other chemicals which can be absorbed by the optical fiber coating. Those sensors exhibit response time in the order of 1 min on the full 0–100% range. To our knowledge, the accuracy of such CO₂ sensors was never characterized extensively, although Melo et al. [146] measured a 4.1% resolution on the full scale. Of note, if multiple sensors are used in the same facilities or geographical area, multiplexing can be used to share the light source and measurement apparatus between them, thus greatly reducing the cost per sensor [148]. Such multiplexing was demonstrated for probing up to 256 sensors on the same fiber, and distances as high as 150 km were reported [149].

2.4. Reduction of CO₂

Sensors based on the reduction of CO₂ into CO₂[−] and CO₃^{2−} radicals operate following several schemes. CO₂ may be reduced following its adsorption on a thin film of metal oxide, thus modifying the conductivity of the oxide layer—Section 2.4.1. A similar adsorption mechanism has also been reported between CO₂ molecules and graphene, leading to graphene-based sensors—Section 2.4.2. Alternatively, the reduction of CO₂ may be used in an electrochemical cell, whose electromotive force yields the surrounding CO₂ activity—Section 2.4.3. Lastly, ionic liquids have been used in CO₂ sensing, either binding to CO₂ to form carbamate species in conductometric sensor or acting as a substrate for CO₂ reduction into peroxydicarbonate ions in amperometric sensors—Section 2.4.4.

2.4.1. Adsorption by Metal Oxide Thin Film

Adsorption-based sensors use the change in conductivity of a thin layer of metal oxide caused by the adsorption of CO₂. Although the latter adsorption has been studied for a number of years [150–154], its mechanism is still not entirely understood and remains a discussed topic in the scientific community [155–158]. Indeed, both physical adsorption and chemisorption appear to take place at the metal-oxide interface, and the reduction of CO₂ into CO₂[−] may not be the only mechanism involved [157]. That being said, the following reaction is often considered in the absence of a more satisfactory alternative [159–161]:



wherein *ads* stands for *adsorbed*, *lat* for *lattice*, and the O[−] radicals and e[−] are supposed to come from the MO lattice—where M may be Zn or Cu, for instance. Overall, despite the use of metal oxide CO₂ sensors by an important number of authors, few of them propose an explicit sensing scheme, and even fewer mind using equilibrated or justified schemes, which may lead to incoherences. For instance, it has been proposed that since the above-mentioned scheme consumes free electrons from the MO lattice, fewer of them remain available for conductivity [162]. The resulting expected behavior would be an increase in the metal oxide resistance with an increase in pCO₂. While this assertion seems to hold in the simple ZnO case [160,162,163], opposite behaviors were observed when doping ZnO with lanthanum [164] or calcium/aluminium [165,166]. Consequently, we believe that further research is needed to gain a deeper insight into the working principle of thin-film metal oxide sensors. Concerning the present review, we are nevertheless able to mention some interesting works and put them into perspective.

The main drawbacks of most metal oxide sensors are their elevated operating temperature—in the 200–600 °C range—and cross-sensitivity towards carbon monoxide (CO), O₂, H₂, and humidity. Along the years, several metals were explored, the most ubiquitous being copper, zinc and—although to a lesser extent—cadmium and tin, but chromium (Cr₂O₃) [153], barium/tungsten (Ba_xWO_y) [167], barium titanate (BaTiO₃) [163] and lan-

thanum ($\text{La}_2\text{O}_2\text{CO}_3$) [168] compounds were also studied. While the performance of chromium-based sensors was not measured, $\text{La}_2\text{O}_2\text{CO}_3$ -based sensors exhibit a fairly good sensitivity but a long response time—over 1 h—and Ba_xWO_y -based sensors showed an important drift. BaTiO_3 -based sensors were loaded with different metal oxides, and promising results were obtained with zirconium and lanthanum oxides, with response times below 10 min, and almost no humidity influence near 600 °C.

Several elements were used as doping agents for CuO or ZnO thin film such as the above mentioned lanthanum and calcium/aluminium, but sodium [169], germanium/neodymium/tungsten [160], manganese [170], gold [161], silver [155,171], and indium [172] were also explored. While the manganese-, gold-, and indium-doped ZnO-based sensors reported in the literature performed worse than their pure ZnO counterpart, all the other above-mentioned doping elements greatly enhanced the sensitivity of the sensors—more than doubling it in certain cases [166].

Overall, metal oxide sensors can only work at an elevated temperature—above 100 °C at least, even if 200–600 °C are more usual. Rare attempts to operate at room temperature resulted in sensors that appeared to be rather unstable and highly sensitive to humidity [173,174], or were not thoroughly characterised [161,169]. Sensitivity to humidity may be mitigated by the addition of silver in the metal oxide [163,175], while some degree of CO and H_2 cross-sensitivity seems to be inevitable at first glance.

Yet, a temperature modulation approach—a.k.a. temperature cycling approach—may be used to isolate the sensor response due to CO_2 from that of other interfering gases. This approach has been first suggested in the early 1980s [176], and was quickly demonstrated in the following years as a proof-of-concept [177–181]. In brief, temperature modulation is performed by cycling the operating temperature of a metal oxide sensor, and recording its dynamic response. Since both (i) the peak sensitivity as a function of temperature and (ii) the kinetics of adsorption/desorption onto the metal oxide layer vary from one gas to another, it is possible to discriminate between different gases using the same sensor operated at different cycling temperatures [182]. This approach has been successfully used to discriminate between organic—e.g., benzene, methane, ethanol [180,181]—and inorganic—e.g., CO, H_2S [178]—gases, or mixture thereof. Both qualitative—i.e., classification of an unknown gas mixture in pre-determined categories [183,184]—and quantitative—i.e., accurately measuring the concentration of each gas in a given mixture [185,186]—have been performed successfully. Applications to CO_2 sensing can also be envisioned, in spite of more scarce literature on the topic [187,188].

Measurements in the physiological range have been reported [163] and response times below 30 s are reachable [160,171,189]. The influence of humidity has also been discussed in detail by Gankanda et al. [159] and the above-mentioned hydration of CO_2 is suspected to alter the sensing properties of metal oxide sensors. Interestingly, while most works focused on the change in conductivity of metal oxide upon CO_2 adsorption, other works were based on capacitive [171,175,190], work function [173,174] or optic properties [161] measurements. Thorough reviews on metal oxide-based sensors for gas sensing—although not focused on CO_2 detection alone—are also available [23,191].

2.4.2. Adsorption by Graphene

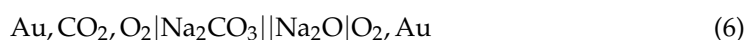
More recently, a similar approach has been used with graphene as the sensing material instead of a metal oxide film [192,193] and—as is the case for metal oxide-based sensor—the working principle of such sensors is also a debated topic. Overall, graphene acts as a room-temperature p-type semiconductor and can be used either in a purely conductometric setup—measuring the bulk resistance or impedance of the graphene layer [194–196]—or in a Field-Effect Transistor (FET) setup—of which graphene is the canal [197]. However, the interaction of the CO_2 molecule with the graphene layer is not exactly known, and different competing theories have been proposed. On the one hand, CO_2 has been presented as an oxidizing or reducing agent, which exchanges electrons with the graphene lattice, the direction of the charge transfer depending on the applied electric field [198]. On the

other hand, it has also been proposed that the change of conductivity of the graphene layer following CO₂ adsorption could be caused by adsorption-induced impurity scattering without formal charge exchange [199].

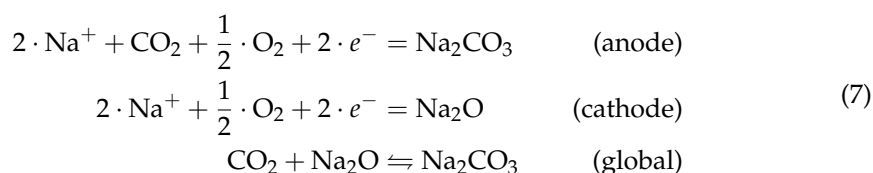
Graphene has been used both as a pristine material [194,200–202] and in its oxidised form [196,203] for CO₂ sensing. Additionally, other authors even considered the fabrication of composite sensors, combining graphene with polyethyleneimine [195] or metal oxides—such as Al₂O₃ [204], Sb₂O₃ [205], In₂O₃ and NiO [206] with mitigated results. Indeed, the performance of graphene-based devices for CO₂ sensing suffers from a high cross-sensitivity to a variety of other gases—e.g., N₂, O₂, NH₃, CO or H₂ [196,200,201]—and humidity [201,202,207]. Encouragingly, however, Akther et al. [196] recently reported temperature and humidity corrections for graphene oxide-based CO₂ sensor, with a mean error below 3% on the full 400–4000 ppm scale, and a response time of 3–5 s, despite showing some degree of cross-sensitivity towards other gases. So as to overcome the latter cross-sensitivity issue in graphene-based sensors, Rumyantsev et al. [208] developed a discrimination method based on the analysis of the low-frequency noise spectrum of a pristine graphene transistor. However—at least to the best of our knowledge—their method is yet to be applied to CO₂ sensing.

2.4.3. Electrochemical Cells

Potentiometric sensors based on electrochemical cells have been proposed for CO₂ sensing since the late seventies [209], and although several ameliorations have been developed in half a century of intense research, their basic working principle remains largely untouched. An extensive description of the sensing principle of such sensors for CO₂ can be found in the work of Maruyama et al. [210] and will be briefly summarised here. The sensor itself consists of the following electrochemical cell:



wherein the ion bridge is made of NASICON (Na₃Zr₂Si₂PO₁₂), which acts as a sodium-ion conductor. The anode, cathode, and global cell reactions are given by:



and the electromotive force of the cell appears to be proportional to $\log(p\text{CO}_2)$. The anode, covered in sodium carbonate (Na₂CO₃) is referred to as the *sensing electrode*, while the cathode is the *reference electrode*. The outline schematic of such a potentiometric sensor is presented in Figure 9.

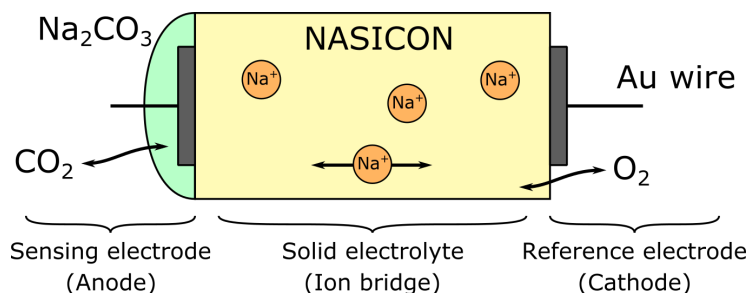


Figure 9. Outline schematic of a potentiometric CO₂ sensor as described by Maruyama et al. [210]. The NASICON sandwich with one end covered in sodium carbonate makes an electrochemical cell, the electromotive force of which yields pCO₂.

A major improvement to the stability of potentiometric sensors has been the addition of a third reference electrode [210–212], or the use of a solid reference electrode instead of the above-mentioned Na₂O/O₂ interface [213–215]. Still, even with this referencing, such sensors usually suffer from some degree of cross-sensitivity towards humidity. In addition, one of their major drawback for biomedical applications is their high operating temperature—in the 300–700 °C range.

The performance of a potentiometric sensor strongly depends on the thickness of its different constituents, but also on the choice of the materials used for the electrolyte and the sensing electrode coating. Concerning the electrodes themselves, their composition does not seem to have any significant influence on the sensing performance, since they are often made out of noble metals—such as gold [210,211,216] or platinum [209,212,217]. The electrode wires are bound to the solid electrolyte using pastes of the same metal—possibly deposited with a stencil—which are further sintered to make an electrical bond between the solid electrolyte and the wires. For a wider contact area, the use of a gold mesh has also been proposed [216]. The solid electrolyte consists more often than not in NASICON, but potassium carbonate (K₂CO₃) [209], Na-beta-alumina [218], lithium phosphate (Li₃PO₄) [213–215], and more recently Yttrium-doped LSBO (La_{9.66}Si_{5.3}B_{0.7}O_{26.14}) [219] and Li₇La₃Zr₂O₁₂ [220] have also been used with some success. As for the coating of the sensing electrode, various carbonates were explored such as Na₂CO₃, Li₂CO₃ or CaCO₃, with similar performance. Reference materials such as yttrium stabilised zirconia [210], BiCuVO_x-perovskite-oxide [211], Li₂TiO₃/TiO₂ [213–215] and Bi₈Nb₂O₁₇ [212] were used exhibiting good stability.

If the objective comparison of one of the combinations of the above-mentioned chemicals with another is made difficult by the change in form-factor and film thicknesses of the reported works, one can still notice some remarkable facts. At first, in an attempt to mitigate the humidity cross-sensitivity of potentiometric sensors, the addition of barium carbonate to a lithium carbonate sensing material (BaCO₃/Li₂CO₃) [211,213,215], or the addition of lithium carbonate to an indium tin oxide sensing material (Li₂CO₃/ITO) [216] have been successfully explored by several authors, yielding potentiometric sensors with no cross-sensitivity toward humidity. Then, room temperature operation of such sensors was also achieved with good sensitivity at 30 °C on the 300–3000 ppm CO₂ range [216]. Finally, thin-film designs were investigated yielding particularly fast—below 1 min—responding sensors [214,215,221]. The full range of potentiometric CO₂ sensors covers the 0–100% CO₂ concentration.

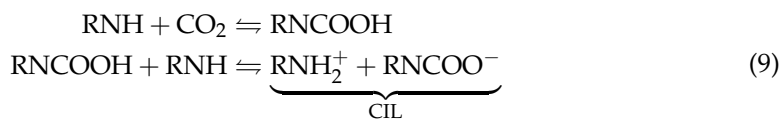
2.4.4. Ionic Liquids-Based Sensors

Room-temperature ionic liquids have been intensively studied since the early 2000s, with targeted applications for gas sensing and CO₂ sequestration in particular [222–225]. Ionic liquids, unlike ordinary liquids, are not made out of neutral molecules but consist exclusively of ion pairs. They also exhibit a negligible vapor pressure and their electrical conductivity makes them appropriate candidates to act as liquid electrolytes. As for metal oxide sensors, the exact mechanisms underlying CO₂ sensing with ionic liquids are still partially unknown, although three main pathways have been proposed. One is the reduction of CO₂ at the anode and its further oxidation at the cathode, possibly following [226]:



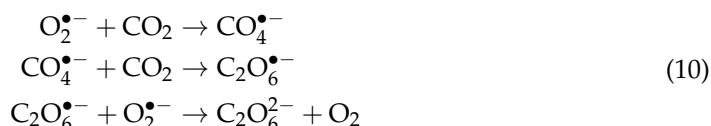
although—since there is a reasonable amount of doubt about the latter equation and the existence of CO_{2(ads)}[−]—most authors did not explicit it, or preferred the R-CO₂ notation—standing for *Reduced*-CO₂—instead of CO₂[−] [227]. CO₂ reduction can be measured either by a change in the impedance of the ionic liquid [228–232], or by amperometric or cyclic voltammetry techniques [226,227,233].

A second sensing scheme has been proposed, in which CO₂ binds with an amine to form a Carbamate Ionic Liquid (CIL) following [234]:



Since the CIL conducts electricity, it can serve as a CO₂ probe using different sensing schemes. Although a simple impedance measurement may be performed, Chen et al. [234] exploited the chemoluminescence of luminol in the presence of O₂ instead. In their sensor, the presence of CO₂ in solution generated a conducting CIL as described by Equation (9). Electric current is then passed through the CIL, reducing dissolved O₂ into O₂^{•-} ions which oxidizes luminol. Oxidized luminol in turn emits light by chemiluminescence, which can be quantified by optical measurements.

A third sensing scheme takes advantage of the irreversible reduction of CO₂ into peroxydicarbonate in the presence of oxygen following [235,236]:



Since it is not reversible, the latter scheme may not be used for a traditional CO₂ sensor, but rather for CO₂ detection, dosimetry, or sequestration. Interestingly, this reduction of CO₂ in the presence of oxygen has been treated as interference by several authors [226,233], who placed an oxygen trap before their CO₂-sensitive ionic liquid layer to prevent it from happening. This reduction may also be the cause of the slight drift observed in some of the afore-mentioned, non-oxygen-protected sensors [228,231,232].

In most cases, ionic liquids sensors are probed by amperometric or conductimetric methods, such as cyclic voltammetry, galvanostatic, or impedance measurements. However, Fabry-Perot interferometry—see Section 2.3.5—has also been reported [237] as well as acoustic resonant sensors using quartz micro-balances, for instance [236,238]. The idea of such sensors is to assess the shift in frequency of a resonant element coated with an ionic liquid. When the ionic liquid adsorbs CO₂, its mass increases, lowering the resonance frequency of the micro-balance. When CO₂ desorbs, the inverse phenomenon occurs. Of note, such acoustic resonant sensors based on CO₂ solubility were also explored with silicone or amine-based polymers instead of ionic liquids [239–243], although they often exhibit significant sensitivity to humidity.

Overall, ionic liquid sensors have been used on the physiological [226] or full 0–100% [227,238] CO₂ range. Response time in the 40–200 s seems reachable [226,234,238] although much longer response times have also been reported, especially for CO₂ desorption when returning to baseline [230–232]. The accuracy of such sensors was seldom characterized, with only Chen et al. [234] mentioning a 2.05% accuracy measured on 10 trials. The same remark holds for the sensor lifetime, reported in only one case to be over 4 months [226]. Ionic liquids sensors also exhibit a temperature-dependent response [226,233], and are often sensitive to CO, O₂, H₂, NO₂, N₂O, SO₂ and humidity [226,228,234].

2.5. Acoustic Properties of CO₂

2.5.1. Time of Flight Acoustic Sensors

Time of flight sensors are based on the difference in sound velocity between CO₂ and other gases—e.g., 349, 326 and 267 m·s⁻¹ for N₂, O₂ and CO₂ respectively [244]. Thus, a simple time of flight sensor can be constructed for CO₂ sensing, consisting of an ultrasound emitter and receiver pair, facing each other in the analyte gas mixture. Joos et al. [245] performed acoustic measurements using a 20 cm tube at the end of which

the ultrasound transducers were attached. The authors were able to measure the CO₂ content of a CO₂/N₂ gas mixture on the full 0–100% CO₂ range with an accuracy of 0.3%. An outline schematic representing the working principle of their experiment is depicted in Figure 10.

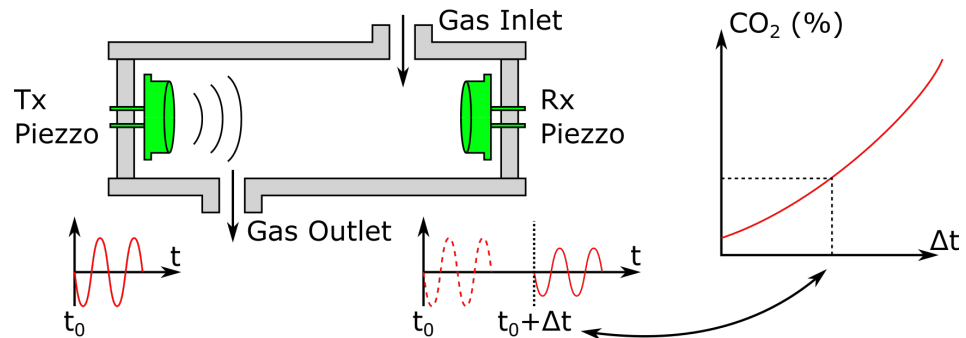


Figure 10. Outline schematic of a time of flight CO₂ sensor as described by Joos et al. [245]. Two ultrasound (40 kHz) transducers—emitter (Tx) and receiver (Rx)—are placed at both ends of an acoustic chamber which may consist in a simple tube. A burst of ultrasound is emitted at t_0 (on the left) and arrives at $t_0 + \Delta t$ at the receiver (on the right). The Δt value can then yield the percentage of CO₂ in the gas mixture using velocity-based calculations.

While this technique may seem interesting at first glance for its low cost and long-term stability, it is usually limited to a mixture of two gases [246]. Consequently, it might be unusable in the context of biomedical CO₂ monitoring. Indeed, most human tissues not only produce CO₂ and consume O₂ but also evaporate water. As such, a gaseous volume equilibrated with human tissues may contain as many as four different gases—CO₂, O₂, N₂ and H₂O—whose amounts cannot be found with a single pulse velocity measurement. These sensors usually have long path lengths—20 cm in the above-mentioned work [245]—which may be difficult to embed in a portable apparatus. Still, they can provide low latency measurements, since their response time is only limited by the time taken by the analyte gas mixture to fill the acoustic chamber. Interestingly, recent research by Cicek et al. [247] demonstrates another exploitation of the difference in sound velocity between N₂ and CO₂, using an array of miniature Helmholtz resonators, whose resonance frequency shifts depending on the CO₂ concentration to which they are exposed. They achieved CO₂ sensing in the 0–1% range with a 70 mm radius sensing array.

2.5.2. Acoustic Attenuation Sensors

The acoustic attenuation sensing scheme is based on the vibrational relaxation phenomenon. Vibrational relaxation consists of the attenuation in the intensity of a propagating acoustic wave in a gas. This attenuation depends on the sound frequency and also on the gas—or gas mixture—in which it takes place [248,249]. Acoustic attenuation measurements performed at different frequencies allow establishing the acoustical absorption spectrum—i.e., attenuation intensity as a function of the acoustic wave frequency—of a gas mixture. Several such spectra are presented in Figure 11 and can be used to identify the different gases that compose an analyte gas mixture as well as their proportion in the latter. To do so, an apparatus similar to that presented in Figure 10 may be used, but with multiple emitter/receiver pairs placed at different distances. Then, measurements of the sound attenuation and velocity can be performed, yielding an absorption value. The latter may in turn be compared with theoretical calculations—or experimental data—for a CO₂/N₂ gas mixture, leading to a pCO₂ value.

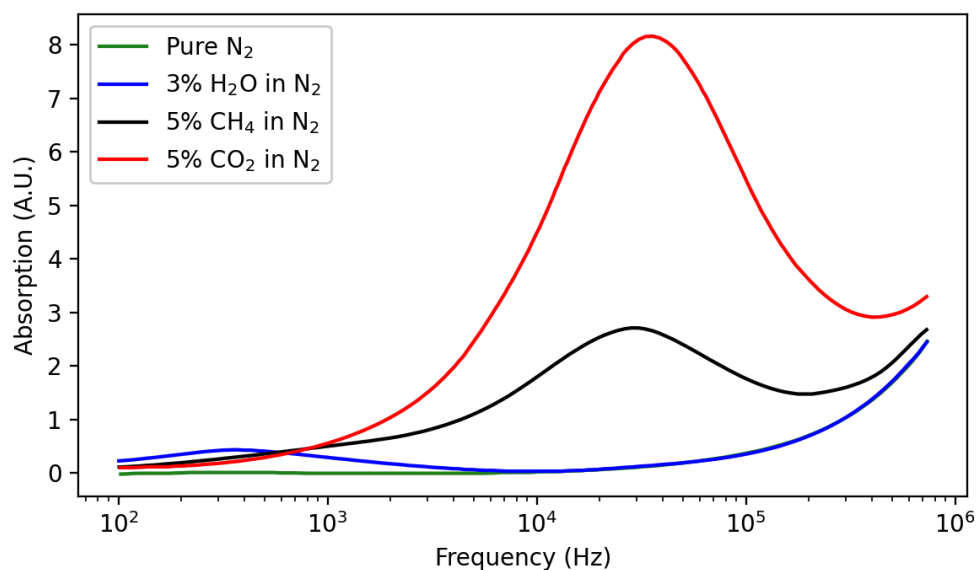


Figure 11. Acoustical absorption spectra of diverse nitrogen mixtures. Data source: Petculescu et al. [250].

Theoretical and practical applications of this phenomenon are available in the literature [250–255]. However, at least to the best of our knowledge, vibrational relaxation applied to CO₂ sensing never went further than the proof of concept presented by Petculescu et al. [254]. Contrary to other sensors presented in this review, cross-sensitivity towards O₂ should be negligible. Indeed, O₂ does not exhibit any vibrational relaxation phenomenon in the 10³–10⁷ Hz·atm^{−1} [253]. The influence of humidity may be another source of concern. If the lower mode of water vibrational relaxation occurs at much lower frequencies than that of CO₂ [256], higher frequencies components are also present at high humidity fraction which can interfere with CO₂ measurements [253]. In addition, the temperature should be measured and compensated for, as it influences sound propagation, and thus the position and amplitude of the acoustical absorption peaks [251].

2.6. Comparison Table

Although an objective comparison of the above-mentioned CO₂ measurement techniques is made exceedingly difficult due to the incompleteness of most of the referenced works, we tried to do our best to gather the state-of-the-art performance for the different sensing schemes presented. The pith and marrow of our literature review are thus summarised in Table 1.

We gently warn the reader that each column of the table contains the best performance reported in the literature for a given criterion and that no sensor may exist with all the characteristics presented in a given row. For instance, concerning ionic liquids-based sensors, Chen et al. [234] reported a 2.05% accuracy but with a 2 min response time, while Mineo et al. [238] reported a 40 s response time without reporting the accuracy of their sensor. Still the “ionic liquid” row of Table 1 contains both the 2.05% accuracy and 40 s response time, even if no sensor exists with such characteristics.

Table 1. An overview of the presented techniques. (∞): expected to be at least several years. ^(a): limited primarily by the diffusion of the analyte gas inside the enclosure of the sensor. Please refer to detailed explanations in Section 2.6.

Criterion → ↓ Technique	Lifetime	Calibration Need	Humidity Cross-Sensitivity	Accuracy	Response Time	Miniaturisation Potential	References
NDIR (Section 2.2.1)	≥15 years	No	No	0.03%	≤1 s ^(a)	Moderate (down to 10 × 10 × 0.5 mm ³)	[32–34,36]
Photoacous. (Section 2.2.2)	? (∞)	No	No	1%	≤1 s ^(a)	Low (~cm)	[51,257,258]
Wet Conduct. (Section 2.3.1)	?	Yes (0.4% drift/h)	Yes (dries out)	?	5 s	High (down to 100 μm thickness)	[60,62]
S-S elec. (Section 2.3.2)	80 days	Yes (0.03 mV/h)	Yes (dries out)	0.03% (0–100 mmHg)	30 s	High (down to 10 μm thickness)	[67,69,73,259]
ISFET (Section 2.3.3)	≥30 days	Yes (0.23 mV/h)	Yes	?	60 s	High (down to 100 μm thickness)	[79,88]
Dye-based (Section 2.3.4)	19 months	No	Yes	0.1%	≤1 s	Excellent (down to 1 μm thickness)	[56,103,112,122,123,260]
Optical fiber (Section 2.3.5)	?	?	Yes	4.1%	40–75 s	Excellent (down to 55 nm coating thickness)	[145–147]
Metal Oxide Ads. (Section 2.4.1)	≥5 months	No	Yes (low)	1.6%	30 s	Excellent (down to 125 nm thickness)	[155,163,164,171,175,189,261]
Graphene (Section 2.4.2)	≥90 days	No	Yes	0.8%	3 s	Excellent (down to 3 nm thickness)	[194,196,207]
Electro. Cells (Section 2.4.3)	≥2 years	No	No	4%	2–4 s	Excellent (down to 1 μm thickness)	[213,214,221,262]
Ionic liquids (Section 2.4.4)	≥4 months	No	No	2.05%	40 s	Excellent (down to 430 nm thickness)	[226,231,233,234,238]
Time of flight (Section 2.5.1)	? (∞)	No	Yes (low)	0.3% (0–10% range)	≤1 s ^(a)	Low (~cm)	[245]
Acous. Att. (Section 2.5.2)	? (∞)	No	?	?	≤1 s ^(a)	Low (~cm)	[250,254]

Finally, although most criteria are self-explanatory, a few additional comments may be necessary for a sound understanding and interpretation of this table. First, the lifetimes of several sensor families—and especially that of the (photo-)acoustical ones—are not explicitly reported in the literature. Yet, since NDIR sensors were reported to reach a lifetime of at least 15 years [36], and since acoustical building blocks—e.g., ultrasonic transducers—usually last for years, the infinity symbol (∞) was used, meaning that a lifetime of at least several years should be expected. Second, the calibration need refers to the need to re-calibrate a sensor frequently—i.e., every few hours or days—due to the presence of a significant drift in its response. This criterion does *not* refer to the initial sensor calibration that may be performed in the factory. Third, the response time of the evaluated sensors was often measured using test benches which flush the sensors with a continuous flow of a gas mixture containing a known CO₂ concentration. In such a configuration, the four sensors noted with an (*a*) are supposed to respond as soon as the latter gas mixture flows inside their embodiment, hence the ≤ 1 s indication. In practice, however, the response time strongly depends on the sensor housing dimensions, since CO₂ will have to diffuse from the analyte gas or medium inside the sensor embodiment.

3. Current Applications to Biomedical CO₂ Sensing

As a by-product of aerobic metabolism, CO₂ is ubiquitous in the human body and its influence on pH—see Section 2.3—makes its regulation in the organism a key parameter to maintain homeostasis [263]. In particular, CO₂ equilibrium is controlled by several mechanisms governing the efficiency of gas exchange [264,265] and by renal regulation of plasma bicarbonate ions [266]. Both the excess or deficiency of CO₂ in the organism—termed hyper- and hypocapnia, respectively—can have either beneficial or deleterious effects on a patient's outcome, depending on their condition [267]. As a consequence, CO₂ monitoring is of major importance in clinical care. Its measurement can be performed in three locations, presented in order of decreasing invasiveness:

1. inside the body with blood or tissues sampling—Section 3.1,
2. in the exhaled air with airway capnometry—Section 3.2,
3. on the skin with transcutaneous capnometry—Section 3.3.

An illustration of these locations is provided in Figure 12. For each one of them, the clinical significance of the corresponding pCO₂ measurement is first presented, and its probing modalities in practice are then described. One should bear in mind through the remainder of this section, that CO₂ transport in the human body takes three distinct forms—dissolved CO₂, bicarbonate ions, and carbamate compounds—which are in constant equilibrium for a given blood pH, and could give rise to as many measurements—blood pCO₂, [HCO₃[−]], Carbamino-Haemoglobin (CO₂ Hb) concentration and pH [268,269]. Yet, for both practical and clinical reasons, pCO₂ measurements have been predominantly adopted from a clinical perspective, as is disclosed below.

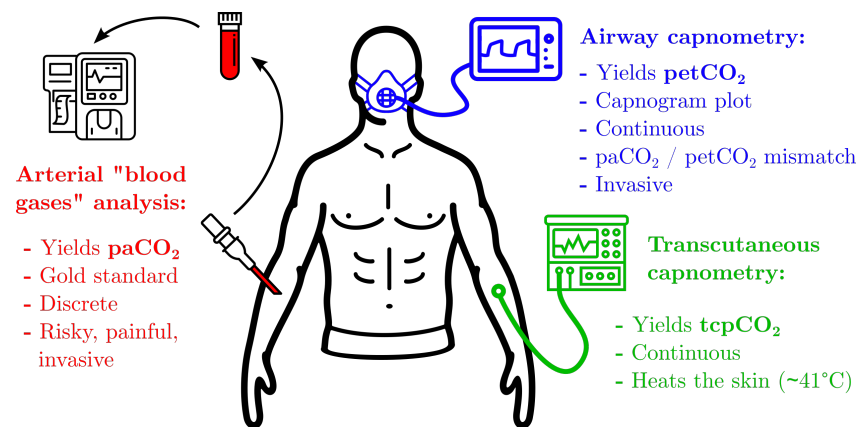


Figure 12. The three in vivo CO_2 probing modalities and their key features.

3.1. Blood Gas Analysis

3.1.1. Clinical Significance

Arterial blood sampling is considered to be the gold standard for the assessment of whole-body CO_2 content. Arterial blood is released from the lungs and is thus fully oxygenated, with a low CO_2 content, which is not the case of capillary or venous blood. Arterial blood pCO_2 — $paCO_2$ —thus best represents the global haemodynamic status of patients and gives important clues on their metabolism and homeostasis [1,270]. There is an extremely large panel of clinical applications of $paCO_2$ measurements including acute and chronic respiratory failures [271,272], mechanical ventilation assessment [273,274], general anaesthesia—but also sedation in patients at risk of hypoventilation—monitoring [275], or resuscitation procedures [276]. Due to the painful and potentially risky aspects of arterial blood puncture [2], other blood sampling techniques have been explored. In particular, arterialized capillary blood sampling was reported to be an acceptable surrogate for arterial blood sampling [277]. In contrast, peripheral venous blood can not be used to this end [278], nor can central venous blood [279–281], even if both may be used for trend analysis. Venous blood pCO_2 measurement is nevertheless interesting in critically ill patients for whom measuring the venous-to-arterial carbon dioxide partial pressure difference ($p_{v-a}CO_2$)—or calculating the venous-to-arterial carbon dioxide content difference—makes it possible to detect organ hypo-perfusion [282].

More localized pCO_2 measurements have also been performed with intra-tissue probing—in particular into the brain [283], liver [284] or skeletal muscles [285]—yielding crucial information about the perfusion of the organ under study. Gastric tonometry and sublingual capnometry have also been explored, but their clinical interest is yet to be fully demonstrated [286,287].

3.1.2. Probing Modalities

In vivo CO_2 probing can be achieved under two distinct modalities. Either pCO_2 is measured in situ or a biological sample is collected to be further analyzed.

In the first case, the sensor is brought to the analyte. This is notably what happens for intra-tissue pCO_2 monitoring. In such cases, the sensor is inserted directly into the organ or blood vessel that is to be probed by mean of a catheter, for instance. This setting allows for continuous monitoring with a low latency, which is only dictated by the response time of the chosen pCO_2 sensor [288].

In the second case, often used for blood pCO_2 measurements, the analyte is brought to an external analyzer and an arterial or venous line placement may be performed to facilitate repeated blood sampling. However, these settings allow only discrete monitoring since a blood sampling must be performed every single time a pCO_2 is desired. In addition, the blood samples must be analyzed quickly upon collection, which may lead to additional logistic difficulties compared to in situ sensing [3], even if recent hand-held blood gas analyzers tend to mitigate this issue [289].

In practice, two main technologies have been used to perform blood gas analysis: optodes using dye-based CO₂ sensing as described in Section 2.3.4 [288,290] and electrochemical sensors such as the Stow-Severinghaus electrode, described in Section 2.3.2 [291].

3.2. Airway Capnometry

3.2.1. Clinical Significance

Airway capnometry—from Greek *capnos* (καπνος), smoke, vapor—is the measurement of the amount of CO₂ in exhaled air, with a distinction between capnometry—which consists in the measurement of petCO₂, the end-tidal pCO₂—and capnography—which usually refers to the plot of a capnogram: pCO₂ in the exhaled air as a function of time, or volume. The distinction between capnometry and capnography is made clear in Figure 13.

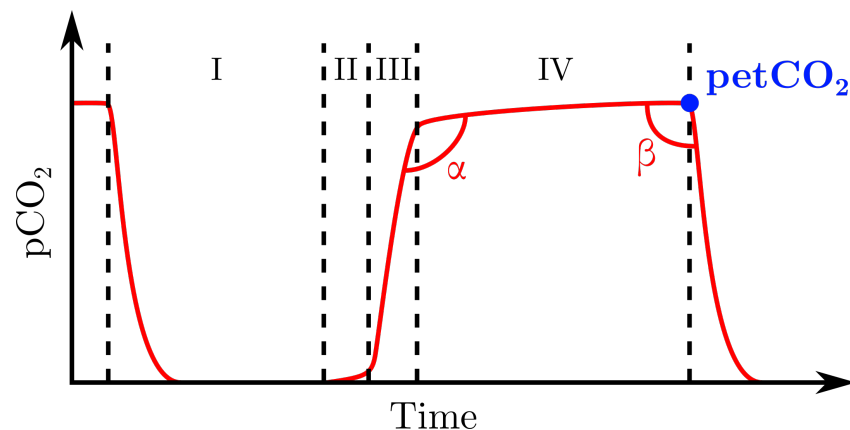


Figure 13. A capnogram yields important clinical clues on the state of the patient or quality of their intubation by analysing the different breathing phases—inspiration (I), and expiration: dead-space volume (II), mixed dead-space and alveolar air (III) and alveolar air (IV)—and the two α and β angles [292,293]. More narrowly, capnometry is only interested in knowing the more concise end-tidal pCO₂ value reached at the end of the plateau (IV): petCO₂.

Capnography is particularly useful in medical practice since it gives information about respiratory airflow, CO₂ production, and elimination, respiratory quotient, or the quality of endotracheal intubation. It can also be used to detect ventilation/perfusion inadequacy, apnea, Chronic Obstructive Pulmonary Disease (COPD), or heart failures [294,295]. For its part, petCO₂ has proven to be a reliable proxy for paCO₂ under stable haemodynamic conditions, with petCO₂ being usually 2–5 mmHg lower than paCO₂ [294]. However, the correlation between petCO₂ and paCO₂ vanishes in case of elevated physiological dead space or ventilation-perfusion mismatch [1,296]. It can also be difficult to use capnometry on neonates due to the small volume of exhaled air that they produce [297].

Interestingly, Siobal et al. [294] pointed out that while airway capnometry is often criticized for its inaccuracy as a paCO₂ proxy—e.g., in case of ventilation/perfusion mismatch, elevated dead space, or poor endotracheal placement—the same roots of this inaccuracy may be identified and quantified by a simultaneous paCO₂ measurement. In other words, if simultaneous paCO₂ and petCO₂ measurements are performed in the same patient, discrepancies between the two values may reveal one of the aforementioned issues.

3.2.2. Probing Modalities

Two distinct modalities exist for airway capnometry: mainstream or sidestream measurements. In mainstream capnometry, the CO₂ sensor is positioned on the main airway of the intubated patient so that the whole breathed air flow is forced through it. This technique yields instantaneous petCO₂ measurement and real-time capnogram plot. Historically, mainstream capnometry has long been criticized, for the additional sensor on the patient's airway was bulky, fragile, and led to an additional respiratory dead space. In particular, the bulkiness of mainstream sensors may dislodge the endotracheal tube

in young patients [294,297]. In response, recent designs have been improved to become more rugged, compact, and with minimal sampling volume, partially mitigating these drawbacks [298,299].

In contrast, sidestream capnometry consists of a small diameter sampling tube, which continuously aspirates a fraction of the patient's breathed air. The air is then conveyed to an external monitor wherein both the analysis and display functions are performed. Contrary to the mainstream technique, a delay is present between air sampling and the monitoring of its CO₂ content [292]. Additionally, distortions of the measured capnogram may occur, especially on its more rapidly changing portions, and sidestream-measured petCO₂ may be slightly underestimated compared to the mainstream-measured one [300].

In practice, airway capnometry is more often than not measured using the infrared absorption of CO₂, either using NDIR sensors—as presented in Section 2.2.1—or photoacoustic sensors—as presented in Section 2.2.2 [292,294]. Additionally, colorimetric dye-based sensors—as described in Section 2.3.4—are also routinely used to assess the correct positioning of endotracheal intubation, although they only provide qualitative information about the latter, and not a quantitative tcpCO₂ reading [301].

3.3. Transcutaneous CO₂ Sensing

3.3.1. Clinical Significance

Transcutaneous pCO₂–tcpCO₂—measurements are clinically relevant in two different situations: either as a surrogate for paCO₂ in patients with normal tissue perfusion or as an evaluation tool to measure the paCO₂–tcpCO₂ gap in patients with an abnormal perfusion [302].

In patients with normal circulation and peripheral perfusion, tcpCO₂ correlates well with paCO₂ and, as such, may be used in all situations where paCO₂ is required [11]. This correlation is particularly influenced by the choice of the measuring site, and by the probe temperature, as will be disclosed in the next section.

Alternatively, measurements of the paCO₂–tcpCO₂ gap proved to be a reliable predictor of mortality in case of shock [303]. In such a view, however, a simultaneous measurement of paCO₂ is required in addition to tcpCO₂ monitoring. One may notice the similarity between this technique, and the proposal of Siobal et al. for petCO₂ mentioned earlier—see Section 3.2.1.

3.3.2. Probing Modalities

tcpCO₂ measurements can be performed with the attachment of a transcutaneous probe on the skin by means of a disposable, adhesive mounting ring. The measuring site and sensor temperature depend on what is to be measured: for instance, when searching for a paCO₂ surrogate, it is recommended to place the tcpCO₂ probe at the earlobe with a setpoint temperature above 42 °C for the best results [11]. However, an elevated skin temperature can be a source of skin burn or thermal injury, especially in the neonates, requiring a frequent change of the probe site. A compromise may then be found between skin temperature—and thus site change frequency—and accuracy of the tcpCO₂ measurement [304]. When assessing local perfusion or shock condition—on the contrary—a temperature as low as 37 °C may be used at the site of interest [305]. Different temperatures can also be used to assess changes in perfusion as a function of temperature [303].

Technically speaking, the tcpCO₂ is measured by means of a miniaturized Stow-Severinghaus electrode similar to that described in Section 2.3.2 which can be heated anywhere in the 37–45 °C range [302].

4. Future Applications to Transcutaneous Monitoring

While the above-mentioned monitors are routinely used in clinical practice, they are not only expensive and invasive but also unpractical—for they require frequent external interventions for calibration or sampling purposes—and bulky, as mentioned in Sections 1 and 3. These drawbacks, in addition to turning pCO₂ monitors into a coveted

resource used sparingly in the hospital, make them unusable outside the hospital. Yet, bringing pCO₂ monitors in homes would allow for telemonitoring, which can reduce hospital admissions and the risk of contracting nosocomial infections. Although literature is inexistent regarding pCO₂ telemonitoring for the obvious reason that an adapted monitor does not exist yet, several clinical trials are encouraging regarding the advantages of telemedicine—a.k.a. telehealth—on patient's outcome and costs of admission in various pathologies [306–308]. Further still, both the emergence of new pandemics such as the COVID-19 outbreak [309] and the rapid growth of health wearables [310–313] may also push medical practice towards telemonitoring.

In this context, the development of a non-invasive, low-cost, and portable—if not wearable—biomedical pCO₂ monitor appears highly desirable. Among the three sensing modalities presented in Section 3, only transcutaneous pCO₂ monitoring meets the non-invasiveness target underlined above. In the following sections, the rare attempts found in the literature at finding an alternative to the drifting Stow-Severinghaus electrode conventionally used for tcpCO₂ monitoring are first given. Then, our recommendations regarding the development of a future sensor meeting the above-mentioned criteria follows, taking into account the technological review presented in Section 2.

4.1. Past Attempts

The Stow-Severinghaus electrode appeared in the late 1950s, underwent only minor improvements since then, and reigns supreme over the tcpCO₂ monitoring market [4,302]. Yet, several authors have been trying to push forward other means to measure tcpCO₂ mainly using NDIR sensing and mass spectroscopy, as disclosed in the following sections. It is also worth mentioning that we measured the absorption spectrum of CO₂Hb—i.e., haemoglobin bound to CO₂—while searching for a non-invasive alternative to tcpCO₂ monitoring. In a nutshell, we wondered whether the optical properties of CO₂Hb could pave the way for an *in vivo* pCO₂ measurement technique analogous to pulse oximetry but for CO₂. Alas, this track proved to be but a dead-end, as CO₂Hb, and Deoxy-Haemoglobin (HHb) have identical absorption spectra [314].

4.1.1. Non-Dispersive Infrared and Transcutaneous Sensing

Regarding NDIR, a couple of works by Eletr, Greenspan et al. surfaced in the early 1980s [315,316], describing a Hewlett-Packard capnometer which collects CO₂ exhaled by the skin in a small sampling chamber probed by infrared radiations. Despite the fair performances achieved—up to 48 h of continuous monitoring, a STD of 0.2 kPa (1.5 mmHg) between paCO₂ and tcpCO₂ on 3–6 h sessions and a response time about 90 s [315]—the main drawback of this sensor was the need to strip the stratum corneum with 20–50 successive applications of adhesive tape so as to reach a reasonable response time.

The NDIR track was then dropped until the mid-2010s and the advent of rate-based approaches by the team of Chatterjee, Ge, Iitani et al. [317–320] at first and by the team of Grangeat et al. [321,322] in a second move. If the latter work is insufficiently detailed—especially the explanations concerning the sensing part itself—the former allows for a sound understanding of the rate-based approach. This approach consists in placing a sampling cup against the skin to collect transcutaneously exhaled CO₂, but—contrary to what was done in the earlier work of Eletr, Greenspan, et al.—no time is left for the gas in the cup to reach an equilibrium with the skin CO₂ content. Rather, the gas in the cup are flushed with fresh air or pure N₂ and its CO₂ fraction measured by a conventional NDIR sensor. Theoretically, the so-obtained CO₂ diffusion rate is only function of (i) the patient's tcpCO₂ and (ii) their skin diffusivity towards CO₂ [318]. However, since the latter parameter is not known accurately and fluctuates a lot depending on the skin temperature [323,324], measurement site [325,326] and subject at hand [327], the rate-based approach is most likely limited to trend analysis at best.

In the afore-mentioned works, it should also be noted that contrary to the teams of Chatterjee, Ge, Iitani, et al., those of Grangeat, Eletr, Greenspan, et al. heated the skin in the 35–43 °C range.

4.1.2. Mass Spectroscopy and Transcutaneous Sensing

Overcoming the issue of the latter rate-based approach, a more sophisticated technique has been explored in parallel by Mc Ilroy et al. in the early 1980s [328–330] using mass spectrometry for CO₂ detection. The main idea behind their work is to perform a per-subject and per-site calibration to first determine the skin permeability towards CO₂ and only then access to the patient's tcpCO₂. While in its first version, their sensor required a change of membrane to perform this calibration [329], a second version with two sampling chambers and an additional valve solved this need for external intervention [330]. In their setup, the skin was also stripped with 5–10 applications of adhesive tape beforehand, and heated to 43–45 °C. They achieved a correlation factor of 0.81 between paCO₂ and tcpCO₂, and a response time below 5 min. The main drawback of their technique is of course the need for a mass spectrometer, which is bulky, requires maintenance, and costs tens if not hundreds of thousands of euros. Their dual-rate technique, however, might presumably be adapted to an NDIR sensing scheme, thus compensating for the fluctuations of skin diffusivity mentioned in the previous section.

4.2. Transcutaneous Sensing Constraints

An effective biomedical tcpCO₂ sensor should fulfill two main objectives: it must respond swiftly to a patient's haemodynamic changes, and it must measure a tcpCO₂ that reflects accurately their state. To do so, the sensor design must take into account the two main characteristics of CO₂ diffusion through the skin, which both are temperature-dependent:

1. The correlation between the pCO₂ measured at the skin surface—that is tcpCO₂—and that of arterial blood—that is paCO₂, which will determine the ability of the sensor to give clues about the patient's status through a tcpCO₂ reading.
2. The exhalation rate of CO₂ through the skin into the sensor, which will determine the response time of the sensor.

4.2.1. Correlation Between paCO₂ and tcpCO₂

The latter correlation has been demonstrated at 42 °C and above [11], but heating the skin is not only uncomfortable for the patient but also energy-consuming—which limits the ability of the sensor to be integrated into a wearable, battery-powered device—and potentially harmful due to risk of thermal injury.

Indeed, literature on the topic suggests a maximum long-term skin temperature of 42 °C, even if higher temperatures can be used for a limited amount of time—up to 45 °C for a few minutes for instance [331], or up to several hours depending on the study [332]. In the medical practice of tcpCO₂ monitoring, temperatures up to 45 °C were used for up to one hour [333] or 42 °C for eight hours [12]. Legally speaking, the Food and Drug Administration (FDA) guidance for tcpCO₂ monitors recommends not to exceed 44 °C for more than four hours [334].

For these reasons, working at low skin temperature seems highly desirable. To the best of our knowledge, only the work of Wimberley et al. [333] studied the influence of skin temperature on the correlation between paCO₂—through arterialized capillary blood, to be accurate—and tcpCO₂. Their study covers the full 37–45 °C range and they show a fair— $r = 0.93$ —correlation between capillary and transcutaneous pCO₂, even at a temperature as low as 37 °C. Yet, further research on the topic would be valuable since other sources argue that a higher probe temperature still yields narrower limits of agreement for tcpCO₂ [11].

4.2.2. Exhalation Rate

The *exhalation rate* of CO₂ through the skin refers here to the macroscopic observation of cutaneous respiration. It corresponds to a volumetric flow rate of gaseous CO₂ per unit area—dimension L¹·T⁻¹, unit cm³·m⁻²·h⁻¹—diffusing from the human skin to the outer air. The phenomenon of CO₂ exhalation—a.k.a. cutaneous respiration—through the skin was particularly studied in the early 20th century and Fitzgerald [335] wrote a complete and critical review on the topic in 1957. With the help of his work and others, the following information could be gathered:

- The exhalation rate of CO₂ through the skin increases with an increasing temperature.
- The CO₂ production rate of the tissues increases with temperature (due to an increase in tissues metabolism).
- Skin humidity, or the presence of various chemicals can change the CO₂ exhalation rate through the skin [336].

The increase in CO₂ exhalation rate through the skin with an increasing temperature is widely accepted by the community [324,335,337] and is often cited as a reason for heating the skin whilst measuring transcutaneous CO₂. Justifying this, the remarkable works of Shaw, Whitehouse et al. in the early 1930s [323,336,338] are of particular interest. Their main findings and that of others are presented in Table 2. Some values that can be found in Fitzgerald’s review [335] were omitted on purpose due to the non-availability of the publications from which they emanate, or because of unusable units.

Table 2. CO₂ exhalation rate through the skin in the literature.

Exhalation Rate [cm ³ ·m ⁻² ·h ⁻¹]	Temp. [°C]	Num. of Subjects	Ref.
25–120	22–36 (air)	2	Shaw (1929) [336]
10–160	25–37 (air)	1	Shaw (1930) [323]
40–125	25–30 (air)	2	Ernstene (1932) [327]
12–143	23–37 (air)	1	Whitehouse (1932) [338]
180–2500 †	-	1	Adamczyk (1966) [325]
25–87	-	5	Thiele (1972) [339]
11–28	25–35 (air)	3	Frame (1972) [340]
50	-	27	Levshankov (1983) [326]
131–206	36 (skin)	14	Eöry (1984) [341]

† Axilla measured value, possibly erroneous.

As pointed out by Fitzgerald, the main drawback of these studies is the fact that the measured temperature is that of the air surrounding the skin, and not that of the skin itself—although the two correlate to some extent [342]. Further research on the influence of skin temperature on its CO₂ exhalation rate would thus be welcome. A plausible explanation for this lack of knowledge is the clinical aspect of further studies led in the 1950s–1990s, aiming at developing a new sensorless intrusive than the more traditional blood gas analysis [4]. In this context, researchers focused less on the response time of the sensor and more on the clinical relevance of the measured tcpCO₂ value [333,343,344].

Nevertheless, the existence of the influence of skin temperature on CO₂ exhalation rate can reasonably be assumed to be true. It has been even further justified by the partially lipid structure of the skin, which strongly affects its permeability towards gases with changes in its temperature [324]. Further still, diminishing response times with an increase in skin temperature were also demonstrated for tcpCO₂ sensors in a clinical setting [345,346].

4.2.3. Impact on the Sensor Form Factor in a Closed-Chamber Design

Of the many constraints imposed by transcutaneous CO₂ sensing, the limited CO₂ exhalation rate by the skin is probably the most challenging one. Indeed, let us consider the simplified, generic, closed-chamber sensor model presented in Figure 14 (Left). In this crude model, the skin is considered as a membrane of thickness e and diffusivity D (m²·s⁻¹)

towards CO₂. The sub-cutaneous tissues are considered as a semi-infinite medium wherein the pCO₂ is constant and equal to tcpCO₂. Finally, the sensor of total volume V_{Se} (contact area with the skin S_{Se} and height h_{Se}) of internal pressure $p_{Se}CO_2$ is enclosed into a supposedly gas-tight body, with non-leaking contacts between the sensor body and the skin. Using Fick's first law of diffusion applied to CO₂ in the membrane with x the vertical axis leads to:

$$J_S = -D \cdot \frac{dC(x)}{dx} \quad (11)$$

wherein J_S is the CO₂ diffusion flux per unit area (mol·m⁻²·s⁻¹) and C the CO₂ concentration (mol·m⁻³). Supposing a constant total pressure and integrating over the membrane's thickness under the hypothesis that $p_{Se}CO_2$ is null at $t = 0$ yields—see Supplementary Material S1 for complete details and calculations:

$$p_{Se}CO_2(t) = tcpCO_2 \cdot \left(1 - \exp\left(-\frac{t}{\tau}\right)\right), \quad \text{with } \tau = h_{Se} \cdot \frac{e}{D} \quad (12)$$

Which is a classic first-order system response, as described in Figure 14 (Right). The response time of the sensor used in this crude model is thus the only function of two elements: the dimensions of the sensor itself, given by h_{Se} —that is the V_{Se}/S_{Se} ratio—on the one hand, and the properties of the skin membrane—the e/D ratio—on the other hand. Quite intuitively, a large surface to volume ratio of the sensor, a thin skin membrane, and an elevated diffusivity all lead to a faster sensor.

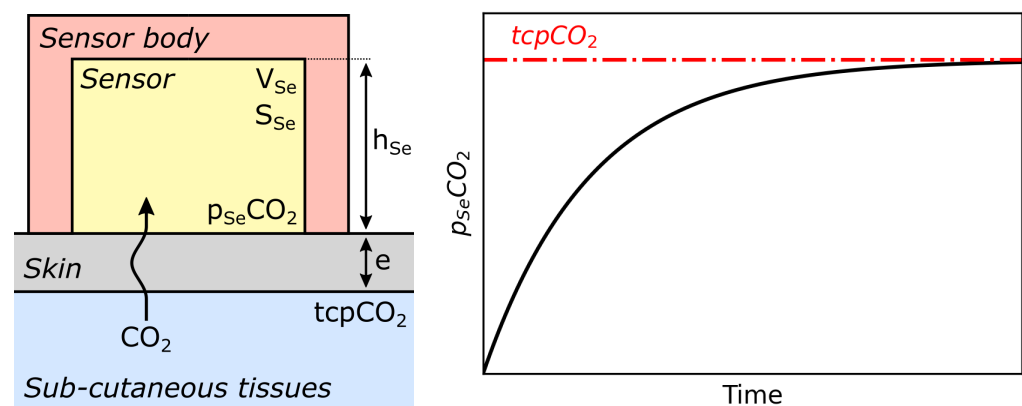


Figure 14. (Left) crude closed-chamber sensor model. Please note the colour matching between this schematic and previous Figures—e.g., Figures 4–7—blue for the analyte medium, yellow for the sensor itself. (Right) typical evolution of $p_{Se}CO_2$ against time when applying the sensor against the skin.

From this crude model, we can learn that in order to decrease the response time of a transcutaneous sensor one can either act on the sensor form factor, by designing a thinner sensor, or on the skin diffusivity and thickness. Indeed, increasing the skin diffusivity can be achieved by heating—hence the positive influence of skin temperature on CO₂ diffusion rate discussed in Section 4.2.2—while stripping the skin upper layers reduces e —mentioned in Section 4.1. However, the last two options can be uncomfortable for the patient.

Estimating the e/D ratio is thus necessary to get an idea of h_{Se} values compatible with a reasonable sensor response time τ . It can be demonstrated—see Supplementary Material S1—that:

$$\tau = h_{Se} \cdot \frac{tcpCO_2}{Q_S \cdot p_0} \Big|_{t=0} \quad (13)$$

with Q_S the CO₂ exhalation rate through the skin and p_0 the total ambient pressure. From Section 4.2.2, $Q_S \approx 100 \text{ cm}^3 \cdot \text{m}^{-2} \cdot \text{h}^{-1}$ for normocapnic—tcpCO₂ $\approx 5.3 \text{ kPa}$ (40 mmHg)—subjects is deemed plausible. These crude estimations lead to the response time presented in Figure 15.

As can be seen, for a sensor to have a reasonable response time—e.g., below 10 min—it must be relatively thin, in the range of 100 μm or below. Given the approximations made above, and the hypotheses presented in the Supplementary Material S1, the reader should bear in mind that this 100 μm threshold is given as an order of magnitude of targeted sensor height.

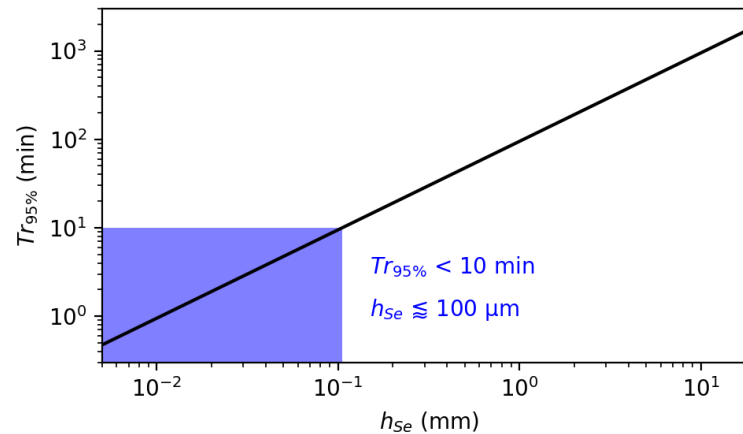


Figure 15. 95% response time ($Tr_{95\%} \approx 3 \cdot \tau$) of a closed-chamber sensor of height h_{Se} . The blue area underlines the portion of the line with a response time below 10 min, which corresponds to a sensor height below approximately 100 μm .

4.3. Recommendations for a Closed-Chamber Design

Summarising the above, when designing a tcpCO₂ sensor two main parameters should be carefully taken into account: (i) the skin temperature—as it influences both the sensor *response time* through the CO₂ rate of diffusion and its *accuracy* through the paCO₂/tcpCO₂ correlation—and (ii) the form factor of the sensor itself—as a crude analysis of a simplified sensor revealed that a volume to surface ratio of approximately 100 μm or below is required to yield reasonable response times. Considering a transcutaneous application, the CO₂ measuring techniques presented in Section 2 are reviewed below.

At first, only some of them can deal with a height limitation of only 100 μm . In that respect, NDIR, photoacoustic, time-of-flight, and acoustic attenuation sensors cannot be miniaturized to reach such a thickness. Second, the use of metal oxide thin films as well as electrochemical cells should be highly discouraged since both operate at several hundreds of degrees ($^{\circ}\text{C}$). As such, using them against the skin may entail a significant safety hazard. Then, conductometric and ISFET-based sensors as well as the Stow-Severinghaus electrode all suffer from important drift issues, making them unusable for more than a few hours, or days. Optical fiber-based sensors, for their part, require an expensive and bulky measurement apparatus that seems hardly embeddable into a wearable device.

Remain the ionic liquid, graphene, and dye-based sensors. While recent research on ionic liquid-based sensors showed definite progress, they are still extremely sensitive to O₂ and often exhibit particularly elevated recovery times [226,232]. Similarly, recent developments pave the way for graphene-based CO₂ sensors [196], but their important cross-sensitivity towards humidity precludes their use without an additional humidity sensor for referencing, due to the skin humidity. Thus, the option of choice appears to be the more mature dry dye-based sensors for they can yield thin enough, fast-responding, and long lasting pCO₂ sensors—see Section 2.3.4. In addition, dye-based sensors can be dissociated into a CO₂ sensing part, on the one hand, and an optical probing part on the other hand, as presented in Figure 16. This design is especially interesting since it makes it possible to use a disposable sensing patch that can be replaced every few days while the sensing head can be reused indefinitely. Finally, the multilayer structure of the patch seems well adapted to existing manufacturing processes—roll-to-roll in particular—for mass production [347,348].

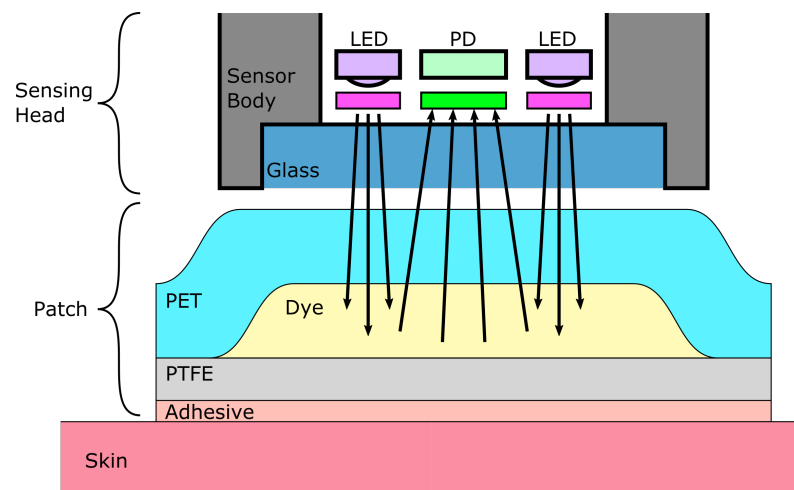


Figure 16. The dye-based fluorescent transcutaneous sensor consists of two parts. **(Top)** a sensing head with the LEDs and photodiode covered with their emission and reception filters (bright purple and green rectangles) and enclosed in a solid body, protected by a covering glass. **(Bottom)** a multilayer sensing patch stuck on the skin, consisting in—from top to bottom—a transparent layer, impermeable towards CO₂—e.g., PET—a layer of CO₂ sensitive dye in a polymer matrix, a layer of ion-impermeable, CO₂-permeable material such as PTFE for CO₂ diffusion from the skin into the dye, and a thin adhesive layer to maintain the patch onto the skin. See Section 2.3.4 for a detailed review of material choices as well as their advantages and drawback, when designing a dye-based CO₂ sensor.

4.4. Other Perspectives

Apart from a closed-chamber design—for which dye-based sensing seems to be the most appropriate sensing technique—transcutaneous CO₂ monitoring may also be envisioned using a rate-based approach, or Diffuse Reflectance Spectrometry (DRS).

4.4.1. Rate-Based Approach

The rate-based approach has already been presented in Section 4.1, and corresponding theoretical developments can be found in the work of Chatterjee et al. [318]. The main advantage of this approach is that it releases the form factor constraint highlighted above in the closed-chamber case. Thus, NDIR sensing can be used instead of a dye-based thin film, with better lifetime, accuracy, and selectivity over the latter. These advantages made NDIR sensing the foremost choice of the authors who considered using a rate-based approach for transcutaneous CO₂ sensing [317–319,321,322].

The biggest issue with this approach is the inter-subject variability in skin diffusivity towards CO₂. Indeed, all studies reporting measurements of the skin CO₂ exhalation rate mention this variability, with a factor 1.5–2 being not unheard of between the exhalation rates of two individuals, even at the same skin site and in the same temperature conditions (see references in Table 2). This variation among individuals precludes the measurement of *absolute* tcpCO₂ by mean of a rate-based approach without further improvements of the technique, as demonstrated by several authors who could only report trend analyses of skin CO₂ exhalation rate, and no rate-based absolute tcpCO₂ readings [319,321,322]. Further still, the recent work of Iitani et al. [320] clearly illustrates the afore-mentioned inter-subject variability with a factor of more than ten between the exhalation rates of two subjects (S2 and S6 on their Figure 4-H). There may be an exception concerning neonates, however, whose exceedingly thin skin may be more homogeneous than that of adults, leading to less variability in their skin CO₂ exhalation rate, and allowing Chatterjee et al. [317] to demonstrate a significant correlation between skin CO₂ exhalation rate and tcpCO₂.

To overcome this challenge, several tracks can be followed. At first, further studies on the CO₂ exhalation rate through human skin would be welcome, since the currently

available literature is aging, and rarely include more than a handful of subjects. In addition, the temperature dependence of the exhalation rate also needs to be carefully studied, by regulating the skin temperature, and not that of the ambient air surrounding it. This would greatly help to better characterize the intra- and inter-subject variations in CO₂ exhalation rate with skin site, skin temperature, or time of the day.

Second, dual membrane techniques—as that presented by Targett et al. [330]—may be adapted to modern sensing techniques in a setup and compactness close to that of Grangeat et al. [321] prototype, using two different sensing channels, for instance.

Third, the need for an absolute tcpCO₂ reading could also be mitigated in two ways. First off, by mean of a punctual per-subject calibration, following the example of non-invasive, cuffless, photoplethysmography (PPG)-based blood pressure measurements [349,350]. In this sensing scheme, the actual tcpCO₂ could be measured from time to time using a reference tcpCO₂ monitor, whose measurements would serve to calibrate a lighter, wearable, rate-based device. This would allow sharing the main tcpCO₂ monitor among multiple patients, in a clinical setting. Alternatively, it could also be envisioned that rate-based devices do not provide any absolute tcpCO₂ reading. Rather, they may provide the user with trend analysis only, raising alarms following the crossing of certain thresholds or abrupt variations. This last approach, however, may be difficult to introduce into medical practice without further clinical studies, even though the clinical interest of similar variability metrics for other physiological variables—such as heart rate [351] or oxygen saturation [352,353]—is encouraging in this perspective.

4.4.2. Diffuse Reflectance Spectrometry (DRS)

As stated in Section 2.2.1, dissolved CO₂ measurements can be performed not only in the gaseous phase, but also in aqueous solution [47]. This result was also demonstrated for whole blood samples, the pCO₂ of which could be retrieved with a standard error of about 5 mmHg, using infrared spectroscopy in the 1024–2290 nm range [354]. Further still, it has been recently suggested in a patent that transcutaneous CO₂ measurements could be performed using mid-infrared LEDs of wavelength “between about 2 μm and about 18 μm” [355].

Although patents do not constitute scientific evidence [356], the idea has been put forth, and further research would be interesting on the topic, in order to assess the feasibility of such transcutaneous CO₂ measurements. *Prima facie*, two major challenges conceivably need to be solved for DRS-based transcutaneous measurements.

First, contrary to pulse oximetry, the possibility to measure a pulsatile absorbance component due to CO₂ dissolved in the arterial blood by transcutaneous DRS probing in the mid-infrared is vastly unknown. If possible though, the whole theoretical background developed over the years for pulse oximetry and PPG signal processing [357] could be translated to CO₂ measurements.

Second, the penetration depth of mid-infrared light in the human tissues may also be a source of concern, especially because of the elevated infrared absorbance of water. Indeed, water absorbance becomes predominant in the tissues in the near and mid infrared [358], with values over 1 cm⁻¹ above 1150 nm, and over 5 cm⁻¹ above 1380 nm [359]. This may cause serious difficulties for mid-infrared tissue probing and lead to a very low signal-to-noise ratio, which may be the reason why Marasco et al. suggest the use of a lock-in amplifier for transcutaneous CO₂ measurement in their patent [355].

In both cases, heating the skin to provoke local hyperaemia—as mentioned in Section 4.2.1—may tackle the above-mentioned probing depth issue, by bringing the CO₂ content of subcutaneous tissues close to that of arterial blood.

4.5. Synthesis

tcpCO₂ is the least invasive and the most accessible proxy for paCO₂—which is of major clinical significance—given that the skin temperature is at least above 37 °C

(Section 4.2.1). tcpCO_2 may be measured by two means: either exploiting the cutaneous respiration phenomenon, or by direct infrared tissue probing, using DRS.

While the feasibility of the latter technique has yet to be demonstrated for in vivo transcutaneous CO_2 monitoring, it seems like an appetizing proposal (Section 4.4.2). Indeed, it would require merely a mid-infrared source and detector—which are readily available components, see Section 2.2.1—and conceivably the same kind of electronic as that already embedded in commercially available pulse oximeters. Yet, such an application of DRS remains vastly hypothetical at the time of writing this review, and further research would be needed on the topic, so as to consolidate the above-mentioned research works.

Cutaneous respiration, on its part, has long proven to be a reliable access route to tcpCO_2 , by capturing the CO_2 exhaled by the skin inside the embodiment of a CO_2 sensor (Section 2.3.2). A simple model for such a closed-chamber sensor design has been extensively described, as well as its expected response time as a function of its form factor (Section 4.2.3). We conclude that in such a closed-chamber design, the compactness of the CO_2 sensor is crucial in order to reach reasonable response times. Taking into account other merit criteria such as response time, long-term stability, and accuracy, we put forth the application of dye-based CO_2 sensing to serve such a purpose.

Alternatively, a rate-based approach may be envisioned using a constant flow of air or N_2 passing over the skin, and being analyzed thereafter (Section 4.4.1). The main advantage of this technique is that the form factor of the sensor itself is not as much a source of concern as in the closed-chamber setup. Thus, other sensing techniques can be envisioned such as NDIR CO_2 sensing. However, several challenges remain, precluding rate-based approaches to yield an absolute tcpCO_2 measurement. In particular, a better characterization of human skin CO_2 exhalation rate, dual membrane approaches, or self-calibration from time to time are all interesting leads that need further exploration.

5. Conclusions

Building on previous knowledge, we present in Section 2 an extensive review of CO_2 sensing techniques, the main characteristics of which are summed up in Table 1. Then, we emphasize the clinical importance of CO_2 monitoring in humans in Section 3. The latter monitoring can be performed through three distinct modalities: (arterial) blood puncture, airway capnometry, or transcutaneous capnography. In the first and last cases, miniature Stow-Severinghaus electrode or ISFET are used for pCO_2 sensing, while NDIR sensors are used for airway capnometry.

Among these three modalities, transcutaneous monitoring is the least invasive one, while still providing a clear picture of a patient's haemodynamic status. However, current commercially available sensors based on the Stow-Severinghaus electrode suffer from several drawbacks—mainly an important drift and an elevated cost—and an alternative would be highly desirable.

In this view, we first present several works aiming at the same target and discuss their advantages and drawbacks. We then propose a simple model of transcutaneous sensor, taking into account early studies on human cutaneous respiration in order to emphasize the importance of the sensor form factor in transcutaneous sensing. More specifically, we conclude that a volume to surface ratio—or equivalent height—as low as possible—ideally below approximately $100\ \mu\text{m}$ —must be achieved in order to obtain reasonable, clinically exploitable response times using a closed-chamber sensor design. The CO_2 sensing techniques presented in Section 2 are then reviewed against these requirements in terms of form factor, cost, and performance. Under the current state of the art, we conclude that a dry dye-based sensor in the form of a thin-film patch seems the most promising approach to develop a new kind of closed-chamber tcpCO_2 sensor.

Finally, perspectives for alternative transcutaneous probing modalities are also discussed, with an emphasis on two exploratory paths that may be pursued in the near future: DRS, and the rate-based approach. At the time of writing this review, these two alternatives

seem both challenging, bringing their share of exciting research questions that have yet to be answered.

Supplementary Materials: The following are available at <https://www.mdpi.com/article/10.3390/s22010188/s1>, Supplementary Material S1: The Dynamic of Transcutaneous Sensing: A Closed Chamber Model.

Author Contributions: Investigation, visualisation and writing—original draft preparation, E.D.; project administration and supervision, M.T. and W.U.; validation, M.T. and W.U.; writing—review and editing; E.D., M.T. and W.U. All authors have read and agreed to the published version of the manuscript.

Funding: This research was funded by BiOSENCEY.

Acknowledgments: We would like to thank James Barrington for his early review of Section 2.3.5, and for his useful advices and suggestions. We also wish to thank Quentin Bodinier, Jean and Isabelle Dervieux, and Alexis Bisiaux for their reviews, corrections and suggestions during the writing of the whole article. In Figure 2, the original cloud picture was drawn by Ecem Afacan, while the light bulb was drawn by Jeremie Sommet. In Figure 12 the human body was drawn by Oleksandr Panasovskyi, the face mask by Darayani, the catheter by AomAm, the blood vial and tcpCO₂ monitor by Eucalyp, the blood analyzer by Muhamad Fuad Afandi, and the airway capnometer by IconMark. In the graphical abstract, the meter gauge was drawn by Adrien Coquet, the nurse by LAFS, and the other already-mentioned elements by the same artists as stated in Figure 12 credits. All the above-mentioned artists are members of the [Noun Project](#). All these resources are distributed under Creative Commons license CCBY and were freely modified and combined to better illustrate the given explanations.

Conflicts of Interest: The authors declare no conflict of interest.

Abbreviations

The following abbreviations are used in this manuscript:

CIL	Carbamate Ionic Liquid
CO	Carbon monoxide
CO ₂	Carbon dioxide
CO ₂ Hb	Carbamino-Haemoglobin
COPD	Chronic Obstructive Pulmonary Disease
CTAH	Cetyltrimethyl ammonium hydroxide
DLR	Dual Lifetime Referencing
DRS	Diffuse Reflectance Spectrometry
FDA	Food and Drug Administration
FET	Field-Effect Transistor
FRET	Fluorescent Resonance Energy Transfer
H ₂ O	Water
HHb	Deoxy-Haemoglobin
HPMC	Hydroxy propyl methylcellulose
HPTS	1-hydroxy-pyrene-3,6,8-trisulfonate
IFE	Inner Filter Effect
ISFET	Ion-Selective Field-Effect Transistor
LED	Light Emitting Diode
MEMS	Micro Electro-Mechanical Systems
MOSFET	Metal Oxyde Semiconductor Field-Effect Transistor
N ₂	Di-nitrogen
NDIR	Non Dispersive Infra-Red
O ₂	Di-oxygen
p _{v-a} CO ₂	Carbon dioxide venous-to-arterial pressure difference

paCO ₂	Arterial carbon dioxide partial pressure
paO ₂	Arterial dioxygen partial pressure
pCO ₂	Carbon dioxide partial pressure
PEN	Polyethylene naphthalate
PET	Polyethylene terephthalate
petCO ₂	End-tidal carbon dioxide partial pressure
PPG	Photoplethysmography
PTFE	Polytetrafluoroethylene
tcpCO ₂	Transcutaneous carbon dioxide partial pressure
TMAH	Tetramethyl ammonium hydroxide
TPB	Tributyl phosphate

References

- Wagner, P.D. The Physiological Basis of Pulmonary Gas Exchange: Implications for Clinical Interpretation of Arterial Blood Gases. *Eur. Respir. J.* **2015**, *45*, 227–243. [\[CrossRef\]](#)
- Scheer, B.V.; Perel, A.; Pfeiffer, U.J. Clinical Review: Complications and Risk Factors of Peripheral Arterial Catheters Used for Haemodynamic Monitoring in Anaesthesia and Intensive Care Medicine. *Crit. Care* **2002**, *6*, 199. [\[CrossRef\]](#)
- Nanji, A.A.; Whitlow, K.J. Is it Necessary to Transport Arterial Blood Samples on Ice for pH and Gas Analysis? *Can. Anaesth. Soc. J.* **1984**, *31*, 568–571. [\[CrossRef\]](#)
- Severinghaus, J.W.; Astrup, P.B. History of Blood Gas Analysis. III. Carbon Dioxide Tension. *J. Clin. Monit.* **1986**, *2*, 60–73. [\[CrossRef\]](#)
- Severinghaus, J.; Astrup, P. History of Blood Gas Analysis. VI. Oximetry. *J. Clin. Monit.* **1986**, *2*, 270–288. [10.1007/BF02851177](#). [\[CrossRef\]](#)
- Huttmann, S.E.; Windisch, W.; Storre, J.H. Techniques for the Measurement and Monitoring of Carbon Dioxide in the Blood. *Ann. Am. Thorac. Soc.* **2014**, *11*, 645–652. [\[CrossRef\]](#)
- Nitzan, M.; Romem, A.; Koppel, R. Pulse Oximetry: Fundamentals and Technology Update. *Med. Devices Evid. Res.* **2014**, *7*, 231–239. [\[CrossRef\]](#)
- Jubran, A. Pulse Oximetry. *Crit. Care* **2015**, *19*, 272. [\[CrossRef\]](#)
- McSwain, S.D.; Hamel, D.S.; Smith, P.B.; Gentile, M.A.; Srinivasan, S.; Meliones, J.N.; Cheifetz, I.M. End-Tidal and Arterial Carbon Dioxide Measurements Correlate Across All Levels of Physiologic Dead Space. *Respir. Care* **2010**, *55*, 288–293.
- Donnellan, M.E. Capnography: Gradient PaCO₂ and PetCO₂. In *Applied Technologies in Pulmonary Medicine*; Karger Publishers: Basel, Switzerland, 2011; pp. 126–131.
- Conway, A.; Tipton, E.; Liu, W.H.; Conway, Z.; Soalheira, K.; Sutherland, J.; Fingleton, J. Accuracy and Precision of Transcutaneous Carbon Dioxide Monitoring: A Systematic Review and Meta-Analysis. *Thorax* **2018**, *74*, 157–163. [\[CrossRef\]](#)
- Bendjelid, K.; Schütz, N.; Stotz, M.; Gerard, I.; Suter, P.; Romand, J.A. Transcutaneous pCO₂ Monitoring in Critically Ill Adults: Clinical Evaluation of a New Sensor. *Crit. Care Med.* **2005**, *33*, 2203–2206. [\[CrossRef\]](#)
- Acock, B.; Wall, G.W. A Simple Conductimetric CO₂ Analyzer With Automatic Recalibration: I. Design, Implementation, and Functionality. *Agron. J.* **1995**, *87*, 70–75. [\[CrossRef\]](#)
- Shitashima, K. Evolution of Compact Electrochemical In-Situ pH-pCO₂ Sensor Using ISFET-pH Electrode. In Proceedings of the Oceans 2010 MTS/IEEE Seattle, Seattle, WA, USA, 20–23 September 2010; doi: 10.1109/OCEANS.2010.5663782. [\[CrossRef\]](#)
- Fanget, S.; Hentz, S.; Puget, P.; Arcamone, J.; Matheron, M.; Colinet, E.; Andreucci, P.; Duraffourg, L.; Myers, E.; Roukes, M. Gas Sensors Based on Gravimetric Detection—A Review. *Sens. Actuators B Chem.* **2011**, *160*, 804–821. [\[CrossRef\]](#)
- Zosel, J.; Oelßner, W.; Decker, M.; Gerlach, G.; Guth, U. The Measurement of Dissolved and Gaseous Carbon Dioxide Concentration. *Meas. Sci. Technol.* **2011**, *22*, 072001. [\[CrossRef\]](#)
- Puligundla, P.; Jung, J.; Ko, S. Carbon Dioxide Sensors for Intelligent Food Packaging Applications. *Food Control* **2012**, *25*, 328–333. [\[CrossRef\]](#)
- Llobet, E. Gas Sensors Using Carbon Nanomaterials: A Review. *Sens. Actuators B Chem.* **2013**, *179*, 32–45. [\[CrossRef\]](#)
- Neethirajan, S.; Jayas, D.; Sadistap, S. Carbon Dioxide (CO₂) Sensors for the Agri-food Industry—A Review. *Food Bioprocess Technol.* **2009**, *2*, 115–121. [\[CrossRef\]](#)
- Barrington, J. Design and Fabrication of Optical Fibre Long Period Gratings for CO₂ Sensing. Ph.D. Thesis, Cranfield University, Cranfield, UK, 2018.
- Rebber, M.; Willa, C.; Koziej, D. Organic-Inorganic Hybrids for CO₂ Sensing, Separation and Conversion. *Nanoscale Horiz.* **2020**, *5*, 431–453. [\[CrossRef\]](#)
- Rezk, M.Y.; Sharma, J.; Gartia, M.R. Nanomaterial-Based CO₂ Sensors. *Nanomaterials* **2020**, *10*, 2251. [nano10112251](#). [\[CrossRef\]](#)
- Bhowmick, T.; Ambardekar, V.; Ghosh, A.; Dewan, M.; Bandyopadhyay, P.P.; Nag, S.; Majumder, S.B. Multilayered and Chemiresistive Thin and Thick Film Gas Sensors for Air Quality Monitoring. In *Multilayer Thin Films*; Basu, S., Ed.; IntechOpen: Rijeka, Croatia, 2020; Chapter 8. [\[CrossRef\]](#)

24. Decker, M.; Oelßner, W.; Zosel, J., Electrochemical CO₂ Sensors with Liquid or Pasty Electrolyte. In *Carbon Dioxide Sensing: Fundamentals, Principles, and Applications*; Wiley: Hoboken, NJ, USA, 2019; pp. 87–116. [CrossRef]
25. Skoog, D.; West, D.; Holler, F.; Crouch, S. *Fundamentals of Analytical Chemistry*; Cengage Learning: Boston, MA, USA, 2013.
26. Harvey, D.T. *Analytical Chemistry 2.1*; 2016. Available online: <https://open.umn.edu/opentextbooks/textbooks/486> (accessed on 7 November 2021).
27. Bernath, P.F. *Spectra of Atoms and Molecules (Topics in Physical Chemistry)*; Oxford University Press: Oxford, UK, 1995.
28. Gordon, I.; Rothman, L.; Hill, C.; Kochanov, R.; Tan, P.B.; Birk, M.; Boudon, V.; Campargue, K.C.; Drouin, B.; Flaud, J.M.; et al. The HITRAN2016 Molecular Spectroscopic Database. *J. Quant. Spectrosc. Radiat. Transf.* **2017**, *203*, 3–69. [CrossRef]
29. Hodgkinson, J.; Smith, R.; Ho, W.; Saffell, J.R.; Tatam, R.P. A Low Cost, Optically Efficient Carbon Dioxide Sensor Based on Nondispersive Infra-Red (NDIR) Measurement at 4.2 μm . In *Optical Sensing and Detection II*; Berghmans, F., Mignani, A.G., Moor, P.D., Eds.; International Society for Optics and Photonics: Bellingham, WA, USA, 2012; Volume 8439, pp. 352–361. [CrossRef]
30. Hodgkinson, J.; Smith, R.; Ho, W.O.; Saffell, J.R.; Tatam, R.P. Non-Dispersive Infra-Red (NDIR) Measurement of Carbon Dioxide at 4.2 μm in a Compact and Optically Efficient Sensor. *Sens. Actuators B Chem.* **2013**, *186*, 580–588. [CrossRef]
31. Liu, W.; Ming, A.; Ren, Y.; Tan, Q.; Ou, W.; Sun, X.; Wang, W.; Chen, D.; Xiong, J. CMOS MEMS Infrared Source Based on Black Silicon. In Proceedings of the 2016 IEEE 11th Annual International Conference on Nano/Micro Engineered and Molecular Systems (NEMS), Sendai, Japan, 17–20 April 2016; pp. 200–204. [CrossRef]
32. Popa, D.; Udrea, F. Towards Integrated Mid-Infrared Gas Sensors. *Sensors* **2019**, *19*, 2076. [CrossRef]
33. Zhang, G.; Li, Y.; Li, Q. A Miniaturized Carbon Dioxide Gas Sensor Based on Infrared Absorption. *Opt. Lasers Eng.* **2010**, *48*, 1206–1212. [CrossRef]
34. Jing, Y.; Cheng, Y.; Yuan, Y.; Li, X.; Zhang, Z.; Xu, M.; Wang, D.; Mu, J.; Mei, Y.; Zhang, Y.; Design and Optimization of an Integrated MEMS Gas Chamber with High Transmissivity. *Digit. Commun. Netw.* **2020**, *7*, 82–91. [CrossRef]
35. Kohsiek, W. Fast-Response Water Vapor and Carbon Dioxide Sensor. In *Fiber Optic Sensors: Engineering and Applications*; Bruinsma, A.J., Culshaw, B., Eds.; International Society for Optics and Photonics: Boston, MA, USA, 1991; Volume 1511, pp. 114–119. [CrossRef]
36. Gibson, D.; Macgregor, C. A Novel Solid State Non-Dispersive Infrared CO₂ Gas Sensor Compatible With Wireless and Portable Deployment. *Sensors* **2013**, *13*, 7079–7103. [CrossRef]
37. Xu, D.; Wang, Y.; Xiong, B.; Li, T. MEMS-Based Thermoelectric Infrared Sensors: A Review. *Front. Mech. Eng.* **2017**, *12*, 557–566. [CrossRef]
38. Lee, K.N.; Lee, D.S.; Jung, S.W.; Jang, Y.H.; Kim, Y.K.; Seong, W.K. A High-Temperature MEMS Heater Using Suspended Silicon Structures. *J. Micromech. Microeng.* **2009**, *19*, 115011. [CrossRef]
39. Vincent, T.; Gardner, J. A Low Cost MEMS Based NDIR System for the Monitoring of Carbon Dioxide in Breath Analysis at ppm Levels. *Sens. Actuators B Chem.* **2016**, *236*, 954–964. [CrossRef]
40. Müller, M.; Graf, P.; Meyer, J.; Pentina, A.; Brunner, D.; Perez-Cruz, F.; Hüglin, C.; Emmenegger, L. Integration and Calibration of Non-Dispersive Infrared (NDIR) CO₂ Low-Cost Sensors and Their Operation in a Sensor Network Covering Switzerland. *Atmos. Meas. Tech.* **2020**, *13*, 3815–3834. [CrossRef]
41. Wang, J.N.; Xue, Q.S.; Lin, G.Y.; Ma, Q.J. Mid-Infrared Carbon Dioxide Sensor With Wireless and Anti-Condensation Capability for Use in Greenhouses. *Spectrosc. Lett.* **2018**, *51*, 266–273. [CrossRef]
42. Fietzek, P.; Fiedler, B.; Steinhoff, T.; Körtzinger, A. In situ Quality Assessment of a Novel Underwater pCO₂ Sensor Based on Membrane Equilibration and NDIR Spectrometry. *J. Atmos. Ocean. Technol.* **2014**, *31*, 181–196. [CrossRef]
43. Gas Sensing Solutions Ltd. *Reducing the Impact of Condensation on CO₂ Sensor*; Technical Report AN008; Gas Sensing Solutions Ltd.: Glasgow, UK, 2020.
44. Jung, D.; Bank, S.; Lee, M.; Wasserman, D. Next Generation Mid-Infrared Sources. *J. Opt.* **2017**, *19*, 123001. 2040-8986/aa939b. [CrossRef]
45. Hodgkinson, J.; Tatam, R.P. Optical Gas Sensing: A Review. *Meas. Sci. Technol.* **2012**, *24*, 012004. [CrossRef]
46. Moumen, S.; Raible, I.; Krauß, A.; Wöllenstein, J. Infrared Investigation of CO₂ Sorption by Amine Based Materials for the Development of a NDIR CO₂ Sensor. *Sens. Actuators B Chem.* **2016**, *236*, 1083–1090. [CrossRef]
47. Schaden, S.; Haberkorn, M.; Frank, J.; Baena, J.R.; Lendl, B. Direct Determination of Carbon Dioxide in Aqueous Solution Using Mid-Infrared Quantum Cascade Lasers. *Appl. Spectrosc.* **2004**, *58*, 667–670. [CrossRef]
48. Bozóki, Z.; Pogány, A.; Szabó, G. Photoacoustic Instruments for Practical Applications: Present, Potentials, and Future Challenges. *Appl. Spectrosc. Rev.* **2011**, *46*, 1–37. [CrossRef]
49. Borri, S.; Patimisco, P.; Galli, I.; Mazzotti, D.; Giusfredi, G.; Akikusa, N.; Yamanishi, M.; Scamarcio, G.; De Natale, P.; Spagnolo, V. Intracavity Quartz-Enhanced Photoacoustic Sensor. *Appl. Phys. Lett.* **2014**, *104*, 091114. [CrossRef]
50. Rousseau, R.; Maurin, N.; Trzpil, W.; Bahriz, M.; Vicet, A. Quartz Tuning Fork Resonance Tracking and Application in Quartz Enhanced Photoacoustics Spectroscopy. *Sensors* **2019**, *19*, 5565. [CrossRef]
51. Scholz, L.; Perez, A.; Bierer, B.; Eaksen, P.; Wollenstein, J.; Palzer, S. Miniature Low-Cost Carbon Dioxide Sensor for Mobile Devices. *IEEE Sens. J.* **2017**, *17*, 2889–2895. [CrossRef]
52. Huber, J.; Wöllenstein, J.; Kolb, S.; Dehé, A.; Jost, F. Miniaturized Photoacoustic CO₂ Sensors for Consumer Applications. *Proc. Sens.* **2015**, *E6*, 688–692. [CrossRef]

53. Pernau, H.F.; Schmitt, K.; Huber, J.; Rademacher, S.; Eberhardt, A.; Wöllenstein, J. Resonant Photoacoustic CO₂ Spectroscopy With LED Light Source. In Proceedings of the 30th Anniversary Eurosensors Conference—Eurosensors 2016, Budapest, Hungary, 4–7 September 2016; Volume 168, pp. 1325–1328. [\[CrossRef\]](#)
54. Lhermet, H.; Verdot, T.; Teulle, A.; Berthelot, A.; Gliere, A.; Desloges, B.; Souchon, F.; Fournier, M.; Fedeli, J.M.; Coutard, J.G. Micro-Photoacoustic Cell With Integrated Microphone for Sub-Ppm Gas Sensing. In Proceedings of the 2019 20th International Conference on Solid-State Sensors, Actuators and Microsystems & Eurosensors XXXIII (Transducers & Eurosensors XXXIII), Berlin, Germany, 23–27 June 2019; pp. 68–71. [\[CrossRef\]](#)
55. Jensen, M.A.; Rechnitz, G.A. Response Time Characteristics of the pCO₂ Electrode. *Anal. Chem.* **1979**, *51*, 1972–1977. [\[CrossRef\]](#)
56. Mills, A. Optical Sensors for Carbon Dioxide and Their Applications. In *Sensors for Environment, Health and Security*; Baraton, M.I., Ed.; Springer: Dordrecht, The Netherlands, 2009; pp. 347–370.
57. Millero, F.J.; Graham, T.B.; Huang, F.; Bustos-Serrano, H.; Pierrot, D. Dissociation Constants of Carbonic Acid in Seawater as a Function of Salinity and Temperature. *Mar. Chem.* **2006**, *100*, 80–94. [\[CrossRef\]](#)
58. Wang, X.; Conway, W.; Burns, R.; McCann, N.; Maeder, M. Comprehensive Study of the Hydration and Dehydration Reactions of Carbon Dioxide in Aqueous Solution. *J. Phys. Chem. A* **2010**, *114*, 1734–1740. [\[CrossRef\]](#)
59. Baker, J.M.; Spaans, E.J.A.; Reece, C.F. Conductimetric Measurement of CO₂ Concentration: Theoretical Basis and Its Verification. *Agron. J.* **1996**, *88*, 675–682. [\[CrossRef\]](#)
60. Roxana Varlan, A.; Sansen, W. Micromachined Conductometric p(CO₂) Sensor. *Sens. Actuators B Chem.* **1997**, *44*, 309–315. [\[CrossRef\]](#)
61. Mirtaheri, P.; Grimnes, S.; Martinsen, Ø.; Tønnessen, T. A New Biomedical Sensor for Measuring PCO₂. *Physiol. Meas.* **2004**, *25*, 421–436. [\[CrossRef\]](#)
62. Mirtaheri, P.; Omtveit, T.; Klotzbuecher, T.; Grimnes, S.; Martinsen, Ø.G.; Tønnessen, T.I. Miniaturization of a Biomedical Gas Sensor. *Physiol. Meas.* **2004**, *25*, 1511–1522. [\[CrossRef\]](#) [\[PubMed\]](#)
63. Tronstad, C.; Pischke, S.; Holhjem, L.; Tønnessen, T.; Martinsen, Ø.; Grimnes, S. Early Detection of Cardiac Ischemia Using a Conductometric pCO₂ Sensor: Real-Time Drift Correction and Parameterization. *Physiol. Meas.* **2010**, *31*, 1241–1255. [\[CrossRef\]](#)
64. Wall, G.W.; Acock, B.; Milliken, G.A. A Simple Conductimetric CO₂ Analyzer with Automatic Recalibration: II. Factors Affecting Calibration. *Agron. J.* **1995**, *87*, 76–80. [\[CrossRef\]](#)
65. Lis, K.; Acker, H.; Lübbers, D.; Halle, M. A PCO₂ Surface Electrode Working on the Principle of Electrical Conductivity. *Pflügers Arch. Eur. J. Physiol.* **1979**, *381*, 289–291. [\[CrossRef\]](#)
66. Neethirajan, S.; Freund, M.; Jayas, D.; Shafai, C.; Thomson, D.; White, N. Development of Carbon Dioxide (CO₂) Sensor for Grain Quality Monitoring. *Biosyst. Eng.* **2010**, *106*, 395–404. [\[CrossRef\]](#)
67. Severinghaus, J.W.; Bradley, A.F. Electrodes for Blood pO₂ and pCO₂ Determination. *J. Appl. Physiol.* **1958**, *13*, 515–520. [\[CrossRef\]](#)
68. Beran, A.V.; Huxtable, R.F.; Sperling, D.R. Electrochemical Sensor for Continuous Transcutaneous PCO₂ Measurement. *J. Appl. Physiol.* **1976**, *41*, 442–447. [\[CrossRef\]](#) [\[PubMed\]](#)
69. Shin, J.H.; Lee, J.S.; Choi, S.H.; Lee, D.K.; Nam, H.; Cha, G.S. A Planar pCO₂ Sensor with Enhanced Electrochemical Properties. *Anal. Chem.* **2000**, *72*, 4468–4473. [\[CrossRef\]](#)
70. Severinghaus, J.W. A Combined Transcutaneous P(O₂)-P(CO₂) Electrode with Electrochemical HCO₃⁻ Stabilization. *J. Appl. Physiol. Respir. Environ. Exerc. Physiol.* **1981**, *51*, 1027–1032. [\[CrossRef\]](#)
71. Zhao, P.; Cai, W.J. An Improved Potentiometric pCO₂ Microelectrode. *Anal. Chem.* **1997**, *69*, 5052–5058. [\[CrossRef\]](#)
72. Suzuki, H.; Arakawa, H.; Sasaki, S.; Karube, I. Micromachined Severinghaus-Type Carbon Dioxide Electrode. *Anal. Chem.* **1999**, *71*, 1737–1743. [\[CrossRef\]](#)
73. Beyenal, H.; Davis, C.C.; Lewandowski, Z. An Improved Severinghaus-Type Carbon Dioxide Microelectrode for Use in Biofilms. *Sens. Actuators B Chem.* **2004**, *97*, 202–210. [\[CrossRef\]](#)
74. Donaldson, T.L.; Palmer, H.J. Dynamic Response of the Carbon Dioxide Electrode. *AIChE J.* **1979**, *25*, 143–151. [\[CrossRef\]](#)
75. McGuire, M.A.; Teskey, R.O. Microelectrode Technique for In Situ Measurement of Carbon Dioxide Concentrations in Xylem Sap of Trees. *Tree Physiol.* **2002**, *22*, 807–811. [\[CrossRef\]](#)
76. Cai, W.J.; Reimers, C.E. The Development of pH and pCO₂ Microelectrodes for Studying the Carbonate Chemistry of Pore Waters Near the Sediment-Water Interface. *Limnol. Oceanogr.* **1993**, *38*, 1762–1773. [\[CrossRef\]](#)
77. Whitehead, M.D.; Pollitzer, M.J.; Parker, D.; Halsall, D.; Delpy, D.T.; Reynolds, E.O.R. Transcutaneous Estimation of Arterial pO₂ and pCO₂ in Newborn Infants with a Single Electrochemical Sensor. *Lancet* **1980**, *315*, 1111–1114. [\[CrossRef\]](#)
78. Bergveld, P. Development of an Ion-Sensitive Solid-State Device for Neurophysiological Measurements. *IEEE Trans. Biomed. Eng.* **1970**, *BME-17*, 70–71. [\[CrossRef\]](#)
79. Hu, B.; Van Den Vlekkert, H.H.; De Rooij, N.F. Carbon Dioxide Gas-Sensing Electrode Based on a pH-ISFET with Back-Side Contacts. *Sens. Actuators* **1989**, *17*, 275–278. [\[CrossRef\]](#)
80. Bergveld, P. The Operation of an ISFET as an Electronic Device. *Sens. Actuators* **1981**, *1*, 17–29. [\[CrossRef\]](#)
81. Jamasb, S. Continuous Monitoring of pH and Blood Gases Using Ion-Sensitive and Gas-Sensitive Field Effect Transistors Operating in the Amperometric Mode in Presence of Drift. *Biosensors* **2019**, *9*, 44. [\[CrossRef\]](#) [\[PubMed\]](#)
82. Star, A.; Han, T.R.; Joshi, V.; Gabriel, J.C.; Grüner, G. Nanoelectronic Carbon Dioxide Sensors. *Adv. Mater.* **2004**, *16*, 2049–2052. [\[CrossRef\]](#)

83. Mohri, S.; Shimizu, J.; Goda, N.; Miyasaka, T.; Fujita, A.; Nakamura, M.; Kajiya, F. Measurements of CO₂, Lactic Acid and Sodium Bicarbonate Secreted by Cultured Cells Using a Flow-Through Type pH/CO₂ Sensor System Based on ISFET. *Sens. Actuators B Chem.* **2006**, *115*, 519–525. [[CrossRef](#)]
84. Ekwińska, M.A.; Jaroszewicz, B.; Domański, K.; Grabiec, P.; Zaborowski, M.; Tomaszewski, D.; Pałko, T.; Przytułski, J.; Łukasik, W.; Dawgul, M.; et al. Transcutaneous Blood Capnometry Sensor Head Based on a Back-Side Contacted ISFET. In *Mechatronics: Recent Technological and Scientific Advances*; Springer: Berlin/Heidelberg, Germany, 2012; pp. 607–614.
85. Lai, C.S.; Lu, T.F.; Yang, C.M.; Lin, Y.C.; Pijanowska, D.; Jaroszewicz, B. Body Effect Minimization Using Single Layer Structure for pH-ISFET Applications. *Sens. Actuators B Chem.* **2010**, *143*, 494–499. [[CrossRef](#)]
86. Sinha, S.; Bhardwaj, R.; Sahu, N.; Ahuja, H.; Sharma, R.; Mukhiya, R. Temperature and Temporal Drift Compensation for Al₂O₃-Gate ISFET-Based pH Sensor Using Machine Learning Techniques. *Microelectron. J.* **2020**, *97*, 104710. [[CrossRef](#)]
87. Shimano, K.; Goto, K.; Obata, K.; Nakata, S.; Sakai, G.; Yamazoe, N. Development of FET-Type CO₂ Sensor Operative at Room Temperature. *Sens. Actuators B Chem.* **2004**, *102*, 14–19. [[CrossRef](#)]
88. Hsieh, C.H.; Hung, W.C.; Chen, P.H.; Huang, I.Y. High-Performance Extended Gate Field-Effect-Transistor-Based Dissolved Carbon Dioxide Sensing System with a Packaged Microreference Electrode. *J. Micro/Nanolithogr. MEMS MOEMS* **2014**, *13*, 033017. [[CrossRef](#)]
89. MacInnes, D.A.; Belcher, D. The Thermodynamic Ionization Constants of Carbonic Acid. *J. Am. Chem. Soc.* **1933**, *55*, 2630–2646. [[CrossRef](#)]
90. Uttamlal, M.; Walt, D.R. A Fiber-Optic Carbon Dioxide Sensor for Fermentation Monitoring. *Bio/Technology* **1995**, *13*, 597–601. [[CrossRef](#)]
91. Vurek, G.G.; Feustel, P.J.; Severinghaus, J.W. A Fiber Optic PCO₂ Sensor. *Ann. Biomed. Eng.* **1983**, *11*, 499–510. [[CrossRef](#)] [[PubMed](#)]
92. DeGrandpre, M.D.; Baehr, M.M.; Hammar, T.R. Calibration-Free Optical Chemical Sensors. *Anal. Chem.* **1999**, *71*, 1152–1159. [[CrossRef](#)]
93. Ge, X.; Kostov, Y.; Rao, G. High-Stability Non-Invasive Autoclavable Naked Optical CO₂ Sensor. *Biosens. Bioelectron.* **2003**, *18*, 857–865. [[CrossRef](#)]
94. Lu, Z.; Dai, M.; Xu, K.; Chen, J.; Liao, Y. A High Precision, Fast Response, and Low Power Consumption in situ Optical Fiber Chemical pCO₂ Sensor. *Talanta* **2008**, *76*, 353–359. [[CrossRef](#)]
95. Hakonen, A.; Hulth, S. A High-Precision Ratiometric Fluorosensor for pH: Implementing Time-Dependent Non-Linear Calibration Protocols for Drift Compensation. *Anal. Chim. Acta* **2008**, *606*, 63–71. [[CrossRef](#)] [[PubMed](#)]
96. Ge, X.; Kostov, Y.; Henderson, R.; Selock, N.; Rao, G. A Low-Cost Fluorescent Sensor for pCO₂ Measurements. *Chemosensors* **2014**, *2*, 108–120. [[CrossRef](#)]
97. Wang, H.; Vagin, S.I.; Rieger, B.; Meldrum, A. An Ultrasensitive Fluorescent Paper-Based CO₂ Sensor. *ACS Appl. Mater. Interfaces* **2020**, *12*, 20507–20513. [[CrossRef](#)] [[PubMed](#)]
98. Opitz, N.; Lübbers, D.W., Compact CO₂ Gas Analyzer with Favourable Signal-to-Noise Ratio and Resolution Using Special Fluorescence Sensors (Optodes) Illuminated by Blue Led's. In *Oxygen Transport to Tissue—VI*; Springer: Boston, MA, USA, 1984; pp. 757–762. [[CrossRef](#)]
99. Zhujun, Z.; Seitz, W.R. A Carbon Dioxide Sensor Based on Fluorescence. *Anal. Chim. Acta* **1984**, *160*, 305–309. [[CrossRef](#)]
100. Wolfbeis, O.S.; Weis, L.J.; Leiner, M.J.P.; Ziegler, W.E. Fiber-Optic Fluorosensor for Oxygen and Carbon Dioxide. *Anal. Chem.* **1988**, *60*, 2028–2030. [[CrossRef](#)]
101. He, X.; Rechnitz, G.A. Linear Response Function for Fluorescence-Based Fiber-Optic CO₂ Sensors. *Anal. Chem.* **1995**, *67*, 2264–2268. [[CrossRef](#)]
102. Marazuela, M.; Moreno Bondi, M.; Orellana, G. Enhanced Performance of a Fibre-Optic Luminescence CO₂ Sensor Using Carbonic Anhydrase. *Sens. Actuators B Chem.* **1995**, *29*, 126–131. [[CrossRef](#)]
103. Mills, A.; Lepre, A.; Wild, L. Breath-by-Breath Measurement of Carbon Dioxide Using a Plastic Film Optical Sensor. *Sens. Actuators B Chem.* **1997**, *39*, 419–425. [[CrossRef](#)]
104. Malins, C.; D. MacCraith, B. Dye-doped Organically Modified Silica Glass for Fluorescence Based Carbon Dioxide Gas Detection. *Analyst* **1998**, *123*, 2373–2376. [[CrossRef](#)]
105. Wolfbeis, O.; Kovacs, B.; Goswami, K.; Klainer, S. Fiber-Optic Fluorescence Carbon Dioxide Sensor for Environmental Monitoring. *Microchim. Acta* **1998**, *129*, 181–188. [[CrossRef](#)]
106. Segawa, H.; Ohnishi, E.; Arai, Y.; Yoshida, K. Sensitivity of Fiber-Optic Carbon Dioxide Sensors Utilizing Indicator Dye. *Sens. Actuators B Chem.* **2003**, *94*, 276–281. [[CrossRef](#)]
107. Oter, O.; Ertekin, K.; Topkaya, D.; Alp, S. Emission-Based Optical Carbon Dioxide Sensing with HPTS in Green Chemistry Reagents: Room-Temperature Ionic Liquids. *Anal. Bioanal. Chem.* **2006**, *386*, 1225–1234. [[CrossRef](#)]
108. Fernández-Sánchez, J.F.; Cannas, R.; Spichiger, S.; Steiger, R.; Spichiger-Keller, U.E. Optical CO₂-Sensing Layers for Clinical Application Based on pH-Sensitive Indicators Incorporated into Nanoscopic Metal-Oxide Supports. *Sens. Actuators B Chem.* **2007**, *128*, 145–153. [[CrossRef](#)]
109. Oter, O.; Ertekin, K.; Derinkuyu, S. Ratiometric Sensing of CO₂ in Ionic Liquid Modified Ethyl Cellulose Matrix. *Talanta* **2008**, *76*, 557–563. [[CrossRef](#)]

110. Chu, C.S.; Lo, Y.L. Fiber-Optic Carbon Dioxide Sensor Based on Fluorinated Xerogels Doped with HPTS. *Sens. Actuators B Chem.* **2008**, *129*, 120–125. [[CrossRef](#)]
111. Chu, C.S.; Lo, Y.L. Highly Sensitive and Linear Optical Fiber Carbon Dioxide Sensor Based on Sol-Gel Matrix Doped with Silica Particles and HPTS. *Sens. Actuators B Chem.* **2009**, *143*, 205–210. [[CrossRef](#)]
112. Dansby-Sparks, R.N.; Jin, J.; Mechery, S.J.; Sampathkumaran, U.; Owen, T.W.; Yu, B.D.; Goswami, K.; Hong, K.; Grant, J.; Xue, Z.L. Fluorescent-Dye-Doped Sol-Gel Sensor for Highly Sensitive Carbon Dioxide Gas Detection below Atmospheric Concentrations. *Anal. Chem.* **2010**, *82*, 593–600. [[CrossRef](#)] [[PubMed](#)]
113. Chu, C.S.; Syu, J.J. Optical Sensor for Dual Sensing of Oxygen and Carbon Dioxide Based on Sensing Films Coated on Filter Paper. *Appl. Opt.* **2017**, *56*, 1225–1231. [[CrossRef](#)] [[PubMed](#)]
114. Perez de Vargas-Sansalvador, I.M.; Erenas, M.M.; Diamond, D.; Quilty, B.; Capitan-Vallvey, L.F. Water Based-Ionic Liquid Carbon Dioxide Sensor for Applications in the Food Industry. *Sens. Actuators B Chem.* **2017**, *253*, 302–309. [[CrossRef](#)]
115. Clarke, J.S.; Achterberg, E.P.; Connelly, D.P.; Schuster, U.; Mowlem, M. Developments in Marine pCO₂ Measurement Technology; towards Sustained in situ Observations. *TrAC Trends Anal. Chem.* **2017**, *88*, 53–61. [[CrossRef](#)]
116. Nakamura, N.; Amao, Y. Optical Sensor for Carbon Dioxide Combining Colorimetric Change of a pH Indicator and a Reference Luminescent Dye. *Anal. Bioanal. Chem.* **2003**, *376*, 642–646. [[CrossRef](#)]
117. Amao, Y.; Nakamura, N. Optical CO₂ Sensor with the Combination of Colorimetric Change of α -naphtholphthalein and Internal Reference Fluorescent Porphyrin Dye. *Sens. Actuators B Chem.* **2004**, *100*, 347–351. [[CrossRef](#)]
118. Amao, Y.; Nakamura, N. An Optical Sensor with the Combination of Colorimetric Change of α -naphtholphthalein and Internal Reference Luminescent Dye for CO₂ in Water. *Sens. Actuators B Chem.* **2005**, *107*, 861–865. [[CrossRef](#)]
119. Amao, Y.; Komori, T. Optical CO₂ Sensor of the Combination of Colorimetric Change of α -naphtholphthalein in poly(isobutyl methacrylate) and Fluorescent Porphyrin in Polystyrene. *Talanta* **2005**, *66*, 976–981. [[CrossRef](#)] [[PubMed](#)]
120. Pérez de Vargas-Sansalvador, I.M.; Carvajal, M.A.; Roldán-Muñoz, O.M.; Banqueri, J.; Fernández-Ramos, M.D.; Capitán-Vallvey, L.F. Phosphorescent Sensing of Carbon Dioxide Based on Secondary Inner-Filter Quenching. *Anal. Chim. Acta* **2009**, *655*, 66–74. [[CrossRef](#)]
121. Aguayo-López, M.L.; Capitán-Vallvey, L.F.; Fernández-Ramos, M.D. Optical Sensor for Carbon Dioxide Gas Determination, Characterization and Improvements. *Talanta* **2014**, *126*, 196–201. [[CrossRef](#)] [[PubMed](#)]
122. Fernández-Ramos, M.D.; Aguayo-López, M.L.; Pérez de Vargas-Sansalvador, I.; Capitán-Vallvey, L.F. Ionic Liquids on Optical Sensors for Gaseous Carbon Dioxide. *Anal. Bioanal. Chem.* **2018**, *410*, 5931–5939. [[CrossRef](#)] [[PubMed](#)]
123. Fernández-Ramos, M.D.; Aguayo-López, M.; De Los Reyes Berbel, E.; Santoyo-González, F.; Capitan-Vallvey, L.F. NIR Optical Carbon Dioxide Gas Sensor Based on Simple azaBODIPY pH Indicators. *Analyst* **2019**, *144*, 3870–3877. [[CrossRef](#)]
124. Klimant, I.; Huber, C.; Liebsch, G.; Neuraüter, G.; Stangelmayer, A.; Wolfbeis, O.S. Dual Lifetime Referencing (DLR)—A New Scheme for Converting Fluorescence Intensity into a Frequency-Domain or Time-Domain Information. In *New Trends in Fluorescence Spectroscopy: Applications to Chemical and Life Sciences*; Springer: Berlin/Heidelberg, Germany, 2001; pp. 257–274. [[CrossRef](#)]
125. von Bültzingslöwen, C.; McEvoy, A.; McDonagh, C.; MacCraith, B.; Klimant, I.; Krause, C.; Wolfbeis, O. Sol-gel Based Optical Carbon Dioxide Sensor Employing Dual Lumiphore Referencing for Application in Food Packaging Technology. *Analyst* **2002**, *127*, 1478–1483. [[CrossRef](#)]
126. Burke, C.S.; Markey, A.; Nooney, R.I.; Byrne, P.; McDonagh, C. Development of an Optical Sensor Probe for the Detection of Dissolved Carbon Dioxide. *Sens. Actuators B Chem.* **2006**, *119*, 288–294. [[CrossRef](#)]
127. Cajlakovic, M.; Bizzarri, A.; Ribitsch, V. Luminescence Lifetime-Based Carbon Dioxide Optical Sensor for Clinical Applications. *Anal. Chim. Acta* **2006**, *573–574*, 57–64. [[CrossRef](#)]
128. Fritzsche, E.; Gruber, P.; Schutting, S.; Fischer, J.P.; Strobl, M.; Müller, J.D.; Borisov, S.M.; Klimant, I. Highly Sensitive Poisoning-Resistant Optical Carbon Dioxide Sensors for Environmental Monitoring. *Anal. Methods* **2017**, *9*, 55–65. [[CrossRef](#)]
129. Staudinger, C.; Strobl, M.; Fischer, J.P.; Thar, R.; Mayr, T.; Aigner, D.; Müller, B.J.; Müller, B.; Lehner, P.; Mistlberger, G.; et al. A Versatile Optode System for Oxygen, Carbon Dioxide, and pH Measurements in Seawater with Integrated Battery and Logger. *Limnol. Oceanogr. Methods* **2018**, *16*, 459–473. [[CrossRef](#)]
130. Pfeifer, D.; Russegger, A.; Klimant, I.; Borisov, S.M. Green to Red Emitting BODIPY Dyes for Fluorescent Sensing and Imaging of Carbon Dioxide. *Sens. Actuators B Chem.* **2020**, *304*, 127312. [[CrossRef](#)]
131. Lakowicz, J.R.; Szmajcinski, H.; Karakelle, M. Optical Sensing of pH and pCO₂ Using Phase-Modulation Fluorimetry and Resonance Energy Transfer. *Anal. Chim. Acta* **1993**, *272*, 179–186. [[CrossRef](#)]
132. Neuraüter, G.; Klimant, I.; Wolfbeis, O.S. Microsecond Lifetime-Based Optical Carbon Dioxide Sensor Using Luminescence Resonance Energy Transfer. *Anal. Chim. Acta* **1999**, *382*, 67–75. [[CrossRef](#)]
133. Valeur, B. Resonance Energy Transfer and Its Applications. In *Molecular Fluorescence*; John Wiley and Sons, Ltd.: Hoboken, NJ, USA, 2001; Chapter 9, pp. 247–272. [[CrossRef](#)]
134. von Bültzingslöwen, C.; McEvoy, A.K.; McDonagh, C.; MacCraith, B.D. Lifetime-Based Optical Sensor for High-Level pCO₂ Detection Employing Fluorescence Resonance Energy Transfer. *Anal. Chim. Acta* **2003**, *480*, 275–283. [[CrossRef](#)]
135. Wolfbeis, O.S. Materials for Fluorescence-Based Optical Chemical Sensors. *J. Mater. Chem.* **2005**, *15*, 2657–2669. [[CrossRef](#)]
136. Kautsky, H. Quenching of Luminescence by Oxygen. *Trans. Faraday Soc.* **1939**, *35*, 216–219. [[CrossRef](#)]

137. Lakowicz, J.R.; Weber, G. Quenching of Fluorescence by Oxygen. A Probe for Structural Fluctuations in Macromolecules. *Biochemistry* **1973**, *12*, 4161–4170. [[CrossRef](#)]
138. Huber, C.; Klimant, I.; Krause, C.; Werner, T.; Mayr, T.; Wolfbeis, O.S. Optical Sensor for Seawater Salinity. *Fresenius J. Anal. Chem.* **2000**, *368*, 196–202. [[CrossRef](#)]
139. Zheng, Y.; Chen, L.; Dong, X.; Yang, J.; Long, H.; So, P.; Chan, C. Miniature pH Optical Fiber Sensor Based on Fabry-Perot Interferometer. *IEEE J. Sel. Top. Quantum Electron.* **2015**, *22*, 331–335. [[CrossRef](#)]
140. Ma, W.; Xing, J.; Wang, R.; Rong, Q.; Zhang, W.; Li, Y.; Zhang, J.; Qiao, X. Optical Fiber Fabry-Perot Interferometric CO₂ Gas Sensor Using Guanidine Derivative Polymer Functionalized Layer. *IEEE Sens. J.* **2018**, *18*, 1924–1929. [[CrossRef](#)]
141. Quintero, S.M.M.; Cremona, M.; Triques, A.L.C.; d’Almeida, A.R.; Braga, A.M.B. Swelling and Morphological Properties of poly(vinyl alcohol) (PVA) and poly(acrylic acid) (PAA) Hydrogels in Solution with High Salt Concentration. *Polymer* **2010**, *51*, 953–958. [[CrossRef](#)]
142. Hill, K.O.; Meltz, G. Fiber Bragg Grating Technology Fundamentals and Overview. *J. Light. Technol.* **1997**, *15*, 1263–1276. [[CrossRef](#)]
143. Herber, S.; Olthuis, W.; Bergveld, P.; van den Berg, A. Exploitation of a pH-Sensitive Hydrogel Disk for CO₂ Detection. *Sens. Actuators B Chem.* **2004**, *103*, 284–289. [[CrossRef](#)]
144. Hu, P.; Dong, X.; Wong, W.C.; Chen, L.; Ni, K.; Chiu Chan, C. Photonic Crystal Fiber Interferometric pH Sensor Based on Polyvinyl Alcohol/Polyacrylic Acid Hydrogel Coating. *Appl. Opt.* **2015**, *54*, 2647–2652. [[CrossRef](#)]
145. Hromadka, J.; Tokay, B.; Correia, R.; Morgan, S.P.; Korposh, S. Carbon Dioxide Measurements Using Long Period Grating Optical Fibre Sensor Coated with Metal Organic Framework HKUST-1. *Sens. Actuators B Chem.* **2018**, *255*, 2483–2494. [[CrossRef](#)]
146. Melo, L.; Burton, G.; Davies, B.; Risk, D.; Wild, P. Highly Sensitive Coated Long Period Grating Sensor for CO₂ Detection at Atmospheric Pressure. *Sens. Actuators B Chem.* **2014**, *202*, 294–300. [[CrossRef](#)]
147. Chong, X.; Kim, K.; Ohodnicki, P.R.; Li, E.; Chang, C.; Wang, A.X. Ultrashort Near-Infrared Fiber-Optic Sensors for Carbon Dioxide Detection. *IEEE Sens. J.* **2015**, *15*, 5327–5332. [[CrossRef](#)]
148. Kersey, A.D. Multiplexed fiber optic sensors. In *Distributed and Multiplexed Fiber Optic Sensors II*; Dakin, J.P., Kersey, A.D., Eds.; International Society for Optics and Photonics: Boston, MA, USA, 1993; Volume 1797, pp. 161–185. [[CrossRef](#)]
149. Perez-Herrera, R.A.; Lopez-Amo, M. Fiber Optic Sensor Networks. *Opt. Fiber Technol.* **2013**, *19*, 689–699. [[CrossRef](#)]
150. Hotan, W.; Göpel, W.; Haul, R. Interaction of CO₂ and CO with Nonpolar Zinc Oxide Surfaces. *Surf. Sci.* **1979**, *83*, 162–180. [[CrossRef](#)]
151. Au, C.T.; Hirsch, W.; Hirschwald, W. Adsorption and Interaction of Carbon Dioxide, Formic Acid and Hydrogen/Carbon Dioxide Mixtures on (1010) Zinc Oxide Surfaces Studied by Photoelectron Spectroscopy (XPS and UPS). *Surf. Sci.* **1988**, *199*, 507–517. [[CrossRef](#)]
152. Freund, H.J.; Roberts, M.W. Surface Chemistry of Carbon Dioxide. *Surf. Sci. Rep.* **1996**, *25*, 225–273. [[CrossRef](#)]
153. Seifert, O.; Wolter, K.; Dillmann, B.; Klivenyi, G.; Freund, H.J.; Scarano, D.; Zecchina, A. IR Investigations of CO₂ Adsorption on Chromia Surfaces: Cr₂O₃ (0001)/Cr(110) Versus Polycrystalline α -Cr₂O₃. *Surf. Sci.* **1999**, *421*, 176–190. [[CrossRef](#)]
154. Lopes Martins, J.B.; Longo, E.; Rodríguez Salmon, O.D.; Espinoza, V.A.; Taft, C.A. The Interaction of H₂, CO, CO₂, H₂O and NH₃ on ZnO Surfaces: An Oniom Study. *Chem. Phys. Lett.* **2004**, *400*, 481–486. [[CrossRef](#)]
155. Herrán, J.; Mandayo, G.; Castaño, E. Semiconducting BaTiO₃-CuO Mixed Oxide Thin Films for CO₂ Detection. *Thin Solid Films* **2009**, *517*, 6192–6197. [[CrossRef](#)]
156. Noei, H.; Wöll, C.; Muhler, M.; Wang, Y. Activation of Carbon Dioxide on ZnO Nanoparticles Studied by Vibrational Spectroscopy. *J. Phys. Chem. C* **2011**, *115*, 908–914. [[CrossRef](#)]
157. Tang, Q.L.; Luo, Q.H. Adsorption of CO₂ at ZnO: A Surface Structure Effect from DFT + U Calculations. *J. Phys. Chem. C* **2013**, *117*, 22954–22966. [[CrossRef](#)]
158. Usseinov, A.B.; Akilbekov, A.T.; Kotomin, E.A.; Popov, A.I.; Seitov, D.D.; Nekrasov, K.A.; Giniyatova, S.G.; Karipbayev, Z.T. The First Principles Calculations of CO₂ Adsorption on (1010) ZnO Surface. *AIP Conf. Proc.* **2019**, *2174*, 020181. [[CrossRef](#)]
159. Gankanda, A.; Cwiertny, D.M.; Grassian, V.H. Role of Atmospheric CO₂ and H₂O Adsorption on ZnO and CuO Nanoparticle Aging: Formation of New Surface Phases and the Impact on Nanoparticle Dissolution. *J. Phys. Chem. C* **2016**, *120*, 19195–19203. [[CrossRef](#)]
160. Çolak, H.; Karaköse, E. Synthesis and Characterization of Different Dopant (Ge, Nd, W)-Doped ZnO Nanorods and Their CO₂ Gas Sensing Applications. *Sens. Actuators B Chem.* **2019**, *296*, 126629. [[CrossRef](#)]
161. Álvarez-Ramos, M.E.; Necochea-Chamorro, J.I.; Carrillo-Torres, R.C.; Sánchez-Zeferino, R. Room Temperature CO₂ Sensing Using Au-Decorated ZnO Nanorods Deposited on an Optical Fiber. *Mater. Sci. Eng. B* **2020**, *262*, 114720. [[CrossRef](#)]
162. Kannan, P.K.; Saraswathi, R.; Rayappan, J.B.B. CO₂ Gas Sensing Properties of DC Reactive Magnetron Sputtered ZnO Thin Film. *Ceram. Int.* **2014**, *40*, 13115–13122. [[CrossRef](#)]
163. Haeusler, A.; Meyer, J.U. A Novel Thick Film Conductive Type CO₂ Sensor. *Sens. Actuators B Chem.* **1996**, *34*, 388–395. [[CrossRef](#)]
164. Jeong, Y.J.; Balamurugan, C.; Lee, D.W. Enhanced CO₂ Gas-Sensing Performance of ZnO Nanopowder by La Loaded during Simple Hydrothermal Method. *Sens. Actuators B Chem.* **2016**, *229*, 288–296. [[CrossRef](#)]
165. Dhahri, R.; Leonardi, S.G.; Hjiri, M.; Mir, L.E.; Bonavita, A.; Donato, N.; Iannazzo, D.; Neri, G. Enhanced Performance of Novel Calcium/Aluminum Co-Doped Zinc Oxide for CO₂ Sensors. *Sens. Actuators B Chem.* **2017**, *239*, 36–44. [[CrossRef](#)]

166. Ghosh, A.; Zhang, C.; Zhang, H.; Shi, S. CO₂ Sensing Behavior of Calcium-Doped ZnO Thin Film: A Study to Address the Cross-Sensitivity of CO₂ in H₂ and CO Environment. *Langmuir* **2019**, *35*, 10267–10275. [[CrossRef](#)]
167. Cavanagh, L.; Binions, R. BaSnO₃ Thick Film as a Carbon Dioxide Sensor. *J. Electrochem. Soc.* **2011**, *159*, 1006–1009. [[CrossRef](#)]
168. Chen, G.; Han, B.; Deng, S.; Wang, Y.; Wang, Y. Lanthanum Dioxide Carbonate La₂O₂CO₃ Nanorods as a Sensing Material for Chemoresistive CO₂ Gas Sensor. *Electrochim. Acta* **2014**, *127*, 355–361. [[CrossRef](#)]
169. Basyooni, M.A.; Shaban, M.; El Sayed, A.M. Enhanced Gas Sensing Properties of Spin-coated Na-doped ZnO Nanostructured Films. *Sci. Rep.* **2017**, *7*, 41716. [[CrossRef](#)]
170. Ghanbari Shohany, B.; Motevalizadeh, L.; Ebrahimizadeh Abrishami, M. Investigation of ZnO Thin-Film Sensing Properties for CO₂ Detection: Effect of Mn Doping. *J. Theor. Appl. Phys.* **2018**, *12*, 219–225. [[CrossRef](#)]
171. Ishihara, T.; Kometani, K.; Mizuhara, Y.; Takita, Y. Capacitive-Type Gas Sensor for the Selective Detection of Carbon Dioxide. *Sens. Actuators B Chem.* **1993**, *13*, 470–472. [[CrossRef](#)]
172. Shokry Hassan, H.; Kashyout, A.B.; Morsi, I.; Nasser, A.A.A.; Ali, I. Synthesis, Characterization and Fabrication of Gas Sensor Devices Using ZnO and ZnO: In Nanomaterials. *Beni-Suef Univ. J. Basic Appl. Sci.* **2014**, *3*, 216–221. [[CrossRef](#)]
173. Tanvir, N.B.; Wilbertz, C.; Steinhauer, S.; Köck, A.; Urban, G.; Yurchenko, O. Work Function Based CO₂ Gas Sensing Using Metal Oxide Nanoparticles at Room Temperature. *Mater. Today Proc.* **2015**, *2*, 4190–4195. [[CrossRef](#)]
174. Tanvir, N.B.; Yurchenko, O.; Urban, G. Optimization Study for Work Function Based CO₂ Sensing Using CuO-nanoparticles in Respect to Humidity and Temperature. *Procedia Eng.* **2015**, *120*, 667–670. [[CrossRef](#)]
175. Ishihara, T.; Kometani, K.; Nishi, Y.; Takita, Y. Improved Sensitivity of CuO–BaTiO₃ Capacitive-Type CO₂ Sensor by Additives. *Sens. Actuators B Chem.* **1995**, *28*, 49–54. [[CrossRef](#)]
176. Heiland, G. Homogeneous Semiconducting Gas Sensors. *Sens. Actuators* **1981**, *2*, 343–361. [[CrossRef](#)]
177. Sears, W.M.; Colbow, K.; Consadori, F. General Characteristics of Thermally Cycled Tin Oxide Gas Sensors. *Semicond. Sci. Technol.* **1989**, *4*, 351–359. [[CrossRef](#)]
178. Nakata, S.; Kaneda, Y.; Nakamura, H.; Yoshikawa, K. Detection and Quantification of CO Gas Based on the Dynamic Response of a Ceramic Sensor. *Chem. Lett.* **1991**, *20*, 1505–1508. [[CrossRef](#)]
179. Wlodek, S.; Colbow, K.; Consadori, F. Signal-Shape Analysis of a Thermally Cycled Tin-Oxide Gas Sensor. *Sens. Actuators B Chem.* **1991**, *3*, 63–68. [[CrossRef](#)]
180. Hiranaka, Y.; Abe, T.; Murata, H. Gas-Dependent Response in the Temperature Transient of SnO₂ Gas Sensors. *Sens. Actuators B Chem.* **1992**, *9*, 177–182. [[CrossRef](#)]
181. Nakata, S.; Akakabe, S.; Nakasuji, M.; Yoshikawa, K. Gas Sensing Based on a Nonlinear Response: Discrimination Between Hydrocarbons and Quantification of Individual Components in a Gas Mixture. *Anal. Chem.* **1996**, *68*, 2067–2072. [[CrossRef](#)] [[PubMed](#)]
182. Lee, A.P.; Reedy, B.J. Temperature Modulation in Semiconductor Gas Sensing. *Sens. Actuators B Chem.* **1999**, *60*, 35–42. [[CrossRef](#)]
183. Vergara, A.; Martinelli, E.; Llobet, E.; D’Amico, A.; Di Natale, C. Optimized Feature Extraction for Temperature-Modulated Gas Sensors. *J. Sens.* **2009**, *2009*, 716316. [[CrossRef](#)]
184. Gosangi, R.; Gutierrez-Osuna, R. Active Temperature Modulation of Metal-Oxide Sensors for Quantitative Analysis of Gas Mixtures. *Sens. Actuators B Chem.* **2013**, *185*, 201–210. [[CrossRef](#)]
185. Vergara, A.; Llobet, E.; Brezmes, J.; Ivanov, P.; Cané, C.; Gràcia, I.; Vilanova, X.; Correig, X. Quantitative Gas Mixture Analysis Using Temperature-Modulated Micro-Hotplate Gas Sensors: Selection and Validation of the Optimal Modulating Frequencies. *Sens. Actuators B Chem.* **2007**, *123*, 1002–1016. [[CrossRef](#)]
186. Madrolle, S.; Grangeat, P.; Jutten, C. A Linear-Quadratic Model for the Quantification of a Mixture of Two Diluted Gases with a Single Metal Oxide Sensor. *Sensors* **2018**, *18*, 1785. [[CrossRef](#)]
187. Choi, N.J.; Shim, C.H.; Song, K.D.; Lee, D.S.; Huh, J.S.; Lee, D.D. Classification of Workplace Gases Using Temperature Modulation of Two SnO₂ Sensing Films on Substrate. *Sens. Actuators B Chem.* **2002**, *86*, 251–258. [[CrossRef](#)]
188. Radhakrishnan, J.K.; Kumara, M. Effect of Temperature Modulation, on the Gas Sensing Characteristics of ZnO Nanostructures, for Gases O₂, CO and CO₂. *Sens. Int.* **2021**, *2*, 100059. [[CrossRef](#)]
189. Mizuno, N.; Yoshioka, T.; Kato, K.; Iwamoto, M. CO₂-Sensing Characteristics of SnO₂ Element Modified by La₂O₃. *Sens. Actuators B Chem.* **1993**, *13*, 473–475. [[CrossRef](#)]
190. Ishihara, T.; Kometani, K.; Hashida, M.; Takita, Y. Application of Mixed Oxide Capacitor to the Selective Carbon Dioxide Sensor: I. Measurement of Carbon Dioxide Sensing Characteristics. *J. Electrochem. Soc.* **1991**, *138*, 173–176. [[CrossRef](#)]
191. Korotcenkov, G.; Cho, B.K. Metal Oxide Composites in Conductometric Gas Sensors: Achievements and Challenges. *Sens. Actuators B Chem.* **2017**, *244*, 182–210. [[CrossRef](#)]
192. Amin, K.R.; Bid, A. Graphene as a Sensor. *Curr. Sci.* **2014**, *107*, 430–436.
193. Singh, E.; Meyyappan, M.; Nalwa, H.S. Flexible Graphene-Based Wearable Gas and Chemical Sensors. *ACS Appl. Mater. Interfaces* **2017**, *9*, 34544–34586. [[CrossRef](#)]
194. Yoon, H.J.; Jun, D.H.; Yang, J.H.; Zhou, Z.; Yang, S.S.; Cheng, M.M.C. Carbon Dioxide Gas Sensor Using a Graphene Sheet. *Sens. Actuators B Chem.* **2011**, *157*, 310–313. [[CrossRef](#)]
195. Zhou, Y.; Jiang, Y.; Xie, G.; Wu, M.; Tai, H. Gas Sensors for CO₂ Detection Based on RGO–PEI Films at Room Temperature. *Chin. Sci. Bull.* **2014**, *59*, 1999–2005. [[CrossRef](#)]

196. Akhter, F.; Alahi, M.E.E.; Siddiquei, H.R.; Gooneratne, C.P.; Mukhopadhyay, S.C. Graphene Oxide (GO) Coated Impedimetric Gas Sensor for Selective Detection of Carbon Dioxide (CO₂) with Temperature and Humidity Compensation. *IEEE Sens. J.* **2021**, *21*, 4241–4249. [[CrossRef](#)]
197. Lu, G.; Ocola, L.E.; Chen, J. Reduced Graphene Oxide for Room-Temperature Gas Sensors. *Nanotechnology* **2009**, *20*, 445502. [[CrossRef](#)]
198. Muruganathan, M.; Sun, J.; Imamura, T.; Mizuta, H. Electrically Tunable van der Waals Interaction in Graphene–Molecule Complex. *Nano Lett.* **2015**, *15*, 8176–8180. [[CrossRef](#)]
199. Sun, J.; Muruganathan, M.; Mizuta, H. Room Temperature Detection of Individual Molecular Physisorption Using Suspended Bilayer Graphene. *Sci. Adv.* **2016**, *2*, e1501518. [[CrossRef](#)] [[PubMed](#)]
200. Chen, G.; Paronyan, T.M.; Harutyunyan, A.R. Sub-ppt Gas Detection with Pristine Graphene. *Appl. Phys. Lett.* **2012**, *101*, 053119. [[CrossRef](#)]
201. Smith, A.D.; Elgammal, K.; Fan, X.; Lemme, M.C.; Delin, A.; Råsander, M.; Bergqvist, L.; Schröder, S.; Fischer, A.C.; Niklaus, F.; et al. Graphene-Based CO₂ Sensing and its Cross-Sensitivity with Humidity. *RSC Adv.* **2017**, *7*, 22329–22339. [[CrossRef](#)]
202. Fan, X.; Elgammal, K.; Smith, A.D.; Östling, M.; Delin, A.; Lemme, M.C.; Niklaus, F. Humidity and CO₂ Gas Sensing Properties of Double-Layer Graphene. *Carbon* **2018**, *127*, 576–587. [[CrossRef](#)]
203. Zaki, S.E.; Basyooni, M.A.; Shaban, M.; Rabia, M.; Eker, Y.R.; Attia, G.F.; Yilmaz, M.; Ahmed, A.M. Role of Oxygen Vacancies in Vanadium Oxide and Oxygen Functional Groups in Graphene Oxide for Room Temperature CO₂ Gas Sensors. *Sens. Actuators A Phys.* **2019**, *294*, 17–24. [[CrossRef](#)]
204. Nemade, K.R.; Waghuley, S.A. Highly Responsive Carbon Dioxide Sensing by Graphene/Al₂O₃ Quantum Dots Composites at Low Operable Temperature. *Indian J. Phys.* **2014**, *88*, 577–583. [[CrossRef](#)]
205. Nemade, K.R.; Waghuley, S.A. Role of Defects Concentration on Optical and Carbon Dioxide Gas Sensing Properties of Sb₂O₃/Graphene composites. *Opt. Mater.* **2014**, *36*, 712–716. [[CrossRef](#)]
206. Amarnath, M.; Gurunathan, K. Highly Selective CO₂ Gas Sensor Using Stabilized NiO-In₂O₃ Nanospheres Coated Reduced Graphene Oxide Sensing Electrodes at Room Temperature. *J. Alloys Compd.* **2021**, *857*, 157584. [[CrossRef](#)]
207. Shaban, M.; Ali, S.; Rabia, M. Design and Application of Nanoporous Graphene Oxide Film for CO₂, H₂, and C₂H₂ Gases Sensing. *J. Mater. Res. Technol.* **2019**, *8*, 4510–4520. [[CrossRef](#)]
208. Rumyantsev, S.; Liu, G.; Shur, M.S.; Potyraiilo, R.A.; Balandin, A.A. Selective Gas Sensing with a Single Pristine Graphene Transistor. *Nano Lett.* **2012**, *12*, 2294–2298. [[CrossRef](#)]
209. Gauthier, M.; Chamberland, A. Solid-State Detectors for the Potentiometric Determination of Gaseous Oxides: I. Measurement in Air. *J. Electrochem. Soc.* **1977**, *124*, 1579–1583. [[CrossRef](#)]
210. Maruyama, T.; Sasaki, S.; Saito, Y. Potentiometric Gas Sensor for Carbon Dioxide Using Solid Electrolytes. *Solid State Ion.* **1987**, *23*, 107–112. [[CrossRef](#)]
211. Kishi, S.; Yuasa, M.; Tetsuya, K.; Lantto, V.; Shimano, K.; Yamazoe, N. A Stable Solid-Reference Electrode of BiCuVOx/Perovskite-Oxide for Potentiometric Solid Electrolyte CO₂ Sensor. *J. Ceram. Soc. Jpn.* **2007**, *115*, 706–711. doi: 10.2109/jcersj2.115.706. [[CrossRef](#)]
212. Dang, H.Y.; Guo, X.M. Characteristics and Performance of NASICON-Based CO₂ Sensor Using Bi₈Nb₂O₁₇ plus Pt as Solid-Reference Electrode. *Sens. Actuators B Chem.* **2013**, *178*, 163–168. [[CrossRef](#)]
213. Lee, I.; Akbar, S.A.; Dutta, P.K. High Temperature Potentiometric Carbon Dioxide Sensor with Minimal Interference to Humidity. *Sens. Actuators B Chem.* **2009**, *142*, 337–341. [[CrossRef](#)]
214. Lee, I.; Akbar, S.A. Potentiometric Carbon Dioxide Sensor Based on Thin Li₃PO₄ Electrolyte and Li₂CO₃ Sensing Electrode. *Ionics* **2014**, *20*, 563–569. [[CrossRef](#)]
215. Lee, H.K.; Choi, N.J.; Moon, S.E.; Heo, J.; Yang, W.S.; Kim, J. Durability Improvement of Solid Electrolyte CO₂ Sensor against Humidity Variations. *J. Nanosci. Nanotechnol.* **2015**, *15*, 404–407. [[CrossRef](#)]
216. Obata, K.; Shimano, K.; Miura, N.; Yamazoe, N. Influences of Water Vapor on NASICON-Based CO₂ Sensor Operative at Room Temperature. *Sens. Actuators B Chem.* **2003**, *93*, 243–249. [[CrossRef](#)]
217. Kida, T.; Miyachi, Y.; Shimano, K.; Yamazoe, N. NASICON Thick Film-Based CO₂ Sensor Prepared by a Sol–Gel Method. *Sens. Actuators B Chem.* **2001**, *80*, 28–32. [[CrossRef](#)]
218. Liu, J.; Weppner, W. Beta'-Alumina Solid Electrolytes for Solid State Electrochemical CO₂ Gas Sensors. *Solid State Commun.* **1990**, *76*, 311–313. [[CrossRef](#)]
219. Ma, N.; Ide, S.; Suematsu, K.; Watanabe, K.; Shimano, K. Novel Solid Electrolyte CO₂ Gas Sensors Based on c-Axis-Oriented Y-Doped La₉66Si₅3B₀7O₂₆14. *ACS Appl. Mater. Interfaces* **2020**, *12*, 21515–21520. [[CrossRef](#)]
220. Struzik, M.; Garbayo, I.; Pfenninger, R.; Rupp, J.L.M. A Simple and Fast Electrochemical CO₂ Sensor Based on Li₇La₃Zr₂O₁₂ for Environmental Monitoring. *Adv. Mater.* **2018**, *30*, 1804098. [[CrossRef](#)]
221. Choi, N.J.; Lee, H.K.; Moon, S.E.; Yang, W.S.; Kim, J. Stacked-Type Potentiometric Solid-State CO₂ Gas Sensor. *Sens. Actuators B Chem.* **2013**, *187*, 340–346. [[CrossRef](#)]
222. Barrosse-Antle, L.; Bond, A.; Compton, R.; O'Mahony, A.; Rogers, E.; Silvester, D. Voltammetry in Room Temperature Ionic Liquids: Comparisons and Contrasts with Conventional Electrochemical Solvents. *Chem. Asian J.* **2010**, *5*, 202–230. [[CrossRef](#)]
223. Rehman, A.; Zeng, X. Methods and Approaches of Utilizing Ionic Liquids as Gas Sensing Materials. *RSC Adv.* **2015**, *5*, 58371–58392. [[CrossRef](#)] [[PubMed](#)]

224. Behera, K.; Pandey, S.; Kadyan, A.; Pandey, S. Ionic Liquid-Based Optical and Electrochemical Carbon Dioxide Sensors. *Sensors* **2015**, *15*, 30487–30503. [[CrossRef](#)]
225. Wasilewski, T. Ionic Liquids in Gas Sensors and Biosensors. In *Green Sustainable Process for Chemical and Environmental Engineering and Science*; Elsevier: Amsterdam, The Netherlands, 2020; Chapter 10, pp. 287–318.
226. Fapyane, D.; Revsbech, N.P. Fast Responding Amperometric CO₂ Microsensor with Ionic Liquid–Aprotic Solvent Electrolytes. *ACS Sens.* **2020**, *5*, 2604–2610. [[CrossRef](#)] [[PubMed](#)]
227. Rosen, B.A.; Salehi-Khojin, A.; Masel, R.I. A Microfabricated Carbon Dioxide Sensor for Portable Applications. In Proceedings of the IEEE Sensors 2010 Conference, Waikoloa, HI, USA, 1–4 November 2010; pp. 365–368. [[CrossRef](#)]
228. Li, Y.; Li, G.; Wang, X.; Zhu, Z.; Ma, H.; Zhang, T.; Jin, J. Poly(Ionic Liquid)-Wwrapped Single-Walled Carbon Nanotubes for Sub-ppb Detection of CO₂. *Chem. Commun.* **2012**, *48*, 8222–8224. [[CrossRef](#)]
229. Honda, M.; Takei, Y.; Ishizu, K.; Imamoto, H.; Itoh, T.; Maeda, R.; Matsumoto, K.; Shimoyama, I. Low-Power-Consumption CO₂ Gas Sensor Using Ionic Liquids for Green Energy Management. In Proceedings of the Sensors, 2012 IEEE, Taipei, Taiwan, 28–31 October 2012; pp. 1–4. [[CrossRef](#)]
230. Ishizu, K.; Takei, Y.; Honda, M.; Noda, K.; Inaba, A.; Itoh, T.; Maeda, R.; Matsumoto, K.; Shimoyama, I. Carbon Dioxide Gas Sensor with Ionic Gel. In Proceedings of the 2013 Transducers Eurosensors XXVII: The 17th International Conference on Solid-State Sensors, Actuators and Microsystems (Transducers Eurosensors XXVII), Barcelona, Spain, 16–20 June 2013; pp. 1633–1636. [[CrossRef](#)]
231. Willa, C.; Yuan, J.; Niederberger, M.; Koziej, D. When Nanoparticles Meet Poly(Ionic Liquid)s: Chemoresistive CO₂ Sensing at Room Temperature. *Adv. Funct. Mater.* **2015**, *25*, 2537–2542. [[CrossRef](#)]
232. Willa, C.; Schmid, A.; Briand, D.; Yuan, J.; Koziej, D. Lightweight, Room-Temperature CO₂ Gas Sensor Based on Rare-Earth Metal-Free Composites—An Impedance Study. *ACS Appl. Mater. Interfaces* **2017**, *9*, 25553–25558. [[CrossRef](#)]
233. Revsbech, N.P.; Garcia-Robledo, E.; Sveegaard, S.; Andersen, M.H.; Gothelf, K.V.; Larsen, L.H. Amperometric Microsensor for Measurement of Gaseous and Dissolved CO₂. *Sens. Actuators B Chem.* **2019**, *283*, 349–354. [[CrossRef](#)]
234. Chen, L.; Huang, D.; Ren, S.; Chi, Y.; Chen, G. Carbon Dioxide Gas Sensor Based on Ionic Liquid-Induced Electrochemiluminescence. *Anal. Chem.* **2011**, *83*, 6862–6867. [[CrossRef](#)]
235. Buzzeo, M.C.; Klymenko, O.V.; Wadhawan, J.D.; Hardacre, C.; Seddon, K.R.; Compton, R.G. Kinetic Analysis of the Reaction between Electrogenerated Superoxide and Carbon Dioxide in the Room Temperature Ionic Liquids 1-Ethyl-3-methylimidazolium Bis(trifluoromethylsulfonyl)imide and Hexyltriethylammonium Bis(trifluoromethylsulfonyl)imide. *J. Phys. Chem. B* **2004**, *108*, 3947–3954. [[CrossRef](#)]
236. Xiao, C.; Zeng, X. In Situ EQCM Evaluation of the Reaction between Carbon Dioxide and Electrogenerated Superoxide in Ionic Liquids. *J. Electrochem. Soc.* **2013**, *160*, H749–H756. [[CrossRef](#)]
237. Wu, J.; Yin, M.j.; Seefeldt, K.; Dani, A.; Guterman, R.; Yuan, J.; Zhang, A.P.; Tam, H.Y. In Situ μ -Printed Optical Fiber-Tip CO₂ Sensor Using a Photocrosslinkable Poly(Ionic Liquid). *Sens. Actuators B Chem.* **2018**, *259*, 833–839. [[CrossRef](#)]
238. Mineo, P.G.; Livoti, L.; Lo Schiavo, S.; Cardiano, P. Fast and Reversible CO₂ Quartz Crystal Microbalance Response of Vinylimidazolium-Based Poly(Ionic Liquid)s. *Polym. Adv. Technol.* **2012**, *23*, 1511–1519. [[CrossRef](#)]
239. Zhou, R.; Vaihinger, S.; Geckeler, K.E.; Göpel, W. Reliable CO₂ Sensors with Silicon-Based Polymers on Quartz Microbalance Transducers. *Sens. Actuators B Chem.* **1994**, *19*, 415–420. [[CrossRef](#)]
240. Gomes, M.; Duarte, A.C.; Oliveira, J.P. Detection of CO₂ Using a Quartz Crystal Microbalance. *Sens. Actuators B Chem.* **1995**, *26*, 191–194. [[CrossRef](#)]
241. Lee, H.J.; Park, K.K.; Kupnik, M.; Khuri-Yakub, B.T. Functionalization Layers for CO₂ Sensing Using Capacitive Micromachined Ultrasonic Transducers. *Sens. Actuators B Chem.* **2012**, *174*, 87–93. [[CrossRef](#)]
242. Hoffmann, R.; Schreiter, M.; Heitmann, J. The Concept of Thin Film Bulk Acoustic Resonators as Selective CO₂ Gas Sensors. *J. Sens. Sens. Syst.* **2017**, *6*, 87–96. [[CrossRef](#)]
243. Siefker, Z.A.; Hodul, J.N.; Zhao, X.; Bajaj, N.; Brayton, K.M.; Flores-Hansen, C.; Zhao, W.; Chiu, G.T.C.; Braun, J.E.; Rhoads, J.F.; et al. Manipulating Polymer Composition to Create Low-Cost, High-Fidelity Sensors for Indoor CO₂ Monitoring. *Sci. Rep.* **2021**, *11*, 13237. [[CrossRef](#)]
244. Zuckerwar, A. *Handbook of the Speed of Sound in Real Gases: Theory*; Academic Press: Cambridge, MA, USA, 2002.
245. Joos, M.; Müller, H.; Lindner, G. An Ultrasonic Sensor for the Analysis of Binary Gas Mixtures. *Sens. Actuators B Chem.* **1993**, *16*, 413–419. [[CrossRef](#)]
246. Gerlach, G. Acoustic CO₂ Sensors. In *Carbon Dioxide Sensing*; John Wiley and Sons, Ltd.: Hoboken, NJ, USA, 2019; Chapter 9, pp. 215–245. [[CrossRef](#)]
247. Cicek, A.; Trak, D.; Arslan, Y.; Korozlu, N.; Kaya, O.A.; Ulug, B. Ultrasonic Gas Sensing by Two-Dimensional Surface Phononic Crystal Ring Resonators. *ACS Sens.* **2019**, *4*, 1761–1765. [[CrossRef](#)] [[PubMed](#)]
248. Evans, L.B.; Bass, H.E.; Sutherland, L.C. Atmospheric Absorption of Sound: Theoretical Predictions. *J. Acoust. Soc. Am.* **1972**, *51*, 1565–1575. [[CrossRef](#)]
249. Bass, H.E.; Sutherland, L.; Zuckerwar, A.J. Atmospheric Absorption of Sound—Update. *J. Acoust. Soc. Am.* **1990**, *88*, 2019–2021. [[CrossRef](#)]
250. Petculescu, A. Future Trends in Acoustic Gas Monitoring and Sensing. *J. Optoelectron. Adv. Mater.* **2006**, *8*, 217.

251. Dain, Y.; Lueptow, R.M. Acoustic Attenuation in a Three-Gas Mixture: Results. *J. Acoust. Soc. Am.* **2001**, *110*, 2974–2979. [[CrossRef](#)]
252. Cottet, A.; Neumeier, Y.; Scarborough, D.; Bibik, A.; Lieuwen, T. Acoustic Absorption Measurements for Characterization of Gas Mixing. *J. Acoust. Soc. Am.* **2004**, *116*, 2081–2088. [[CrossRef](#)]
253. Ejakov, S.; Phillips, S.; Dain, Y.; Lueptow, R.; H Visser, J. Acoustic Attenuation in Gas Mixtures with Nitrogen: Experimental Data and Calculations. *J. Acoust. Soc. Am.* **2003**, *113*, 1871–1879. [[CrossRef](#)]
254. Petculescu, A.; Hall, B.; Fraenzle, R.; Phillips, S.; Lueptow, R. A Prototype Acoustic Gas Sensor Based on Attenuation (L). *J. Acoust. Soc. Am.* **2006**, *120*. [[CrossRef](#)]
255. Jia, Y.; Yu, B.; Du, M.; Wang, X. Gas Composition Recognition Based on Analyzing Acoustic Relaxation Absorption Spectra: Wavelet Decomposition and Support Vector Machine Classifier. In Proceedings of the 2018 2nd International Conference on Electrical Engineering and Automation (ICEEA 2018), Chengdu, China, 25–26 March 2018; pp. 126–130. [[CrossRef](#)]
256. Zuckerwar, A.J.; Griffin, W.A. Effect of Water Vapor on Sound Absorption in Nitrogen at low Frequency/Pressure Ratios. *J. Acoust. Soc. Am.* **1981**, *69*, 150–154. [[CrossRef](#)]
257. Wysocki, G.; Kosterev, A.; Tittel, F. Influence of Molecular Relaxation Dynamics on Quartz-enhanced Photoacoustic Detection of CO₂ at $\lambda = 2 \mu\text{m}$. *Appl. Phys. B Lasers Opt.* **2006**, *85*, 301–306. [[CrossRef](#)]
258. Eberl, M.; Jost, F.; Kolb, S.; Schaller, R.; Dettmann, W.; Gassner, S.; Skorupa, F. Miniaturized Photoacoustic CO₂ Gas Sensors—A New Approach for the Automotive Sector. In Proceedings of the AmE 2019—Automotive meets Electronics, 10th GMM-Symposium, Dortmund, Germany, 12–13 March 2019; pp. 1–5.
259. Hahn, C.E.W. Techniques for Measuring the Partial Pressures of Gases in the Blood. I. In Vitro Measurements. *J. Phys. E Sci. Instrum.* **1980**, *13*, 470–482. [[CrossRef](#)]
260. Atamanchuk, D.; Tengberg, A.; Thomas, P.J.; Hovdenes, J.; Apostolidis, A.; Huber, C.; Hall, P.O. Performance of a Lifetime-Based Optode for Measuring Partial Pressure of Carbon Dioxide in Natural Waters. *Limnol. Oceanogr. Methods* **2014**, *12*, 63–73. [[CrossRef](#)]
261. Joshi, S.; Jones, L.A.; Sabri, Y.M.; Bhargava, S.K.; Sunkara, M.V.; Ippolito, S.J. Facile Conversion of Zinc Hydroxide Carbonate to CaO-ZnO for Selective CO₂ Gas Detection. *J. Colloid Interface Sci.* **2020**, *558*, 310–322. [[CrossRef](#)]
262. Kaneyasu, K.; Otsuka, K.; Setoguchi, Y.; Sonoda, S.; Nakahara, T.; Aso, I.; Nakagaichi, N. A Carbon Dioxide Gas Sensor Based on Solid Electrolyte for Air Quality Control. *Sens. Actuators B Chem.* **2000**, *66*, 56–58. [[CrossRef](#)]
263. Jones, N.L. An obsession with CO₂. *Appl. Physiol. Nutr. Metab.* **2008**, *33*, 641–650. [[CrossRef](#)]
264. Guyenet, P.G.; Bayliss, D.A. Neural Control of Breathing and CO₂ Homeostasis. *Neuron* **2015**, *87*, 946–961. [[CrossRef](#)] [[PubMed](#)]
265. Lumb, A. Control of Breathing. In *Nunn's Applied Respiratory Physiology*, 8th ed.; Elsevier: Amsterdam, The Netherlands, 2016; Chapter 4, pp. 61–82.
266. Hamm, L.L.; Nakhoul, N.; Hering-Smith, K.S. Acid-Base Homeostasis. *Clin. J. Am. Soc. Nephrol.* **2015**, *10*, 2232–2242. [[CrossRef](#)]
267. Curley, G.; Laffey, J.G.; Kavanagh, B.P. Bench-to-Bedside Review: Carbon Dioxide. *Crit. Care* **2010**, *14*, 220. cc8926. [[CrossRef](#)]
268. Geers, C.; Gros, G. Carbon Dioxide Transport and Carbonic Anhydrase in Blood and Muscle. *Physiol. Rev.* **2000**, *80*, 681–715. [[CrossRef](#)]
269. Lumb, A. Carbon Dioxide. In *Nunn's Applied Respiratory Physiology*, 8th ed.; Elsevier: Amsterdam, The Netherlands, 2016; Chapter 9, pp. 159–177.
270. Larkin, B.G.; Zimmanck, R.J. Interpreting Arterial Blood Gases Successfully. *AORN J.* **2015**, *102*, 343–357. [[CrossRef](#)] [[PubMed](#)]
271. Foster, S.; Lopez, D.; Thomas, H.M. Pulmonary Rehabilitation in COPD Patients with Elevated PCO₂. *Am. Rev. Respir. Dis.* **1988**, *138*, 1519–1523. [[CrossRef](#)] [[PubMed](#)]
272. Cukic, V. The Changes of Arterial Blood Gases in COPD During Four-Year Period. *Med. Arch.* **2014**, *68*, 14–18. [[CrossRef](#)] [[PubMed](#)]
273. Nava, S.; Rubini, F.; Zanotti, E.; Ambrosino, N.; Bruschi, C.; Vitacca, M.; Fracchia, C.; Rampulla, C. Survival and Prediction of Successful Ventilator Weaning in COPD Patients Requiring Mechanical Ventilation for More Than 21 Days. *Eur. Respir. J.* **1994**, *7*, 1645–1652. [[CrossRef](#)]
274. Tsuboi, T.; Ohi, M.; Oga, T.; Machida, K.; Chihara, Y.; Harada, Y.; Takahashi, K.; Sumi, K.; Handa, T.; Niimi, A.; et al. Importance of the PaCO₂ from 3 to 6 Months after Initiation of Long-Term Non-Invasive Ventilation. *Respir. Med.* **2010**, *104*, 1850–1857. [[CrossRef](#)]
275. Campbell, R.L.; Saxen, M.A. Respiratory Effects of a Balanced Anesthetic Technique—Revisited Fifteen Years Later. *Anesth. Prog.* **1994**, *41*, 1–5.
276. Schneider, A.G.; Eastwood, G.M.; Bellomo, R.; Bailey, M.; Lipcsey, M.; Pilcher, D.; Young, P.; Stow, P.; Santamaria, J.; Stachowski, E.; et al. Arterial Carbon Dioxide Tension and Outcome in Patients Admitted to the Intensive Care Unit After Cardiac Arrest. *Resuscitation* **2013**, *84*, 927–934. [[CrossRef](#)]
277. Zavorsky, G.S.; Cao, J.; Mayo, N.E.; Gabbay, R.; Murias, J.M. Arterial Versus Capillary Blood Gases: A Meta-Analysis. *Respir. Physiol. Neurobiol.* **2007**, *155*, 268–279. [[CrossRef](#)]
278. Byrne, A.L.; Bennett, M.; Chatterji, R.; Symons, R.; Pace, N.L.; Thomas, P.S. Peripheral Venous and Arterial Blood Gas Analysis in Adults: Are They Comparable? A Systematic Review and Meta-Analysis. *Respirology* **2014**, *19*, 168–175. [[CrossRef](#)]
279. Malinoski, D.J.; Todd, S.R.; Slone, D.S.; Mullins, R.J.; Schreiber, M.A. Correlation of Central Venous and Arterial Blood Gas Measurements in Mechanically Ventilated Trauma Patients. *Arch. Surg.* **2005**, *140*, 1122–1125. [[CrossRef](#)] [[PubMed](#)]

280. Treger, R.; Pirouz, S.; Kamangar, N.; Corry, D. Agreement between Central Venous and Arterial Blood Gas Measurements in the Intensive Care Unit. *Clin. J. Am. Soc. Nephrol.* **2010**, *5*, 390–394. [[CrossRef](#)] [[PubMed](#)]
281. Walkey, A.J.; Farber, H.W.; O'Donnell, C.; Cabral, H.; Eagan, J.S.; Philippides, G.J. The Accuracy of the Central Venous Blood Gas for Acid-Base Monitoring. *J. Intensive Care Med.* **2010**, *25*, 104–110.10.1177/0885066609356164. [[CrossRef](#)]
282. Scheeren, T.W.; Wicke, J.N.; Teboul, J.L. Understanding the Carbon Dioxide Gaps. *Curr. Opin. Crit. Care* **2018**, *24*, 181–189. [[CrossRef](#)] [[PubMed](#)]
283. Charbel, F.T.; Du, X.; Hoffman, W.E.; Ausman, J.I. Brain Tissue PO₂, PCO₂, and pH During Cerebral Vasospasm. *Surg. Neurol.* **2000**, *54*, 432–437. [[CrossRef](#)]
284. Brooks, A.J.; Hammond, J.S.; Girling, K.; Beckingham, I.J. The Effect of Hepatic Vascular Inflow Occlusion on Liver Tissue pH, Carbon Dioxide, and Oxygen Partial Pressures: Defining the Optimal Clamp/Release Regime for Intermittent Portal Clamping. *J. Surg. Res.* **2007**, *141*, 247–251. [[CrossRef](#)]
285. McKinley, B.A.; Butler, B.D. Comparison of Skeletal Muscle PO₂, PCO₂, and pH with Gastric Tonometric PCO₂ and pH in Hemorrhagic Shock. *Crit. Care Med.* **1999**, *27*, 1869–1877. [[CrossRef](#)] [[PubMed](#)]
286. Mythen, M.G. Does Gastric Tonometry-Guided Therapy Reduce Total Mortality in Critically Ill Patients? *Crit. Care* **2015**, *19*, 172. [[CrossRef](#)] [[PubMed](#)]
287. Mallat, J.; Vallet, B. Regional Capnography. In *Monitoring Tissue Perfusion in Shock: From Physiology to the Bedside*; Pinto Lima, A.A., Silva, E., Eds.; Springer International Publishing: Berlin/Heidelberg, Germany, 2018; pp. 181–192.13. [[CrossRef](#)]
288. Ganter, M.; Zollinger, A. Continuous Intravascular Blood Gas Monitoring: Development, Current Techniques, and Clinical Use of a Commercial Device. *BJA Br. J. Anaesth.* **2003**, *91*, 397–407. [[CrossRef](#)]
289. Luukkonen, A.A.; Lehto, T.M.; Hedberg, P.S.; Vaskivuo, T.E. Evaluation of a Hand-Held Blood Gas Analyzer for Rapid Determination of Blood Gases, Electrolytes and Metabolites in Intensive Care Setting. *Clin. Chem. Lab. Med. (CCLM)* **2016**, *54*, 585–594. [[CrossRef](#)]
290. Menzel, M.; Soukup, J.; Henze, D.; Engelbrecht, K.; Senderreck, M.; Scharf, A.; Rieger, A.; Grond, S. Experiences with Continuous Intra-Arterial Blood Gas Monitoring: Precision and Drift of a Pure Optode-System. *Intensive Care Med.* **2003**, *29*, 2180–2186. [[CrossRef](#)]
291. Badnjevic, A.; Beganovic, E.; Music, O. Facts About Solution Based and Cartridge Based Devices for Blood Gas Analysis. In Proceedings of the 2011 18th International Conference on Systems, Signals and Image Processing, Sarajevo, Bosnia and Herzegovina, 16–18 June 2011; pp. 1–5.
292. Gravenstein, J.; Jaffe, M.; Gravenstein, N.; Paulus, D. *Capnography*, 2nd ed.; Cambridge University Press: Cambridge, UK, 2011; doi:10.1017/CBO9780511933837. [[CrossRef](#)]
293. Kodali, B.S. *Capnography*, 11th ed.; Cambridge University Press: Cambridge, UK, 2021.
294. Siobal, M.S. Monitoring Exhaled Carbon Dioxide. *Respir. Care* **2016**, *61*, 1397–1416. [[CrossRef](#)]
295. Long, B.; Koyfman, A.; Vivirito, M.A. Capnography in the Emergency Department: A Review of Uses, Waveforms, and Limitations. *J. Emerg. Med.* **2017**, *53*, 829–842. [[CrossRef](#)]
296. Amaddeo, A.; Fauroux, B. Oxygen and Carbon Dioxide Monitoring During Sleep. *Paediatr. Respir. Rev.* **2016**, *20*, 42–44. [[CrossRef](#)]
297. Hochwald, O.; Borenstein-Levin, L.; Dinur, G.; Jubran, H.; Ben-David, S.; Kugelman, A. Continuous Noninvasive Carbon Dioxide Monitoring in Neonates: From Theory to Standard of Care. *Pediatrics* **2019**, *144*, e20183640. [[CrossRef](#)]
298. Jaffe, M.B. *Mainstream or Sidestream Capnography?* Respironics White Paper; Respironics Novamatrix, Inc.: Wallingford, CT, USA, 2002.
299. Barter, L.S. Capnography. In *Advanced Monitoring and Procedures for Small Animal Emergency and Critical Care*; John Wiley & Sons, Ltd.: Hoboken, NJ, USA, 2012; Chapter 26, pp. 340–348. [[CrossRef](#)]
300. Balogh, A.L.; Petak, F.; Fodor, G.H.; Tolnai, J.; Csorba, Z.; Babik, B. Capnogram Slope and Ventilation Dead Space Parameters: Comparison of Mainstream and Sidestream Techniques. *Br. J. Anaesth.* **2016**, *117*, 109–117. [[CrossRef](#)]
301. Nakatani, K.; Yukioka, H.; Fujimori, M.; Maeda, C.; Noguchi, H.; Ishihara, S.; Yamanaka, I.; Tase, C. Utility of Colorimetric End-Tidal Carbon Dioxide Detector for Monitoring During Prehospital Cardiopulmonary Resuscitation. *Am. J. Emerg. Med.* **1999**, *17*, 203–206. [[CrossRef](#)]
302. Mari, A.; Nougue, H.; Mateo, J.; Vallet, B.; Vallée, F. Transcutaneous PCO₂ Monitoring in Critically Ill Patients: Update and Perspectives. *J. Thorac. Dis.* **2019**, *11*, S1558–S1567. [[CrossRef](#)] [[PubMed](#)]
303. Vallée, F.; Nougé, H.; Mari, A.; Vodovar, N.; Dubreuil, G.; Damoiseil, C.; Dépret, F.; Mateo, J. Variations of Cutaneous Capnometry and Perfusion Index During a Heating Challenge is Early Impaired in Septic Shock and Related to Prognostic in Non-Septic Shock. *Shock* **2019**, *51*, 585–592. [[CrossRef](#)] [[PubMed](#)]
304. Restrepo, R.D.; Hirst, K.R.; Wittnebel, L.; Wettstein, R. AARC Clinical Practice Guideline: Transcutaneous Monitoring of Carbon Dioxide and Oxygen: 2012. *Respir. Care* **2012**, *57*, 1955–1962. [[CrossRef](#)]
305. Vallée, F.; Mateo, J.; Dubreuil, G.; Poussant, T.; Tachon, G.; Ouanounou, I.; Payen, D. Cutaneous Ear Lobe PCO₂ at 37 °C to Evaluate Microperfusion in Patients with Septic Shock. *Chest* **2010**, *138*, 1062–1070. [[CrossRef](#)]
306. Steventon, A.; Bardsley, M.; Billings, J.; Dixon, J.; Doll, H.; Hirani, S.; Cartwright, M.; Rixon, L.; Knapp, M.; Henderson, C.; et al. Effect of Telehealth on Use of Secondary Care and Mortality: Findings From the Whole System Demonstrator Cluster Randomised Trial. *BMJ* **2012**, *344*, e3874. [[CrossRef](#)]

307. Kruse, C.; Pesek, B.; Anderson, M.; Brennan, K.; Comfort, H. Telemonitoring to Manage Chronic Obstructive Pulmonary Disease: Systematic Literature Review. *JMIR Med. Inf.* **2019**, *7*, e11496. [[CrossRef](#)] [[PubMed](#)]
308. Yun, J.E.; Park, J.E.; Park, H.Y.; Lee, H.Y.; Park, D.A. Comparative Effectiveness of Telemonitoring Versus Usual Care for Heart Failure: A Systematic Review and Meta-analysis. *J. Card. Fail.* **2018**, *24*, 19–28. [[CrossRef](#)] [[PubMed](#)]
309. Garfan, S.; Alamoodi, A.H.; Zaidan, B.B.; Al-Zobbi, M.; Hamid, R.A.; Alwan, J.K.; Ahmaro, I.Y.; Khalid, E.T.; Jumaah, F.M.; Albahri, O.S.; et al. Telehealth Utilization During the COVID-19 Pandemic: A Systematic Review. *Comput. Biol. Med.* **2021**, *138*, 104878. [[CrossRef](#)] [[PubMed](#)]
310. Dunn, J.; Runge, R.; Snyder, M. Wearables and the Medical Revolution. *Pers. Med.* **2018**, *15*, 429–448. [[CrossRef](#)]
311. Yetisen, A.K.; Martinez-Hurtado, J.L.; Ünal, B.; Khademhosseini, A.; Butt, H. Wearables in Medicine. *Adv. Mater.* **2018**, *30*, 1706910. [[CrossRef](#)] [[PubMed](#)]
312. Chung, M.; Fortunato, G.; Radacsi, N. Wearable Flexible Sweat Sensors for Healthcare Monitoring: A Review. *J. R. Soc. Interface* **2019**, *16*, 20190217. [[CrossRef](#)]
313. Dagher, L.; Shi, H.; Zhao, Y.; Marrouche, N.F. Wearables in Cardiology: Here to Stay. *Heart Rhythm* **2020**, *17*, 889–895. [[CrossRef](#)]
314. Dervieux, E.; Bodinier, Q.; Uhring, W.; Théron, M. Measuring Hemoglobin Spectra: Searching for Carbamino-Hemoglobin. *J. Biomed. Opt.* **2020**, *25*, 105001. [[CrossRef](#)]
315. Eletr, S.; Jimison, H.; Ream, A.K.; Dolan, W.M.; Rosenthal, M.H. Cutaneous Monitoring of Systemic Pco₂ on Patients in the Respiratory Intensive Care Unit Being Weaned From the Ventilator. *Acta Anaesthesiol. Scand.* **1978**, *22*, 123–127. [[CrossRef](#)]
316. Greenspan, G.H.; Block, A.J.; Haldeman, L.W.; Lindsey, S.; Martin, C.S. Transcutaneous Noninvasive Monitoring of Carbon Dioxide Tension. *Chest* **1981**, *80*, 442–446. [[CrossRef](#)]
317. Chatterjee, M.; Ge, X.; Kostov, Y.; Tolosa, L.; Rao, G. A Novel Approach Toward Noninvasive Monitoring of Transcutaneous CO₂. *Med. Eng. Phys.* **2014**, *36*, 136–139. [[CrossRef](#)]
318. Chatterjee, M.; Ge, X.; Kostov, Y.; Luu, P.; Tolosa, L.; Woo, H.; Viscardi, R.; Falk, S.; Potts, R.; Rao, G. A Rate-Based Transcutaneous CO₂ Sensor for Noninvasive Respiration Monitoring. *Physiol. Meas.* **2015**, *36*, 883–894. [[CrossRef](#)]
319. Ge, X.; Adangwa, P.; Young Lim, J.; Kostov, Y.; Tolosa, L.; Pierson, R.; Herr, D.; Rao, G. Development and Characterization of a Point-of Care Rate-Based Transcutaneous Respiratory Status Monitor. *Med. Eng. Phys.* **2018**, *56*, 36–41. [[CrossRef](#)]
320. Iitani, K.; Tyson, J.; Rao, S.; Ramamurthy, S.S.; Ge, X.; Rao, G. What do Masks Mask? A Study on Transdermal CO₂ Monitoring. *Med. Eng. Phys.* **2021**, *98*, 50–56. [[CrossRef](#)]
321. Grangeat, P.; Gharbi, S.; Accensi, M.; Grateau, H. First Evaluation of a Transcutaneous Carbon Dioxide Monitoring Wristband Device during a Cardiopulmonary Exercise Test. In Proceedings of the 41st Annual International Conference of the IEEE Engineering in Medicine and Biology Society (EMBC), Berlin, Germany, 23–27 July 2019; pp. 3352–3355. [[CrossRef](#)]
322. Grangeat, P.; Gharbi, S.; Koenig, A.; Comsa, M.P.; Accensi, M.; Grateau, H.; Ghaith, A.; Chacaroun, S.; Doutreleau, S.; Verges, S. Evaluation in Healthy Subjects of a Transcutaneous Carbon Dioxide Monitoring Wristband during Hypo and Hypercapnia Conditions. In Proceedings of the 42nd Annual International Conference of the IEEE Engineering in Medicine Biology Society (EMBC), Montreal, QC, Canada, 20–24 July 2020; pp. 4640–4643. [[CrossRef](#)]
323. Shaw, L.A.; Messer, A.C. Cutaneous Respiration in Man: II. The Effect of Temperature and of Relative Humidity upon the Rate of Carbon Dioxide Elimination and Oxygen Absorption. *Am. J. Physiol.-Leg. Content* **1930**, *95*, 13–19. [[CrossRef](#)]
324. Scheuplein, R.J. Permeability of the Skin: A Review of Major Concepts and Some New Developments. *J. Investig. Dermatol.* **1976**, *67*, 672–676. [[CrossRef](#)]
325. Adamczyk, B.; Boerboom, A.J.; Kistemaker, J. A Mass Spectrometer for Continuous Analysis of Gaseous Compounds Excreted by Human Skin. *J. Appl. Physiol.* **1966**, *21*, 1903–1906. [[CrossRef](#)] [[PubMed](#)]
326. Levshankov, A.I.; Pushkina, M.A.; Slutskaia, M.E.; Uvarov, B.S. Determination of Local Gas Exchange on the Body Surface by the Method of Mass Spectrometry. *Meditainskaia Tekhnika* **1983**, *1*, 21–26.
327. Ernstene, A.C.; Volk, M.C. Cutaneous Respiration in Man: IV. The Rate of Carbon Dioxide Elimination and Oxygen Absorption in Normal Subjects. *J. Clin. Investig.* **1932**, *11*, 363–376. [[CrossRef](#)] [[PubMed](#)]
328. McIlroy, M.B.; Simbruner, G.; Sonoda, Y. Transcutaneous Blood Gas Measurements Using a Mass Spectrometer. *Acta Anaesthesiol. Scand.* **1978**, *22*, 128–130. [[CrossRef](#)]
329. Hansen, T.N.; Sonoda, Y.; McIlroy, M.B. Transfer of Oxygen, Nitrogen, and Carbon Dioxide through Normal Adult Human Skin. *J. Appl. Physiol.* **1980**, *49*, 438–443. [[CrossRef](#)]
330. Targett, R.C.; Kocher, O.; Muramatsu, K.; McIlroy, M.B. Skin Gas Tensions and Resistances Measured by Mass Spectrometry in Adults. *J. Appl. Physiol.* **1984**, *56*, 1431–1435. [[CrossRef](#)]
331. Lawrence, J.C.; Bull, J.P. Thermal Conditions which Cause Skin Burns. *Eng. Med.* **1976**, *5*, 61–63. [[CrossRef](#)]
332. Moritz, A.R.; Henriques, F.C. Studies of Thermal Injury: II. The Relative Importance of Time and Surface Temperature in the Causation of Cutaneous Burns. *Am. J. Pathol.* **1947**, *23*, 695–720.
333. Wimberley, P.D.; Grønlund Pedersen, K.; Olsson, J.; Siggaard-Andersen, O. Transcutaneous Carbon Dioxide and Oxygen Tension Measured at Different Temperatures in Healthy Adults. *Clin. Chem.* **1985**, *31*, 1611–1615. [[CrossRef](#)]
334. Food and Drug Administration. *Cutaneous Carbon Dioxide (PcCO₂) and Oxygen (PcO₂) Monitors—Class II Special Controls Guidance Document for Industry and FDA*; Technical Report; U.S. Department Of Health and Human Services: Washington, DC, USA, 2002.
335. Fitzgerald, L.R. Cutaneous Respiration in Man. *Physiol. Rev.* **1957**, *37*, 325–336. [[CrossRef](#)]

336. Shaw, L.A.; Messer, A.C. Cutaneous Respiration in Man: I. Factors Affecting the Rate of Carbon Dioxide Elimination and Oxygen Absorption. *Am. J. Physiol.-Leg. Content* **1930**, *95*, 107–118. [[CrossRef](#)]
337. Barratt, W. On the Normal and Pathological Elimination of Carbonic Acid and of Water by the Skin. *J. Physiol.* **1897**, *21*, 192–208. [[CrossRef](#)]
338. Whitehouse, A.G.R.; Hancock, W.; Haldane, J.S. The Osmotic Passage of Water and Gases through the Human Skin. *Proc. R. Soc. Lond. Ser. B* **1932**, *111*, 412–429. [[CrossRef](#)]
339. Thiele, F.A.J.; Van Kempen, L.H.J. A Micro Method for Measuring the Carbon Dioxide Release by Small Skin Areas. *Br. J. Dermatol.* **1972**, *86*, 463–471. [[CrossRef](#)]
340. Frame, G.W.; Strauss, W.G.; Maibach, H.I. Carbon Dioxide Emission of the Human Arm and Hand. *J. Investig. Dermatol.* **1972**, *59*, 155–158. [[CrossRef](#)] [[PubMed](#)]
341. Eöry, A. In-Vivo Skin Respiration (CO₂) Measurements in the Acupuncture Loci. *Acupunct. Electro-Ther. Res.* **1984**, *9*, 217–223. [[CrossRef](#)]
342. Montgomery, L.D.; Williams, B.A. Effect of Ambient Temperature on the Thermal Profile of the Human Forearm, Hand, and Fingers. *Ann. Biomed. Eng.* **1976**, *4*, 209–219. [[CrossRef](#)] [[PubMed](#)]
343. Grønlund, J. Evaluation of Factors Affecting Relationship Between Transcutaneous PO₂ and Probe Temperature. *J. Appl. Physiol.* **1985**, *59*, 1117–1127. [[CrossRef](#)]
344. Palmisano, B.W.; Severinghaus, J.W. Transcutaneous Pco₂ and Po₂: A multicenter study of Accuracy. *J. Clin. Monit.* **1990**, *6*, 189–195. [[CrossRef](#)]
345. Herrell, N.; Martin, R.J.; Pultusker, M.; Lough, M.; Fanaroff, A. Optimal Temperature for the Measurement of Transcutaneous Carbon Dioxide Tension in the Neonate. *J. Pediatr.* **1980**, *97*, 114–117. [[CrossRef](#)]
346. Tremper, K.K.; Mentelos, R.A.; Shoemaker, W.C. Clinical And Experimental Transcutaneous PCO₂ Monitoring. *J. Clin. Eng.* **1981**, *6*, 143–147. [[CrossRef](#)]
347. Briand, D.; Oprea, A.; Courbat, J.; Bârsan, N. Making Environmental Sensors on Plastic Foil. *Mater. Today* **2011**, *14*, 416–423. [[CrossRef](#)]
348. Köstler, S.; Kraker, E.; Sagmeister, M.; Lamprecht, B.; Bizzari, A.; Stadlober, B.; Ribitsch, B.; Abel, T.; Mayr, T. C7.3—From Optochemical Sensors for Industrial Processes to Large-Area Printing of Sensor Systems Integrated with Organic Electronics. In Proceedings of the Sensor + Test Conferences 2011, Nürnberg, Germany, 7–9 June 2011.
349. Xing, X.; Ma, Z.; Zhang, M.; Zhou, Y.; Dong, W.; Song, M. An Unobtrusive and Calibration-Free Blood Pressure Estimation Method Using Photoplethysmography and Biometrics. *Sci. Rep.* **2019**, *9*, 8611. [[CrossRef](#)]
350. Shao, J.; Shi, P.; Hu, S.; Yu, H. A Revised Point-to-Point Calibration Approach with Adaptive Errors Correction to Weaken Initial Sensitivity of Cuff-Less Blood Pressure Estimation. *Sensors* **2020**, *20*, 2205. [[CrossRef](#)]
351. Kim, H.G.; Cheon, E.J.; Bai, D.S.; Lee, Y.H.; Koo, B.H. Stress and Heart Rate Variability: A Meta-Analysis and Review of the Literature. *Psychiatry Investig.* **2018**, *15*, 235–245. [[CrossRef](#)]
352. Moret-Bonillo, V.; Alvarez-Estévez, D.; Fernández-Leal, A.; Hernández-Pereira, E. Intelligent Approach for Analysis of Respiratory Signals and Oxygen Saturation in the Sleep Apnea/Hypopnea Syndrome. *Open Med. Inform. J.* **2014**, *8*, 1–19. [[CrossRef](#)]
353. Clarke, M.; Gokalp, H.; Fursse, J.; Jones, R.W. Dynamic Threshold Analysis of Daily Oxygen Saturation for Improved Management of COPD Patients. *IEEE J. Biomed. Health Inform.* **2016**, *20*, 1352–1360. [[CrossRef](#)] [[PubMed](#)]
354. Domján, G.; Kaffka, K.J.; Jákó, J.M.; Vályi-Nagy, I.T. Rapid Analysis of Whole Blood and Blood Serum Using Near Infrared Spectroscopy. *J. Infrared Spectrosc.* **1994**, *2*, 67–78. [[CrossRef](#)]
355. Marasco, C.; Perez, A.; Ehrman, J.; Hoilett, O. Metabolic Rate Measurement Apparatus and Method Thereof. U.S. Patent 2020/0113516 A1, 16 April 2020.
356. Freilich, J. Prophetic patents. *UC Davis L. Rev.* **2019**, *53*, 663. [[CrossRef](#)]
357. Tamura, T. Current Progress of Photoplethysmography and SpO₂ for Health Monitoring. *Biomed. Eng. Lett.* **2019**, *9*, 21–36. [[CrossRef](#)]
358. Jacques, S.L. Optical Properties of Biological Tissues: A Review. *Phys. Med. Biol.* **2013**, *58*, R37–R61. [[CrossRef](#)] [[PubMed](#)]
359. Kou, L.; Labrie, D.; Chylek, P. Refractive Indices of Water and Ice in the 0.65- to 2.5- μ m Spectral Range. *Appl. Opt.* **1993**, *32*, 3531–3540. [[CrossRef](#)]